# Mechanisms of Smac mimetic and proteasome inhibitor-induced cell death in diffuse large B-cell lymphoma

Dissertation

zur Erlangung des Doktorgrades der Naturwissenschaften

vorgelegt beim Fachbereich 14 Biochemie, Chemie und Pharmazie

der Johann Wolfgang Goethe-Universität

in Frankfurt am Main

von

Anna Dietz geb. Schwendler

aus Wiesbaden

Frankfurt am Main, 2020

(D30)

Vom Fachbereich 14 der Johann Wolfgang Goethe-Universität als Dissertation angenommen.

Dekan: Prof. Dr. Clemens Glaubitz

Gutachter 1: Prof. Dr. Volker Dötsch

Gutachter 2: Prof. Dr. Simone Fulda

Datum der Disputation: 23.11.2020

# List of contents

# List of abbreviations

| | |
|---|---|
| **%** | Percent/Prozent (German) |
| **µl** | Microliter |
| **µM** | Micrometer |
| **ABC** | Activated B cell |
| **ATCC** | American Type Culture Collection |
| **α-Toc** | α-Tocopherol |
| **BAD** | BCL-2-Antagonist of Cell Death |
| **BAK** | BCL-2 homologous antagonist/killer |
| **BAX** | BCL-2 associated X protein |
| **BCA** | Bicinchoninic acid |
| **BCL-2** | B cell lymphoma 2 |
| **BCR** | B cell receptor |
| **BH** | BCL-2 homology |
| **BID** | BH3 interacting-domain death agonist |
| **BIK** | BCL-2-interacting killer |
| **BIM** | BCL-2-like protein 11 |
| **BIR** | Baculovirus IAP repeat |
| **BMF** | BCL-2 modifying factor |

| | |
|---|---|
| **BTZ** | Bortezomib |
| **BSA** | Bovine serum albumin |
| **CARD** | Caspase recruitment domain |
| **cFLIP$_{L/S}$** | Cellular FLICE-like inhibitory protein long/short |
| **CHAPS** | 3-((3-cholamidopropyl) dimethylammonio)-1-propanesulfonate |
| **CI** | Combination index |
| **cIAP** | Cellular inhibitor of apoptosis |
| **CLL** | Chronic lymphocytic leukemia |
| **Ctrl** | Control |
| **DCF** | CM-H2DCFDA |
| **DISC** | Death-inducing signaling complex |
| **DLBCL** | Diffuse large B-cell lymphoma |
| **DMEM** | Dulbecco's modified Eagle medium |
| **DMSO** | Dimethyl sulfoxide |
| **DNA** | Deoxyribonucleic acid |
| **DSMZ** | Deutsche Sammlung von Mikroorganismen und Zellkulturen |
| **DTT** | Dithiothreitol |
| **e.g.** | Exempli gratia (Latin); for example |
| **ECL** | Enhanced chemiluminescence |

| | |
|---|---|
| **EDTA** | Ethylenediaminetetraacetic acid |
| **ER** | Endoplasmatic reticulum |
| **Et al.** | Et alii (Latin); and other |
| **FACS** | Fluorescence-activated cell sorting |
| **FADD** | Fas-associated protein with death domain |
| **Fas** | First apoptosis signal |
| **FCS** | Fetal calf serum |
| **FDA** | US food and drug Association |
| **FSC** | Forward scatter |
| **GAPDH** | Glyceraldehyde 3-phosphate dehydrogenase |
| **GCB** | Germinal center B-cell |
| **GSH** | Glutathione |
| **HCL** | Hydrogen chloride |
| **HEPES** | 4-(2-hydroxyethyl)-1-piperazineethanesulfonic acid |
| **HRP** | Horseradish peroxidase |
| **i.e.** | Id est (Latin); that is |
| **IAP** | Inhibitor of apoptosis |
| **IgG** | Immunoglobulin G |
| **IMDM** | Iscove's Modified Dulbecco's Medium |

**IP**            Immunoprecipitation

**JNK**           Jun N-terminal kinase

**KD**            Knockdown

**kDa**           Kilo Daltons

**LOMMP**         Loss of mitochondrial membrane potential

**LUBAC**         Linear ubiquitin chain assembly complex

**M**             Molar

**MBR**           Membrane binding region

**MCL**           Mantle cell lymphoma

**MCL-1**         Induced myeloid leukemia cell differentiation protein

**Mg**            Milligram

**min**           minute

**ml**            Milliliter

**mM**            Millimolar

**MMP**           Mitochondrial membrane potential

**MnTBAP**        Manganese (III) tetrakis (4-benzoic acid) porphyrin chloride

**MOMP**          Mitochondrial outer membrane permeabilization

**mRNA**          Messenger ribonucleic acid

**mTOR**          Mammalian target of rapamycin

| | |
|---|---|
| **NAC** | N-acetylcysteine |
| **NaCl** | Sodium chloride |
| **NEMO** | NF-κB essential modulator |
| **NF-κB** | Nuclear factor κ-light-chain-enhancer of activated B-cells |
| **NIK** | NF-κB inducing kinase |
| **nM** | Nanomolar |
| **NOXA** | Phorbol-12-myristate-13-acetate-induced protein 1 |
| **PBS** | Phosphate-buffered saline |
| **PBMC** | Peripheral-blood mononuclear cell |
| **PBML** | Primary mediastinal B-cell lymphoma |
| **Pen/Strep** | Penicillin/streptomycin |
| **PI** | Propidium iodide |
| **PI3K** | Phosphatidylinositol-4,5-bisphosphate 3-kinase |
| **PIC** | Protease inhibitor cocktail |
| **PMSF** | Phenylmethylsulfonyl fluoride |
| **PTP** | Permeability transition pore |
| **PUMA** | P53 upregulated modulator of apoptosis |
| **qRT-PCR** | Quantitative real time polymerase chain reaction |
| **RHIM** | RIP homotypic interaction motif |

| | |
|---|---|
| **RING** | Really interesting new gene |
| **RIPK1** | Receptor-interacting protein kinase 1 |
| **RNA** | Ribonucleic acid |
| **ROS** | Reactive oxygen species |
| **rpm** | Revolutions per minute |
| **RPMI** | Roswell Park Memorial Institute medium |
| **RSL3** | RAS selective lethal 3 |
| **RT** | Room temperature |
| **SDS** | Sodium dodecyl sulfate |
| **SDS-PAGE** | Sodium dodecyl sulfate–polyacrylamide gel electrophoresis |
| **SEM** | Standard error of mean |
| **siRNA** | Silencing RNA |
| **Smac** | Second mitochondria-derived activator of caspases |
| **SSC** | Side scatter |
| **tBID** | Truncated BID |
| **TEMED** | Tetramethylethylenediamine |
| **TMRM** | Tetramethylrhodamine methylester |
| **TNFR** | Tumor necrosis factor receptor |
| **TNFα** | Tumor necrosis factor α |

| | |
|---|---|
| **TRADD** | TNFR type 1-associated deathdomain protein |
| **TRAF2** | TNFR-associated factor 2 |
| **TRAIL** | T-related apoptosis-inducing ligand |
| **UT** | Untreated |
| **V** | Volt |
| **WB** | Western Blot |
| **XIAP** | X-linked IAP |
| **zVAD.fmk** | N-benzyloxycarbonyl-Val-Ala-Asp-[O-methyl]- fluoromethylketone |
| **z.B.** | zum Beispiel (German), for example |

# List of tables

# List of figures

# 1    Abstract

Inhibitor of apoptosis proteins (IAPs) play an important role in regard to cell death regulation and it is likely that their dysregulation contribute to tumor development and progression. Elevated expression levels of IAPs promote the evasion of programmed cell death and different studies could already show increased expression level of IAPs in different cancer cell lines and primary tumor samples. Moreover, increased expression levels of IAPs in human cancer have been correlated with treatment resistance and poor prognosis. Diffuse large B-cell lymphoma (DLBCL) is the most common type of non-Hodgkin lymphomas (NHL) and was initially classified into three subtypes: activated B-cell (ABC), germinal center B-cell (GCB) and primary mediastinal B-cell lymphoma (PMBL). Copy number gains and increased expression levels of cellular IAP1 (cIAP1) and cIAP2 have also been identified in primary tumor samples of DLBCL. Smac mimetics were designed to antagonize IAPs, therefore being a promising treatment strategy for DLBCL, as around 40% of DLBCL patients relapse or fail to achieve remission under standard immune-chemotherapy. Nevertheless, the effect of Smac mimetics as single agent is limited, thus combination treatment represents a strategy for their clinical development. Therefore, we investigated the Smac mimetic BV6 in combination with different proteasome inhibitors and analyzed the molecular mechanism of action focusing on programmed cell death pathways.

Combination treatment with different concentrations of BV6 and carfilzomib (CFZ) induces cell death in all three tested DLBCL subtypes (ABC, GCB and PMBL). Calculation of the combination index (CI) as well as Bliss score, two quantitative parameters for synergism, reveal that nearly all tested combinations are synergistic, demonstrating that the co-treatment of BV6 and CFZ is a potent combination to induce cell death in DLBCL. Furthermore, combination of BV6 with other proteasome inhibitors like ixazomib (IXA) or oprozomib (OPR) also synergistically reduce cell viability, highlighting the general efficiency of Smac mimetics with proteasome inhibitors to reduce cell viability in DLBCL.

BV6 and CFZ induce an apoptotic cell death, since they promote cleavage of initiator and effector caspases (caspase-3, -7, -8 and -9) and cell death could be blocked by pre-treatment with the pan-caspase inhibitor N-benzyloxycarbonyl-Val-Ala-Asp-[O-methyl]- fluoromethylketone (zVAD.fmk). Furthermore, BV6/CFZ treatment lead to an accumulation of NF-κB inducing kinase (NIK) but mechanistic studies reveal that BV6/CFZ-mediated cell death is independent of non-canonical NF-κB signaling, as genetic silencing of NIK by siRNA did not reduce cell death. Moreover, BV6/CFZ-induced cell death is independent of TNFα signaling, as neither treatment with the TNFα inhibitor Enbrel reduced BV6/CFZ-induced cell death nor did additional TNFα enhance cell death. Further mechanistically studies reveal that involvement of the mitochondrial pathway is critical for BV6/CFZ-mediated cell death induction. We demonstrate an activation of the two pore former proteins BAX and BAK upon BV6/CFZ co-treatment, as well as loss of mitochondrial membrane potential (LOMMP). In addition, genetic silencing of BAX and BAK significantly reduce BV6/CFZ-mediated cell death, indicating a central role of the mitochondria for cell death induction. In line with the involvement of mitochondria in BV6/CFZ-mediated cell death, we detect accumulation of mitochondrial reactive oxygen species (ROS) as well as an increase in overall ROS production. Additionally, BV6/CFZ treatment lead to an accumulation of the pro-apoptotic protein NOXA, which is functionally relevant for cell death induction, as knockdown of NOXA protein level lead to a significant reduction of cell death induced by BV6 and CFZ. Immunoprecipitation studies demonstrate that NOXA is constitutively bound to its anti-apoptotic binding partner MCL-1 in RIVA and U2932, initially priming these cells to undergo apoptosis.This priming for intrinsic apoptosis is enhanced by BV6/CFZ co-treatment, further increasing NOXA binding to MCL-1 and rebalancing the ratio of pro-and anti-apoptotic BCL-2 proteins towards pro-apoptotic proteins to favor apoptosis.

Here, we demonstrate that DLBCL cells are sensitive to Smac mimetic and proteasome inhibitor treatment and that this combination might be a new treatment strategy for this heterogeneous disease.

# 2 Introduction

## 2.1 Diffuse large B-cell lymphoma (DLBCL)

Lymphoma is a cancer that originates from lymphocytes of the lymphatic system and is distinguished into Hodgkin and non-Hodgkin lymphomas (NHL) [1-3]. NHL is more common and 90% of all diagnosed lymphomas belong to the NHL group. Diffuse large B-cell lymphoma is the most common type of NHL accounting for around 40% of all NHL cases [4]. This type of tumor often occurs at the age between sixty and seventy [5] and is a very aggressive cancer entity, which is characterized by rapidly growing tumors in lymph nodes, bone marrow, spleen, liver and other organs [6]. DLBCL is a very heterogeneous disease and was initially classified into three groups on the basis of gene expression and cell of origin studies: activated B-cell (ABC), germinal center B-cell (GCB) and primary mediastinal B-cell lymphoma (PMBL) [7-10].

The ABC subtype originates from B cells that arrested in plasma cell differentiation because of different genetic abnormalities in *PRDM1*, *BCL6* or *SPIB* genes [7, 10]. Further, ABC DLBCL patients harbor a gain or amplification of the *BCL-2* gene, which leads to an overexpression of BCL-2 [11, 12]. Another characteristic of this subtype is chronic active BCR signaling, which is induced by mutations or deletions in *CD79A/B* that encode for parts of the BCR receptor [13]. A hallmark of ABC DLBCL is the constitutive activation of nuclear factor-kappa B (NF-κB) signaling induced by *CARD11*, *A20* or *MYD88* mutations [14-17]. Furthermore, deletions in *INK4α/ARF* are associated with genomic instability [11, 18].

The GCB lymphoma arises from germinal center B cells that are blocked at different stages of B cell development [8, 10]. GCB DLBCL patients often show a BCL-2 t(14;18) translocation, which leads to a constitutive activation of the anti-apoptotic BCL-2 protein [7]. Another pathogenic feature of GCB DLBCL is a deregulation of the signaling pathways PI3K and mTOR as consequence of a PTEN deletion and

amplification of miR-17-92 [11, 19]. A further hallmark is a gain or amplification of *MDM2*, which negatively regulates the tumor suppressor p53 [7] as well as deletions of *TP73* and *ING1*, two other tumor suppressor genes [11]. All these deletions and amplifications are associated with genomic instability.

The third DLBCL subtype PBML originates from thymic asteroid medulla B cells and shows characteristics of late post-germinal center thymic B cells [5]. A hallmark of PMBL is a gain or amplification of the chromosomal band 9p24 [11] which leads to a constitutive activation of the JAK2 pathway [20, 21]. Furthermore, this amplification leads to an upregulation of two T-cells PD receptor ligands (PD-L1/2), which change the interaction of PMBL cells with T cells [22]. Another pathogenic feature of PMBL subtype is the constitutive activation of NF-κB signaling, which is often attributable to an inactivation of A20, a negative regulator of NF-κB signaling [22-24].

However, despite the former classification of these three subtypes, new DLBCL subtypes have been identified based on shared genomic abnormalities [25]. In this study of Reddy and colleagues, four prominent genetic subtypes were identified, termed MCD based on the co-occurrence of MYD88L265P and CD79B mutations, BN2 based on BCL6 fusions and NOTCH2 mutations, N1 based on NOTCH1 mutations and EZB based on EZH2 mutations and BCL2 translocations.

This new classification highlights the heterogeneity of DLBCL tumors and the need for new targeted therapeutic approaches even more, as around 40% of DLBCL patients relapse or fail to achieve remission under standard immuno-chemotherapy [26]. Standard therapy for DLBCL comprises the so-called R-CHOP treatment regimen a combination of immuno-chemotherapy composed of cyclophosphamide, hydroxyldaunorubicin, vincristine, and prednisone (CHOP) plus the anti-CD20 monoclonal antibody rituximab (R) [5].

For the sake of convenience, we decided to use the more common three subtype classification (ABC, GCB, PMBL) in the following study.

## 2.2 Mechanisms of programmed cell death

The response of tumors to cytotoxic therapies depend on intact cell death programs in cancer cells, as anticancer drugs exert their cytotoxic effects largely by promoting programmed cell death [27]. Apoptosis is the best-studied mode of programmed cell death and is mediated via two distinct pathways, the extrinsic (death receptor) and the intrinsic (mitochondrial) pathway, both leading to the activation of caspases and execution of cell death [28]. Both pathways are described below and shown in Figure 1.
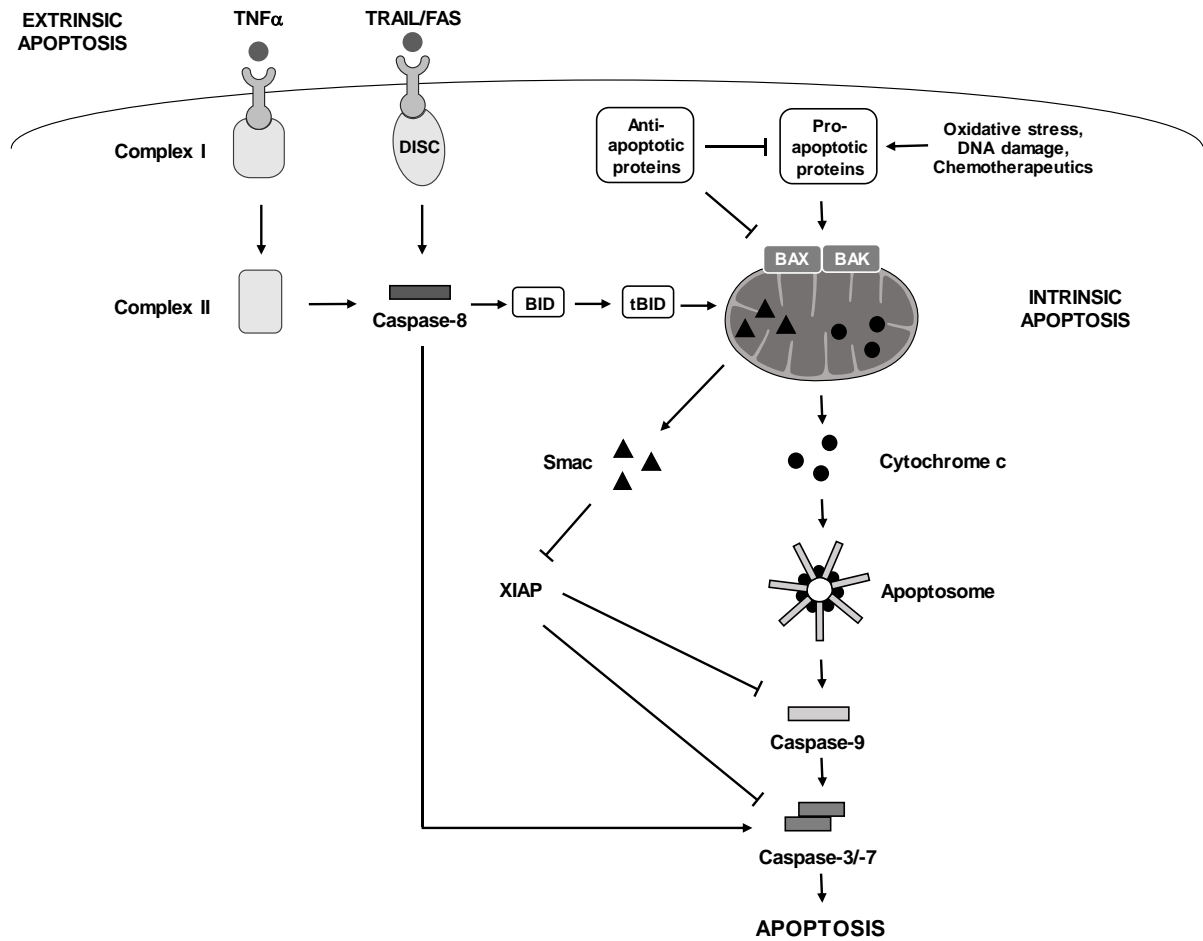
**Figure 1: Schematic pathways of intrinsic and extrinsic apoptosis**

The extrinsic pathway is initiated by ligation of a certain death receptor ligand to its corresponding death receptor. Ligand binding induces complex formation (DISC or complex I), which results in activation of caspase-8. Activated caspase-8 can directly activate caspase-3 and -7, leading to apoptosis. Caspase-8 can also cleave BID to tBID initiating BAX/ BAK activation and the release of mitochondrial intermembrane space proteins (SMAC, cytochrom c) leading to caspase activation and induction of apoptosis. The intrinsic pathway is induced by e.g. DNA damage and depends on mitochondrial outer membrane permeabilization (MOMP), which is tightly regulated by members of the BCL-2 family. Activation of BAX/BAK by pro-apoptotic BCL-2 proteins lead to the release of SMAC and cytochrom c, which results in the formation of the apoptosome and activation of caspase-9. Activated caspase-9 then activates the effector caspases -3 and -7, leading to apoptosis induction. Figure based on [29].

## 2.2.1    Extrinsic pathway of apoptosis

The initiation of extrinsic apoptosis is mediated via ligand binding to cell death receptors at the cell surface. There are different ligands like tumor necrosis factor (TNF), Fas ligand (FasL)/CD95 and TNF-related apoptosis-inducing ligand (TRAIL), which transduce death signals into the cell by binding to their corresponding receptors [30, 31]. After binding of FasL or TRAIL to its receptor, an intracellular death-inducing

6

signaling complex (DISC) is formed, which recruits other adaptor proteins like Fas-associated death domain protein (FADD), cellular FLICE-like inhibitory protein (cFLIP) and inactive caspase-8 to the complex [31, 32]. This complex formation then leads to an auto processing and activation of caspase-8 [29]. After activation of caspase-8, the death signal can be further continued by two distinct mechanisms. On the one hand, caspase-8 can proteolytically process and activate the effector caspases-3 and -7, which provoke further activation of other caspases and induce cell death [29]. On the other hand, caspase-8 can also process BID to truncated BID (tBID), which leads to a translocation of tBID to the mitochondria and activation of BAX and BAK leading to cytochrome c release and activation of initiator and effector caspases, thereby triggering apoptotic cell death [33, 34] and linking the extrinsic apoptosis with the intrinsic apoptosis pathway. Upon binding of TNF$\alpha$ to its receptor, the complex I is formed, consisting of TNFR-associated death domain protein (TRADD), TNFR-associated factor 2 (TRAF2), receptor-interacting protein kinase 1 (RIPK1) and cellular inhibitor of apoptosis (cIAP) proteins 1 and 2 [35, 36]. Complex I builds the basis for regulation of cell death via complex II, which consists of RIPK1, FADD and caspase-8 and promotes activation of caspase-8 and subsequent cleavage and activation of caspase-3 and -7 [37].

### 2.2.2    Intrinsic pathway of apoptosis

The intrinsic apoptosis is activated via different intrinsic stress factors like chemotherapeutics, DNA damaging agents, ionizing radiation, growth factor depletion and other cellular stresses [38]. This pathway is also termed mitochondrial apoptosis because it is mediated via the mitochondria [39]. Intrinsic apoptosis is controlled by the distribution of pro-and anti-apoptotic BCL-2 (B-cell CLL/Lymphoma 2) proteins [39].

The family of BCL-2 proteins is composed of three groups based on their structure and function (illustrated in Figure 2). First, anti-apoptotic proteins (BCL-2, BCL-X$_L$, BCL-W, MCL-1, BFL-1/A1) second, pro-apoptotic pore-former proteins (BAX, BAK, BOK) and third, pro-apoptotic BH3-only proteins (NOXA, PUMA, BAD, BID, BIM, BIK, BMF, HRK) [40]. All BCL-2 proteins contain one to four BCL-2 homology (BH) domains, which allow them to interact with each other [41]. The anti-apoptotic proteins as well as the pro-apoptotic pore-former proteins contain all four BH domains, whereas the pro-apoptotic

BH3-only proteins only contain the BH3 domain [40]. Anti-apoptotic BCL-2 proteins can inhibit the function of pro-apoptotic proteins by forming a hydrophobic BH3 domain-binding groove that binds to the BH3 domain of pro-apoptotic proteins, thereby sequestering them [42, 43].

**Anti-apoptotic**

**BCL-2** — BH4 — BH3 — BH1 — BH2 — MBR —

**BCL-XL** — BH4 — BH3 — BH1 — BH2 — MBR —

**MCL-1** — BH4 — BH3 — BH1 — BH2 — MBR —

**Pro-apoptotic**

**BAX** — BH4 — BH3 — BH1 — BH2 — MBR —

**BAK** — BH4 — BH3 — BH1 — BH2 — MBR —

**BID** — BH4 — BH3 — MBR —

**BIM/BAD** — BH3 — MBR —

**NOXA** — BH3 — MBR —
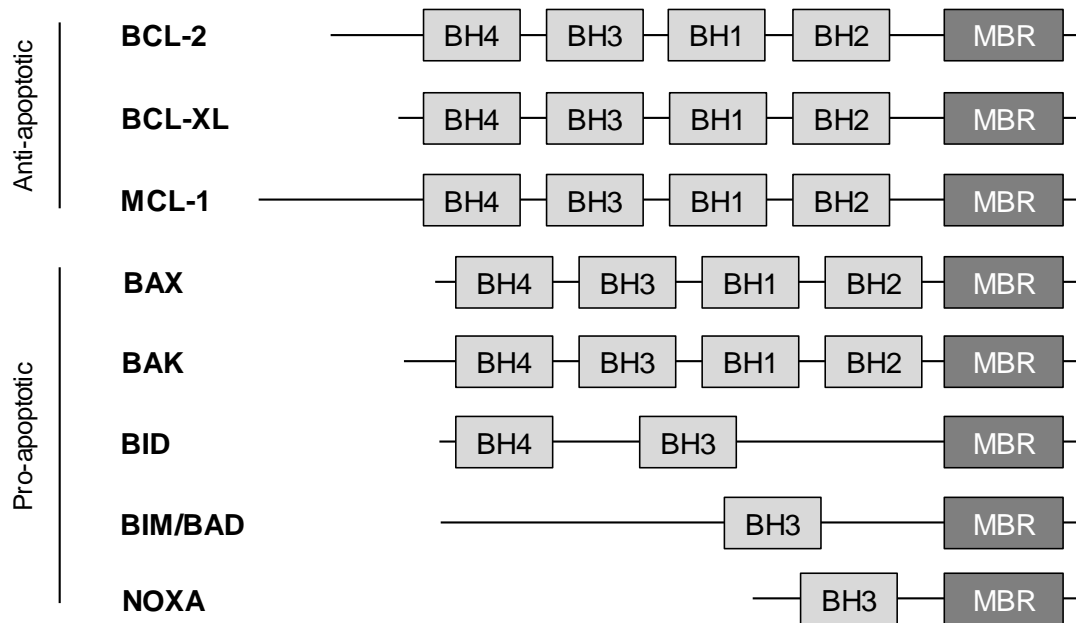
**Figure 2: Schematic structure of BCL-2 proteins**

The family of BCL-2 proteins is divided into pro-and anti-apoptotic proteins based on their function. The group of pro-apoptotic proteins is further subdivided into those that oligomerize and permeabilize the mitochondrial outer membrane (BAX, BAK) and those that promote apoptosis by activating BAX and BAK or inhibiting anti-apoptotic proteins such as BID, BIM, BAD and NOXA. All members of the BCL-2 family contain one to four BCL-2 homology (BH) regions and most members have a membrane-binding region (MBR) facilitating binding and localization of BCL-2 proteins to the membrane. Figure based on [44].

There are different models proposed for the regulation of mitochondrial outer membrane permeabilization (MOMP) by BCL-2 proteins. One model is called the direct activation model, which categorizes the BH3-only proteins into activators (tBID, BIM, PUMA) and sensitizers (NOXA, BAD, BMF, BIK, HRK) [45, 46]. Activator proteins can directly activate BAX and BAK, while sensitizer proteins only bind to anti-apoptotic proteins, thereby releasing activator proteins from being sequestered by anti-apoptotic proteins and promoting activation of BAX and BAK and subsequent MOMP [45, 47, 48]. In this model, anti-apoptotic proteins only bind to activator and sensitizer proteins, but are not able to bind to BAX and BAK [46]. Another model is called the displacement model and proposes that BAX and BAK are constitutively active and held in check by anti-apoptotic proteins to prevent cell death [44]. To induce MOMP and subsequent apoptosis, according to this model BH3 only proteins displace BAX and BAK from anti-

apoptotic proteins [44]. The third model, called embedded together model, highlights the membrane as the "locus of action" because BCL-2 proteins insert into it and change their conformations, which regulate their functions [44, 49]. The interaction of the different BCL-2 proteins with the mitochondrial membrane changes the affinities of the interactions and influences protein function, thus highlighting the membrane as an active player in cell death induction in this scenario [40]. Upon a death signal activator BH3 only proteins migrate to the membrane and are integrated into it, which increases their affinity for BAX and BAK, thus leading to conformational changes of BAX/BAK and their oligomerization followed by MOMP [40]. Furthermore, activator and sensitizer proteins recruit anti-apoptotic proteins to the membrane, thereby preventing their inhibitory function on BAX and BAK [44]. In this proposed model, all interactions are reversible and the functional interactions are controlled by the dynamic equilibria of protein-membrane and protein-protein interactions [40].

Finally, all models propose the activation of the effector proteins BAX and BAK, which mediate their oligomerization followed by pore formation within the outer mitochondrial membrane, resulting in the release of mitochondrial intermembrane space proteins such as cytochrome c or Second mitochondrial derived activator of caspases (Smac) into the cytosol [50]. Cytochrome c release facilitates the formation of the apoptosome, a caspase activation platform, leading to subsequent activation of initiator caspase-9, which in turn cleaves and activates effector caspases-3 and -7 executing apoptotic cell death [29, 38, 51].

## 2.3    Inhibitor of apoptosis proteins

### 2.3.1    Structure of inhibitor of apoptosis proteins

Inhibitor of apoptosis proteins (IAPs), which were originally found in baculovirus [52], have an important impact on the regulation of cell death. The mammalian IAP family is composed of eight proteins, however, only four are directly involved in the regulation of apoptosis, namely cellular IAP1/2 (cIAP1/2), X-chromosome-linked IAP (XIAP) and melanoma IAP (ML-IAP) [53] (Figure 3). All IAPs contain either one or three

baculovirus IAP repeats (BIR) domains, which give them the ability to bind and inhibit caspases. Furthermore, all IAPs include a really interesting gene (RING) domain, which enables them to function as E3 ubiquitin ligase and to mediate the transfer of ubiquitin onto different target proteins [54-56]. CIAP1 and 2 as well as XIAP also contain a ubiquitin-associated domain (UBA) which enables them to interact with ubiquitylated proteins whereas cIAP1/2 additionally contain a caspase recruitment domain (CARD) that mediates interaction with caspases [55-57]. In this study we focused on three of the IAPs, namely cIAP1, cIAP2 and XIAP.
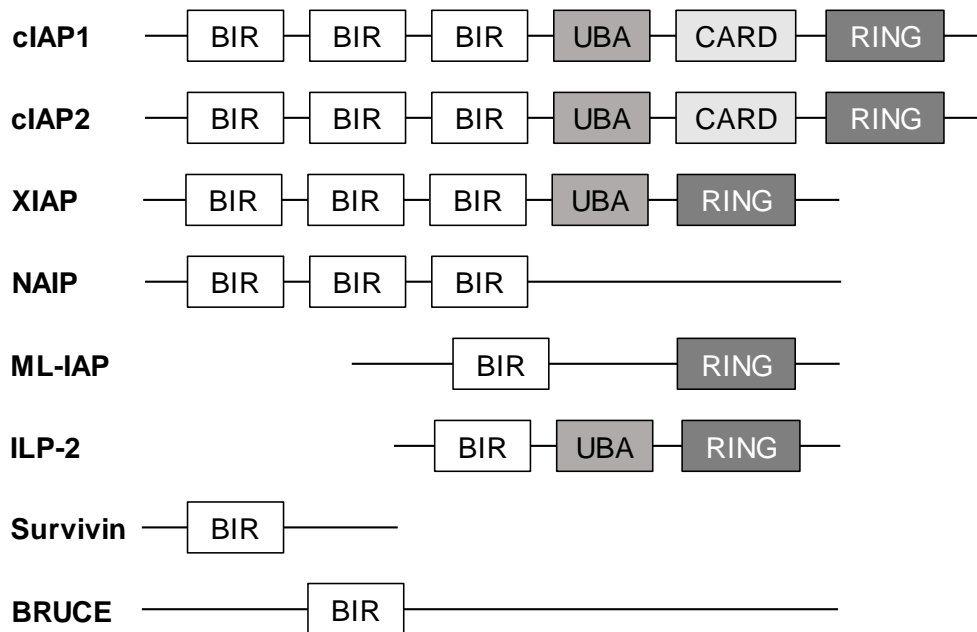


**Figure 3: Schematic structure of mammalian IAP proteins**

BIR: baculovirus IAP repeat, UBA: ubiquitin-associated domain, CARD: caspase recruitment domain, RING: really interesting new gene. Figure based on [58].

### 2.3.2 Role of IAPs in cell death induction

IAPs exert their role as inhibitors of apoptosis via different mechanisms. On the one hand, they negatively influence apoptotic signaling and on the other hand, IAPs positively influence pro-survival pathways of the cell.

XIAP blocks the execution of apoptosis by inhibition of caspase-3, -7 and -9, independent of other external or internal signals [59] [60]. Via its BIR3 domain, XIAP is able to interact with caspase-9 and prevent its homodimerization and subsequent activation [60-62]. Responsible for the inhibition of caspase-3 and -7 is the linker region

between the BIR1 and BIR2 domain of XIAP [63-65]. Furthermore, XIAP can promote proteasomal degradation of caspase-3 and -7 as well as Smac via its RING domain [56, 66, 67].

Cellular IAPs function as inhibitors of apoptosis by modulating cell death signaling via their E3 ubiquitin ligase activity. CIAP1 and cIAP2 ubiquitylate RIPK1, thereby regulating ripoptosome formation. In the absence of cIAPs, RIPK1 is no longer ubiquitylated and can bind to FADD and caspase-8, thus promoting ripoptosome formation and subsequent induction of apoptosis [68-70]. Moreover, it was shown that cIAP1 is able to ubiquitylate caspase-3 and -7, thereby leading to their proteasomal degradation [71]. Interestingly, cIAP1 and 2 are also able to ubiquitylate Smac, an inhibitor of IAPs, leading to Smac degradation [72].

Furthermore, cIAP1 and cIAP2 exert their inhibitory function on apoptosis by modulating pro-survival NF-κB signaling [36]. In the presence of cIAPs and the binding of TNFα to its receptor, the recruitment of the receptor-associated complex consisting of TRADD, TRAF2, cIAP1, cIAP2 and RIPK1 is triggered [73]. Within this complex cIAP1 and cIAP2 ubiquitylate RIPK1 leading to the assembly of different complexes; IKK complex (IKKα, IKKβ, NEMO), TAB-TAK1 complex and LUBAC (HOIP, HOIL-1L, SHARPIN), resulting in the phosphorylation and activation of IKKβ [74]. Once IKKβ is activated, the IKK complex leads to IκBα phosphorylation and its subsequent proteasomal degradation [75]. Degradation of IκBα by the proteasome liberates p65 and RelA (p50), resulting in the translocation of the heterodimer (p65/RelA) to the nucleus and activation of pro-survival NF-κB gene expression [76]. This implies a positive regulation of cIAP1 and cIAP2 on canonical NF-κB signaling. Furthermore, cIAP1 and cIAP2 have a negative regulatory function on non-canonical NF-κB signaling. In unstimulated cells cIAP1 and cIAP2 constitutively ubiquitylate NF-kappa-B-inducing kinase (NIK), a key regulator of non-canonical NF-κB signaling, leading to its proteasomal degradation, thus preventing NIK accumulation and activation of non-canonical NF-κB signaling [77, 78]. Ligation of specific TNFR superfamily members by their ligands (e.g. CD40L or TWEAK), facilitates the recruitment of TRAF2, TRAF3, cIAP1 and cIAP2 to the receptor complex, which induces ubiquitination of TRAF3 as well as auto ubiquitination of cIAP1 and cIAP2 leading to proteasome degradation of these proteins [79, 80]. Consequently, NIK accumulates and mediates IKKα

phosphorylation followed by proteolysis of p100 to p52. Subsequent p52/RelB heterodimers translocate to the nucleus and activate NF-κB gene expression [81, 82]. Alternatively, IAP inhibitors like Smac mimetics lead to an auto ubiquitination of cIAP1 and cIAP2 followed by proteasomal degradation, which then also results in an accumulation of NIK and activation of non-canonical NF-κB signaling [70, 83].

In summary, the presence of IAPs lead to an activation of canonical NF-κB signaling and upregulation of pro-survival protein expression, whereas in the absence of cIAP1/2, canonical NF-κB signaling gene expression is downregulated and non-canonical NF-κB signaling is activated via accumulation of NIK.

### 2.3.3    Role of IAPs in cancer

Since IAPs play an important role in regulation of cell death, it is tempting to reason that their dysregulation could contribute to tumor development and progression. Indeed, a lot of different studies could show elevated expression levels of IAPs in a variety of cancer cells lines and primary tumor samples [68, 84-88]. Moreover, expression level of IAPs in human cancers have been correlated with treatment resistance and poor prognosis [58]. Different studies revealed that XIAP protein expression is upregulated in a variety of cancers like breast, lung, renal and bladder carcinoma and correlates with disease severity and prognosis [87, 89-91]. Furthermore, cIAPs have been observed to be upregulated and are able to function as oncogenes induced by amplification of the 11q21-q23 chromosome region in different cancer entities including medulloblastoma, renal-cell carcinoma, glioblastoma, gastric carcinoma and non-small cell lung carcinoma [92]. Interestingly, copy number gains and increased expression levels of cIAP1 and cIAP2 have been identified in primary tumor samples of DLBCL [93], thus indicating that the IAP protein family could be a promising target for DLBCL treatment strategies.

These studies indicate that the expression of IAPs could play an important role in the development and progression of cancer cells due to their impact on different cell death and survival pathways.

## 2.3.4    Targeting IAPs by Smac mimetics for treatment of cancer

Since cancer cells frequently show elevated expression levels of IAPs, thereby promoting the evasion of cell death and tumor progression, development of IAP antagonists were considered as promising treatment strategy. Pharmaceutical efforts to inhibit IAPs were inspired by structural and functional analysis of Smac, which play a central role in mediating cell death and small-molecule inhibitors called Smac mimetics were subsequently designed for IAP inhibition. They are named Smac mimetics because they mimic the N-terminal four amino acid residues (Ala-Val-Pro-Ile) of the endogenous Smac protein, which is required for its IAP binding properties [94].

Many different monovalent IAP inhibitors were developed and were able to induce cell death as well as to sensitize cancer cells to other apoptotic stimuli [95-98]. Since it has been reported that the Smac protein forms homodimers under physiological conditions, in a next step bivalent Smac mimetics were designed composed of two monomeric Smac mimetics combined with a chemical linker [99]. Furthermore, bivalent Smac mimetics showed higher binding affinities for IAP proteins compared to monovalent Smac mimetics [70]. In this study, we therefore used the bivalent Smac mimetic BV6 whose structure is shown in Figure 4.
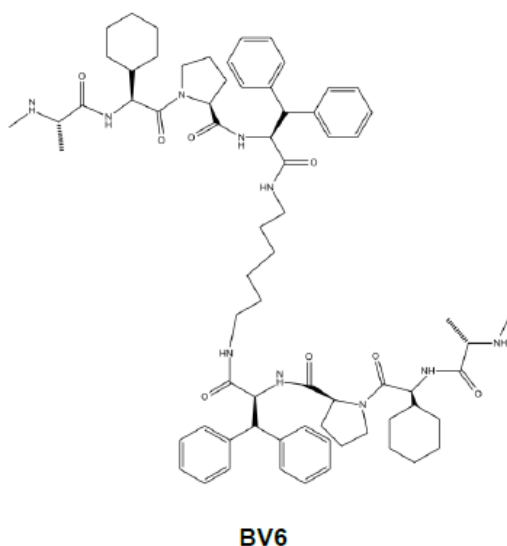


**Figure 4: Chemical structure of the bivalent Smac mimetic BV6**

Smac mimetics bind to the BIR3 domain of cIAPs, thereby blocking the BIR3-RING domain interaction and thus inducing a conformational change of the cIAP protein. This

conformational change then induces exposure of the RING domain followed by dimerization of two cIAP proteins at their RING domains and subsequent activation of their E3 ligase [100-102]. Activation of their E3 ligase leads to a rapid auto ubiquitination and subsequent proteasomal degradation of the cIAPs [70, 83]. Depletion of cIAPs is followed by NIK accumulation and subsequent activation of the non-canonical NF-κB pathway as well as formation of the ripoptosome as described in 2.3.2. Furthermore, bivalent Smac mimetics are able to inhibit BIR2 and BIR3 domains of XIAP simultaneously, thus preventing XIAP-mediated inhibition of caspase-3, -7 and -9 leading to caspase activation and induction of apoptotic cell death. [103, 104].

Preclinical studies could demonstrate that Smac mimetics are potent inducers of cell death as single agent and they have been extensively studied in combination with other cytotoxic agents like chemotherapeutics, death receptor ligands or radiation therapy showing promising results in targeting cancer cells for cell death induction in vitro and in vivo [58, 99, 105]. Moreover, Smac mimetics have been tested in phase I/II clinical trials for treatment of solid tumors, leukemia and lymphomas [106].

## 2.4    The proteasome system

### 2.4.1    Function and structure of the proteasome

The proteasome is a crucial component of the ubiquitin proteasome system (UPS), which is a central structure in eukaryotic cells responsible for protein degradation and regulation of homeostasis within the cell [107-110]. The UPS controls processes like cell cycle, growth and proliferation as well as pro-and anti-apoptotic signaling pathways [111]. The active 26S proteasome is a multi-unit protease complex composed of a 20S catalytic complex and two 19S regulatory subunits at either end of the 20S subunit [112, 113]. The 20S complex is composed of four stacked ring structures. The two outer rings ($\alpha$ rings) interact with the 19S subunit and the two inner rings ($\beta$ rings) form the catalytic chamber [114]. Each $\beta$-ring contains seven $\beta$-subunits whereof three perform the proteasome enzymatic activity namely chymotrypsin-like ($\beta$5), trypsin-like ($\beta$2) and post-glutamyl peptide hydrolase-like (caspase-like, $\beta$1) [108, 115, 116].

Ubiquitylated proteins are degraded inside the core 20S subunit to peptides of a length of 3-25 amino acids [117].

## 2.4.2    Targeting the proteasome for cancer therapy

Tumor cells are highly proliferating cells that in general require a high protein expression [118-120].   Therefore, it is presumed that they are more vulnerable to proteasome inhibition than non-malignant cells [120]. Furthermore, the proteasome plays a critical role in regulating many different processes involving cell cycle and proliferation, which makes the proteasome a relevant target for actively proliferating cancer cells. In fact, different studies reported that cancer cells are more sensitive to proteasome inhibition than non-cancerous cells. Masdehors et al. could show that the proteasome inhibitor lactacystin induces apoptosis in human chronic lymphocytic leukemia (CLL) cells, whereas it had no effect on normal lymphocytes [121]. Similar results were observed in multiple myeloma cells, which were more sensitive to the proteasome inhibitor bortezomib (BTZ) than normal peripheral-blood mononuclear cells (PBMCs) [122].

Proteasome inhibitors can be classified into five different groups: peptide aldehydes, peptide vinyl sulphones, peptide boronates, peptide epoxiketones and β-lactones [123]. Proteasome inhibitors bind to the active core sites of the 20S proteasome, predominantly to the chymotrypsin-like site, thereby inhibiting the enzymatic function of the proteasome [111].

One of the first-generation proteasome inhibitors was BTZ, which binds reversibly to the chymotrypsin-like side [124]. BTZ has been approved for the treatment of multiple myeloma and mantle cell lymphoma by the US Food and Drug Administration (FDA) and was also tested in DLBCL patients [125-128] but a fraction of patients remained refractory to the treatment [125, 129, 130]. Furthermore, side effects like painful peripheral neuropathy and thrombocytopenia occurred during treatment with BTZ [131, 132]. Therefore, second-generation proteasome inhibitors were developed aiming to be more potent and less toxic for patients. One of these second-generation proteasome inhibitors is carfilzomib (CFZ). CFZ is a highly selective epoxyketone analog of epoxomicin that irreversibly inhibits the proteasome by binding primarily to its chymotrypsin-like side [133-135], whereas at high doses it also inhibits the trypsin-

like and caspase-like sites [136]. Because of its highly specific binding profile, CFZ has less side effects than BTZ [137, 138]. CFZ is approved for multiple myeloma[139] and pre-clinical studies evaluated the potential role of CFZ as single agent in lymphoma [140, 141]. Furthermore, different studies have demonstrated synergistic interactions between CFZ and BCL-2 inhibitors or HDAC inhibitors in DLBCL cells [142, 143]. Moreover, preclinical studies reported synergistic interaction of proteasome inhibitor with chemotherapeutic agents [144] as well as with a panel of different cytotoxic substance including BCL-2 inhibitors [145-149], CDK inhibitors [150], histone deacetylase inhibitors [151-155], heat shock protein inhibitors [156] and TRAIL [157-159] in lymphoma. These studies indicate the potential relevance of combination treatment with proteasome inhibitors to treat NHL.

### 2.4.3 Mechanism of action of proteasome inhibitors

Since the proteasome is involved in many different cellular pathways, inhibition of the proteasome leads to a broad disruption of intracellular processes.

First, inhibition of the proteasome leads to an accumulation of misfolded proteins because they are not proteasomally degraded any more. Malignant cells have an increased protein turnover compared to non-malignant cells and therefore depend more on effective degradation of misfolded proteins. Accumulation of misfolded proteins elicit the unfolded protein response, which leads to proteotoxic stress and eventually to cell death [160, 161]. Second, proteasome inhibitors can induce generation of reactive oxygen species (ROS) in solid tumors as well as in malignant hematopoietic cells [146, 162, 163]. Third, as a consequence of proteasome inhibition, the NF-κB inhibitor IκBα is stabilized, which leads to an inactivation of the pro-survival canonical NF-κB signaling pathway [164]. However, the ability of proteasome inhibitors to completely block NF-κB activation is controversially discussed [165]. Fourth, inhibition of the proteasome results in an accumulation of pro-apoptotic proteins like NOXA and BIM as well as activation of pro-apoptotic BCL-2 proteins leading to the induction of apoptotic cell death[146, 166-169]. Fifth, proteasome inhibition can furthermore lead to an upregulation of the tumor suppressor gene p53 as well as p21 and p27, two inhibitors of cyclin-dependent kinase (CDK), thereby leading to cell cycle and growth arrest and induction of apoptosis [123, 168, 170-172]. Seventh, distribution

of the proteasome function can induce an accumulation of c-Jun N-terminal kinase (JNK), a stress related kinase, which plays a role in apoptosis induction [173-175].

Taken together, inhibition of the proteasome has a major impact on many different important pathways involved in proliferation, survival and cell death.

# 3    Aim of the study

IAPs play an important role for the development and treatment of DLBCL, as copy number gains of cIAP1/2 as well as increased expression levels of cIAP1/2 have been identified in DLBCL [93]. Furthermore, high expression levels of XIAP correlates with a poor outcome in DLBCL patients [176]. Therefore, Smac mimetics provide a possible treatment strategy for DLBCL. Besides the use of Smac mimetic as single agent, a number of promising strategies have been developed to combine Smac mimetics with chemotherapeutic drugs or different types of molecular targeted agents aiming to improve their clinical application [177, 178]. A previous study of our lab indicated that combination of the Smac mimetic BV6 with the proteasome inhibitor BTZ may synergistically induce cell death in NHL [179].

In this study we therefore explored the potential of different proteasome inhibitors to increase the sensitivity to Smac mimetic in a range of DLBCL cell lines, a combination that has so far only been investigated in selected cases e.g. in multiple myeloma [180], melanoma [181] or NHL [179]. After exploring the induction of cell death by these combinations, we investigate the molecular mechanisms of action with a specific focus on programmed cell death pathways.

# 4 Materials and Methods

## 4.1 Materials

### 4.1.1 Cell lines

All cell lines were authenticated by STR profiling/DNA fingerprinting at Leibniz Institute, German Collection of Microorganisms and Cell Cultures (DSMZ, Deutsche Sammlung von Mikroorganismen und Zellkulturen). Constant tests for mycoplasma contamination ensured the maintenance of contamination-free cell lines.

**Table 1: DLBCL cell lines**

| Cell line | Subtype | Source |
|---|---|---|
| MedB1 | PMBL | DSMZ |
| OCI-LY1 | GCB | DSMZ |
| OCI-LY3 | ABC | DSMZ |
| OCI-LY10 | ABC | Kindly provided by S. Dave |
| Pfeiffer | GCB | ATCC |
| RCK8 | GCB | DMSZ |
| RIVA | ABC | DSMZ |
| SUDHL2 | ABC | ATCC |
| SUDHL8 | GCB | DSMZ |
| SUDHL10 | GCB | DSMZ |

| Cell line | Subtype | Source |
|---|---|---|
| **TMD8** | ABC | Kindly provided by T.Yoshizawa |
| **U2932** | ABC | DSMZ |
| **U2946** | GCB | DSMZ |

**Table 2: Acute lymphoblastic leukemia cell line**

| Cell line | Source |
|---|---|
| **Jurkat** | DSMZ |

### 4.1.2 Cell culture reagents

**Table 3: Cell culture reagents**

| Reagent | Company |
|---|---|
| **Iscove's Modified Dulbecco's Medium (IMDM) GlutaMAX™** | Thermo Fisher Scientific |
| **Roswell Park Memorial Institute Medium (RPMI) 1640 GlutaMAX™** | Thermo Fisher Scientific |
| **Fetal calf serum** | Thermo Fisher Scientific |
| **Penicillin/Streptomycin (pen/strep)** | Thermo Fisher Scientific |
| **Phosphate-buffered saline (PBS)** | Thermo Fisher Scientific |
| **Trypan blue solution** | Thermo Fisher Scientific |
| **b-Mercaptoethanol** | Thermo Fisher Scientific |

| Reagent | Company |
| --- | --- |
| 4-(2-hydroxyethyl)-1-piperazineethanesulfonic acid HEPES | Thermo Fisher Scientific |

### 4.1.3 Cell death inducing compounds

**Table 4: Cell death inducing compounds**

| Compound | Company |
| --- | --- |
| BV6 | Genentech |
| Tumor necrosis factor $\alpha$ | Peprotech |
| RSL3 | InterBIOScreen Ltd |
| Carfilzomib | Selleckchem |
| Ixazomib | Selleckchem |
| Oprozomib | Selleckchem |

### 4.1.4 Cell death inhibitor

**Table 5: Cell death inhibitor**

| Inhibitor | Target | Company |
| --- | --- | --- |
| zVAD.fmk | Caspases | Bachem |

### 4.1.5 ROS scavengers

**Table 6: ROS scavengers**

| ROS scavenger | Company |
|---|---|
| $\alpha$-Tocopherol ($\alpha$-Toc) | Sigma |
| Glutathione (GSH) | Carl Roth |
| Manganese (III) tetrakis (4-benzoic acid) porphyrin chloride (MnTBAP) | Thermo Fisher Scientific |
| N-Acetyl-cysteine (NAC) | Sigma |

### 4.1.6 Fluorescent dyes

**Table 7: Fluorescent dyes used for FACS and microscope measurements**

| Reagent | Company |
|---|---|
| Annexin V-FITC | In-house production |
| CellEventTM Caspase-3/-7 Green Detection Reagent | Thermo Fisher Scientific |
| CellROX | Thermo Fisher Scientific |
| CM-H2DCFDA | Thermo Fisher Scientific |
| Hoechst-33342 | Sigma-Aldrich |
| MitoSOX™ Red Mitochondrial Superoxide Indicator | Thermo Fisher Scientific |
| Propidium iodid (PI) | Sigma |
| Tetramethylrhodamine methylester (TMRM) | Thermo Fisher Scientific |

### 4.1.7    Western blot materials

**Table 8: Western Blot reagents**

| Reagent | Company |
| --- | --- |
| **Albumin Fraction V (BSA)** | Carl Roth |
| **Amersham™ Protran 0.2 nitrocellulose Western blotting membrane** | GE Lifescience |
| **Ammonium persulfate (APS)** | Carl Roth |
| **Bromphenolblue** | Amersham |
| **complete™ Protease Inhibitor Cocktail (PIC)** | Roche |
| **Dithiothreitol (DTT)** | Merck |
| **PageRuler™ Plus Prestained Protein Ladder** | Thermo Fisher Scientific |
| **Pierce ECL western blotting substrate** | Thermo Fisher Scientific |
| **Phenylmethylsulfonyl fluoride (PMSF)** | Carl Roth |
| **Rotiphorese® Gel 30** | Carl Roth |
| **Sodium dodecyl sulfate (SDS)** | Carl Roth |
| **Sodium fluoride** | Sigma |
| **Sodium orthovanadate** | Sigma |
| **Starter for x-ray developer** | TETENAL |
| **Superfix MRP x-ray fixing solution** | TETENAL |
| **Tetramethylethylenediamine (TEMED)** | Carl Roth |
| **Tris HCl** | Carl Roth |
| **Whatman paper** | Carl Roth |

| Reagent | Company |
|---|---|
| β-glycerophosphate | Sigma |

### 4.1.8    Buffer for Western blotting

**Table 9: Western Blot Buffer**

| Buffer | Ingredients |
|---|---|
| Lysis Buffer | 30 mM Tris HCl pH 7.4, 150 mM NaCl, 1% Triton-X, 10% Glycerol, 1 tablet PIC, 0.5 mM PMSF, 2 mM DTT, 1 mM sodium-orthovanadate, 1 mM β-glycerophosphate, 5 mM sodium fluoride |
| Loading Buffer (6x) | 350 mM Tris Base pH 6.8, 3.8% Glycerol, 10% SDS, 0.12 mg/ml Bromphenolblue |
| Running Buffer (5x) | 15.1 g/l Tris Base, 94 g/l Glycin, 0.5% SDS |
| Blotting Buffer | 5.8 g/l Tris Base, 2.9 g/l Glycin, 0.04% SDS, 20% Methanol |
| Blocking Buffer | 5% milk powder in PBS-Tween (0.1% Tween) |
| Wash Buffer | PBS-Tween (0.1% Tween) |

### 4.1.9    Antibodies for Western blotting

Primary antibodies were diluted in PBS-Tween (0.1%) with 2% BSA and .1% Proclin 150.

**Table 10: Primary antibodies**

| Antibody | Dilution | Company |
|---|---|---|
| Goat anti-cIAP1 | 1:1000 | R&D Systems |
| Mouse anti-Bad | 1:1000 | BD Bioscience |

| Antibody | Dilution | Company |
|---|---|---|
| **Mouse anti-caspase-8** | 1:1000 | Enzo Life Science |
| **Mouse anti-GAPDH** | 1:2000 | BioTrend |
| **Mouse anti-Noxa** | 1:1000 | Enzo Life Science |
| **Mouse anti-p52** | 1:1000 | Merck Millipore |
| **Mouse anti-p-IkBa,** | 1:1000 | Cell Signaling |
| **Mouse anti-Tubulin** | 1:2000 | Calbiochem |
| **Mouse anti-Vinculin** | 1:2000 | BioTrend |
| **Mouse anti-XIAP** | 1:1000 | BD Bioscience |
| **Mouse anti-$\beta$-actin** | 1:2000 | Sigma-Aldrich |
| **Rabbit anti-Bcl-2** | 1:1000 | BD Bioscience |
| **Rabbit anti-Bid** | 1:1000 | Cell Signaling |
| **Rabbit anti-Bim** | 1:1000 | Cell Signaling |
| **Rabbit anti-caspase-3** | 1:1000 | Cell Signaling |
| **Rabbit anti-caspase-9** | 1:1000 | Cell Signaling |
| **Rabbit anti-cIAP2** | 1:1000 | Cell Signaling |
| **Rabbit anti-IkBa** | 1:1000 | Cell Signaling |
| **Rabbit anti-Mcl-1** | 1:1000 | Enzo Life Science |
| **Rabbit anti-NIK** | 1:1000 | Cell Signaling |
| **Rat anti-Bmf** | 1:1000 | Enzo Life Science |

Secondary antibodies were diluted in PBS-Tween (0.1%) with 5% milk powder.

**Table 11: Secondary antibodies**

| Antibody | Dilution | Company |
|---|---|---|
| **Goat anti-mouse IgG HPR** | 1:10.000 | Abcam |
| **Goat anti-rabbit IgG HPR** | 1:10.000 | Abcam |
| **Goat anti-rat HPR** | 1:5000 | Abcam |
| **Donkey-anti-goat IgG HPR** | 1:5000 | Santa Cruz Biotechnology |

## 4.1.10 Material for transfection of cells

Small interfering RNA (siRNA) were all purchased from Thermo Fisher Scientific as Silencer® Select siRNA.

**Table 12: Small interfering RNA (siRNA)**

| siRNA | Target | Sequence Code |
|---|---|---|
| **siBAK #1** | BAK | s1880 |
| **siBAK #2** | BAK | s1881 |
| **siBAX #1** | BAX | s1888 |
| **siBAX #3** | BAX | s1889 |
| **cIAP1 #2** | cIAP1 | s1450 |
| **cIAP1 #3** | cIAP1 | s1448 |
| **cIAP2 #1** | cIAP2 | s1451 |
| **cIAP2 #2** | cIAP2 | s1452 |
| **siCtrl** | Non-silencing control | 4390843 |
| **siNIK #1** | NIK | s17187 |

| siRNA | Target | Sequence Code |
|---|---|---|
| **siNIK #2** | NIK | s17188 |
| **siNOXA #1** | NOXA | s10708 |
| **siNOXA #2** | NOXA | s10709 |
| **siNOXA #3** | NOXA | s10710 |
| **siCaspase-8 #1** | Caspase-8 | s2427 |
| **siCaspase-8 #2** | Caspase-8 | s2425 |
| **siCaspase-8 #3** | Caspase-8 | s2426 |
| **siXIAP #1** | XIAP | s1454 |
| **siXIAP #2** | XIAP | s1455 |
| **siXIAP #3** | XIAP | s1456 |

## 4.1.11 Material for immunoprecipitations

**Table 13: Buffer for immunoprecipitations**

| Buffer | Ingredients |
|---|---|
| **CHAPS** | 1% CHAPS, 150 mM NaCl, 10 mM HEPES pH 7.4, PIC |
| **Triton-X** | 50 mM TRIS-HCl, 150 mM NaCl, 5 mM MgCl2, 1 mM EGTA, 10% Glycerol, 1% TritonX100, pH 7.4, PIC |

### 4.1.12 Material for RNA analysis

**Table 14: Reagents for qRT-PCR**

| Reagent | Company |
| --- | --- |
| SYBR ® Green PCR Master Mix | Thermo Fisher Scientific |

**Table 15: Oligonucleotides for qRT-PCR**

| Target | Sequence |
| --- | --- |
| 28S_forward | TTGAAAATCCGGGGGAGAG |
| 28S_reverse | ACATTGTTCCAACATGCCAG |
| NOXA_forward | GGAGATGCCTGGGAAGAAG |
| NOXA_reverse | CCTGAGTTGAGTAGCACACTCG |

### 4.1.13 Kits

**Table 16: Kits**

| Kit | Company |
| --- | --- |
| 20S Proteasome Activity Assay Kit | Chemicon; Merck |
| Neon ® Transfection System 100µl Kit | Thermo Fisher Scientific |
| peqGOLD Total RNA Kit | Peqlab; VWR |
| Pierce BCA Protein Assay Kit | Thermo Fisher Scientific |
| RevertAid H Minus First Strand cDNA Synthesis Kit | Thermo Fisher Scientific |

### 4.1.14 General chemicals

**Table 17: General chemicals**

| Chemical | Company |
|---|---|
| Dimethyl pimelimidate (DMP) | Sigma-Aldrich |
| Dimethyl sulfoxide (DMSO) | Sigma-Aldrich |
| Dynabeads ® pan mouse IgG | Thermo Fisher Scientific |
| Ethanol | Carl Roth |
| Ethylenediaminetetraacetic acid (EDTA) | Carl Roth |
| FACS Rinse solution | BD Bioscience |
| FACS Clean solution | BD Bioscience |
| FACS Flow | BD Bioscience |
| FACS Shutdown solution | BD Bioscience |
| Glycerol | Carl Roth |
| Glycine | Carl Roth |
| Hydrochloride acid (HCl) | Carl Roth |
| HEPES | Sigma-Aldrich |
| Hybond enhanced chemiluminescence (ECL) 0.45 Amersham | Bioscience |
| Isopropanol | Carl Roth |
| Magnesium chloride (MgCl2) | Carl Roth |
| Methanol | Carl Roth |
| Milk powder | Carl Roth |

| Chemical | Company |
| --- | --- |
| **Pasteur pipettes** | Carl Roth |
| **Postassium chloride (KCl)** | Carl Roth |
| **Potassium dihydrogen phosphate (KH2PO4)** | Carl Roth |
| **Sodium chloride (NaCl)** | Carl Roth |
| **Sodium hydrogen phosphate (Na2HPO4)** | Carl Roth |
| **Triethanolamine (TEA)** | Sigma-Aldrich |
| **Tris Base** | Carl Roth |
| **Tris HCl** | Carl Roth |
| **Tween ® 20** | Carl Roth |

### 4.1.15 Plastic material

**Table 18: Plastic material**

| Plastic | Company |
| --- | --- |
| **Cell culture flasks (25 cm2, 75 cm2)** | Greiner Bio-One |
| **Cell culture plates (96-well, 6-well)** | Greiner Bio-One |
| **Combi tips (0.5 ml, 1 ml, 5 ml, 10 ml)** | Eppendorf |
| **Cryogenic vials** | Starlab |
| **Falcon (15 ml, 50 ml) dark/ transparent** | Greiner Bio-One |
| **Hyperfilm ECL Amersham** | Bioscience |

| Plastic | Company |
| --- | --- |
| **MicroAMP™ optical reaction plate (96-well)** | Thermo Fisher Scientiic |
| **PCR tubes** | Starlab |
| **Pipette tips (10 µl, 200 µl, 1000 µl)** | Starlab |
| **Reaction tubes (0.5 ml, 1.5 ml, 2 ml, 5 ml)** | Starlab |
| **Round bottom tubes (FACS tubes)** | BD Bioscience |
| **Sterile filter (0.22 µM)** | Merck |
| **Sterile pipettes (2 ml, 5 ml, 10 ml, 25 ml, 50 ml)** | Greiner |
| **Syringe (5 ml, 10 ml)** | B.Braun |

### 4.1.16    Equipment

**Table 19: Equipment**

| Equipment | Company |
| --- | --- |
| **Autoclave VX 150** | Systec |
| **Balances Kern 770/EW** | Kern |
| **Biowizard biosafety cabinet** | Kojair |
| **Centrifuge Mikro 200R** | Hettich |
| **Centrifuge Rotixa 50 RS** | Hettich |
| **CO2 incubator MCO-19AIC** | Sanyo |
| **Easypet® 3** | Eppendorf |

| Equipment | Company |
| --- | --- |
| **FACS Canto II** | BD Bioscience |
| **Heating magnetic stirrer ARE** | VELP Scientifica |
| **Image Xpress Micro XLS system** | Molecular devices |
| **Infinite M1000 microplate reader/ Sunrise microplate reader** | Tecan |
| **Inolab ® pH 7310** | WTW |
| **Mastercycler ® pro** | Eppendorf |
| **Micro centrifuge SD** | Carl Roth |
| **Microplate reader** | Tecan |
| **Microscope CKX41** | Olympus |
| **Mini-PROTEAN Tetra Cell** | Bio-Rad |
| **Multipette ® M4** | Eppendorf |
| **Nalgene ® Mr Frosty** | Sigma-Aldrich |
| **NanoDrop 1000** | Peqlab |
| **Neon ® Transfection System** | Thermo Fisher Scientific |
| **Neubauer bright line** | Marienfeld-Superior |
| **PCR thermocycler** | Eppendorf |
| **PerfectBlue TM Gel system** | Peqlab |
| **Pipette Research plus** | Eppendorf |
| **PowerPac TM Universal Power Supply** | Bio-Rad |
| **QuantStudio 7 Flex Real-Time PCR System** | Applied Biosystems |

| Equipment | Company |
| --- | --- |
| Roller | neoLab |
| Shaker | neoLab |
| Thermomixer comfort | Eppendorf |
| Trans-Blot® SD Semi-Dry Transfer Cell | Bio-Rad |
| Vortex mixer Wizard | VELP Scientifica |
| Water bath WBT 22 | Carl Roth |
| X-Ray cassette type G | Rego |

### 4.1.17　Software

**Table 20: Software**

| Software | Company |
| --- | --- |
| Applied Biosystems QuantStudio™ | Thermo Fisher Scientific |
| CalcuSyn 2.0 | Biosoft |
| FACS Diva™ | BD Bioscience |
| GraphPad Prism | GraphPad Software |
| I-control™ | Tecan |
| ImageJ | Open Source |
| Magellan™ Data Analysis Software | Tecan |
| MetaXpress® | Molecular Devices |
| MS Office 2013 | Microsoft |

| Software | Company |
| --- | --- |
| **NanoDrop software** | Peqlab |
| **SigmaPlot** | Systat Software |
| **Synergy Finder (Bliss Score)** | Free web application: https://synergyfinder.fimm.fi |

## 4.2 Methods

### 4.2.1 Cell culture

#### 4.2.1.1 Cultivation of cells

All cell lines were cultured at 37°C with 5% $CO_2$ in a humidified atmosphere. DLBCL cell lines and acute lymphoblastic leukemia cell line (OCI-LY3, RIVA, U2932, SUDHL2, -8, -10, TMD8, RCK8, MedB1, Pfeiffer, U2946 and Jurkat) were cultured in RPMI medium supplemented with 10% FCS and 1% penicillin/streptomycin or in IMDM supplemented with 20% FCS, 1% penicillin/streptomycin and 0.01% β-Mercaptoethanol (OCI-LY1, -10), respectively. Cells were passaged twice a week 1:3 to 1:10 by adding the appropriate amount of cells to a new flask with fresh medium.

#### 4.2.1.2 Freezing and thawing of cells

For long term storage cells were freezed at -80°C or transferred into a nitrogen tank. For freezing 10 ml of a dense cell culture suspension were centrifuged at 1000 rpm for 5 min (RT) and suspended in 1.5 ml of culture medium supplemented with 10% DMSO, which served as a cryoprotectant. Cells were transferred into a cryogenic vial and kept at -80°C over night. Afterwards, cell were transferred into a nitro gen tank for long term storage. To defreeze cells, cryogenic vial was placed into a water bath at 37°C and cells were transferred into a 15 ml falcon with 10 ml pre-warmed medium and gently mixed. Afterwards, cells were centrifuged at 1000 rpm for 5 min (RT) to dispose DMSO and resuspended in 10 ml pre-warmed medium and transferred into a new cell culture flask. For the first three days 20% FCS was added to the medium, followed by a reduction to 10% on day four.

#### 4.2.1.3 Seeding and treatment of cells

Cells were counted before every experiment to assure comparable cell numbers by adding 60 µl of trypan blue solution to 20 µl cell suspension. Dead cells were stained blue by the trypan blue solution and living cell number was assessed by counting in a Neubauer chamber. The suitable number of cells was then diluted in medium in the required density. DLBCL cell lines were seeded in a density of 5 x $10^5$ cells per ml.

Depending on the experiment cells were seeded in a 96-well plate (100/ 150 µl), 6-well plate (3 ml), 25 cm$^2$ flask (5 -10 ml) or 75 cm$^2$ flask (50 ml).

DLBCL cell lines were treated at the same day of seeding. Treatment was prepared in medium in a 20 fold concentration and added to the cells to reach a final concentration of 1 fold in each well or flask depending on the experiment.

## 4.2.2  Transfection of cells

### 4.2.2.1  siRNA transfection of cells

One day before transfection, cells were splitted in a ratio of 1 to 2. Electroporation was performed with the Neon® transfection system to transiently transfect RIVA and U2932 cells with siRNA for gene silencing. 4 x 10$^6$ cells per siRNA construct were centrifuged (1000 rpm, 5 min, RT) and pre-suspended in pre-warmed PBS to remove medium. After a second centrifugation step (1000 rpm, 5 min, RT) cells were resuspended in 120 µl Resuspension Buffer. 100 µl of cells were then added to 100nM of corresponding siRNA and gently mixed. Electroporation was performed with Neon ® transfection system with 1200 V, 20 ms and 2 pulses. In order to increase transfection efficiencies cells were electroporated for a second time, 24 hours after the first electroporation. After electroporation cells were transferred into a 6-well plate with 3 ml of pen/strep-free medium. After 24 hours cell were seeded for further experiments as described above (4.2.1.3). For knockdown of NOXA, cells were directly seeded after the second electroporation. Knockdown efficiency was verified by Western blot analysis.

## 4.2.3  Flow cytometry-based analysis

For flow cytometry analysis cells were seeded and treated as described above (4.2.1.3) for different time points. For FACS analysis cells were transferred into FACS tubes and stained with different fluorescent dyes.

### 4.2.3.1 Annexin V-FITC/ PI staining

After treatment for different time points cell death was assessed by Annexin V-FITC and PI double staining. For FACS analysis 100 µl of cell suspension were stained with Annexin V labelled with FITC for exposure of phosphatidylserine on the cell surface as an indicator of early apoptosis and with propidium iodide (PI) for detection of late apoptotic cell death. Per sample 0,05 µl Annexin V-FITC and 5 µl PI (50µg/ml) were added to 100 µl Annexin V binding buffer (10 mM HEPES, 150 mM NaCl, 5 mM KCl, 1 mM MgCl2, 1.8 mM CaCl2) and mixed with 100 µl cell suspension. After 10 min of incubation at room temperature in the dark cells were analyzed by flow cytometry.

### 4.2.3.2 TMRM staining

For determination of loss of mitochondrial membrane potential 100 µl of cell suspension were stained with 25 nM Tetramethylrhodamine, methyl ester (TMRM), a cell-permeant fluorescent dye that accumulates in active negatively charged mitochondria with intact membrane potentials. Upon loss of the mitochondrial membrane potential, TMRM accumulation is diminished and the signal disappears. After incubation for 30 min at 37°C cells were analyzed by flow cytometry.

### 4.2.3.3 ROS staining

Detection for ROS production ensued at time points before cells undergo cell death. For ROS staining, cells were transferred to FACS tubes and centrifuged for 5 min and 1800 rpm at RT. The supernatant was discarded and 100 µl phenol red free medium with 1 µM CellROX, 5 µM MitoSOX or 5 µM CM-H2DCFDA (DCF) was added. Cells were vortexed and incubated for 30 min (CellROX, DCF) or 10 min (MitoSOX) at 37°C in the dark. Living cell population was analyzed in the APC (CellROX), PE (MitoSOX) or FITC (DCF) channel by flow cytometry.

**4.2.4    Western blot analysis**

4.2.4.1        Protein extraction

After indicated treatment periods, cell suspension was transferred into falcon tubes and centrifuged at 1800 rpm for 5 min (4°C). After centrifugation supernatant was discarded and cell pellets were washed with 1 ml cold PBS and transferred into Eppendorf tubes. Cells were centrifuged for a second time at 1800 rpm for 5 min (4°C). The supernatant was again discarded and cell pellets were either stored at -20°C or directly lysed. For cell lysis, the pellet was resuspended in the same volume as the pellet (20- 100 µl) in lysis buffer and rested on ice for 30 min. Afterwards, cells were centrifuged at 14000 rpm for 25 min (4°C) and the supernatant was collected to determine protein concentration. Protein concentration was determined by the Pierce$^{TM}$ BCA protein assay kit according to the manufactor's instructions. For western blot analysis a defined amount of protein (50-100 µg) was supplemented with ddH$_2$O and 6x loading buffer. Protein samples were denaturated for 5 min at 96°C and subsequent stored at -20°C or directly loaded on a gel.

4.2.4.2        SDS-PAGE and Western blot

SDS-PAGE (sodium dodecylsulfate polyacrylamide gel electrophoresis) is a biochemical method to separate proteins according to their size and molecular weight. For protein separation 50-100 µg of total protein lysate supplemented with ddH$_2$O and 6x loading buffer was loaded onto gels. The polyacrylamide gels consisted of a 5% stacking gel (consisting of 5% polyacrylamide, 125 mM TrisHCl pH 6.8, 0.1% SDS, 0.1% APS, 0.1% TEMED ad ddH$_2$O) and a 12%, 13.5% or 15% resolving gel (consisting of 12%, 13.5% or 15% polyacrylamide, 250 mM TrisHCl pH 8.8, 0.1% SDS, 0.1% APS, 0.04% TEMED ad ddH$_2$O). Additionally a protein ladder ranking from 10 kDa to 250 kDa was loaded to visualize molecular weight of standard bands for comparison of detected proteins. Gels were run at lower voltage (small gels: 80 V, big gels: 100 V) until all samples reached the resolving gel. Afterwards, voltage was increased up to 120 V (small gel) or 140 V (big gel), respectively.

After protein separation the proteins were transferred to a nitrocellulose membrane using a semi-dry blotting system. Therefore, membrane and Whatman paper were soaked in blotting buffer and stacked in a package containing two Whatman papers,

membrane, gel and again two Whatman papers. This package was placed on the anode plate of a blotting chamber and proteins were blotted for 1 hour 25 min with 1mA/cm$^2$.

### 4.2.4.3    Detection of proteins

After finishing the blotting process, the membrane was once washed with PBS-Tween (0.1%) (PBS-T) and then blocked for 1 hour at RT with 5% milk powder in PBS-T to avoid unspecific binding of antibodies. Subsequent the membrane was washed three times for 10 min with PBS-T and afterwards incubated with primary antibody overnight at 4°C on an orbital shaker. On the next day, membrane was washed three times with PBS-T for 10 min and incubated with secondary antibody conjugated to horseradish peroxidase (HRP) for 1.5 hours on an orbital shaker at RT. Afterwards, membrane was again washed three times with PBS-T for 5 - 10 min and HRP-conjugated antibodies were detected using enhanced chemiluminescence with Pierce$^{TM}$ ECL Western Blotting Substrate, according to the manufactor's instructions.

### 4.2.5    Immunoprecipitation

### 4.2.5.1    Immunoprecipitation of BAX and BAK

To determine the activation of BAX and BAK, immunoprecipitation (IP) with an active conformation-specific antibody was used, which allows to specifically enrich active BAX or BAK [182]. Cells were seeded and treated as described above (4.2.1.3) and lysed as described in 4.2.4.1 in CHAPS buffer. Afterwards, 800µg protein were incubated overnight at 4°C with 2 µl anti-BAX or anti-BAK antibody, 10 µl pan mouse IgG Dynabeads and filled up to a total volume of 400 µl with CHAPS buffer. On the next day, samples were washed at least three times with CHAPS buffer using the magnetic particle concentrator and beads were resuspended in 20 µl 1x loading dye. To remove proteins from the beads samples were denaturated for 5 min at 96°C and afterwards frozen at -20°C or directly loaded on a gel without beads using the magnetic particle concentrator.

4.2.5.2        Immunoprecipitation of MCL-1, NOXA and BAK

To enable elution of proteins with little antibody contamination (for cleaner protein preparation and cleaner western blots), it is recommended to cross-link the antibody to the beads. Therefore, 30 µl of pan mouse IgG Dynabeads per IP were washed three times with PBS + 0.05% Tween and 5 µl antibody was added and incubated for 1 hour on the roller at 4°C. Afterwards, supernatant was removed by using the magnetic particle concentrator and beads were washed two times with 0.2 M triethanolamine (TEA). Afterwards, beads were resuspended in 20 mM DMP resolved in 0.2 M TEA and incubated for 30 min on the roller at RT. Next, supernatant was removed and 50 mM Tris solution was added to the beads and incubated for another 15 min on the roller (RT). Finally, beads were washed three times with PBS + 0.5% Tween and resuspended in lysis buffer. 1000 µg protein was filled up to a volume of 250 µl with CHAPS buffer and 50µl of crosslinked antibody was added. Protein was incubated with antibody overnight at 4°C and afterwards treated as describe in 4.2.5.1.

## 4.2.6    RNA analysis

4.2.6.1        RNA isolation

After indicated treatment periods, cell suspension was transferred into falcon tubes and centrifuged at 1800 rpm for 5 min (4°C). Supernatant was discarded and RNA was isolated using peqGOLD Total RNA Kit following the manufacturer's instructions. RNA concentration and purity was analyzed by absorbance at 260 nm, 260/280 nm ratio and 260/230 nm ratio using NanoDrop 1000.

4.2.6.2        cDNA synthesis

1 µg of RNA was used for cDNA synthesis using RevertAid H Minus First Strand cDNA Synthesis Kit according to the manufacturer's instructions.

4.2.6.3        qRT-PCR

Quantitative real-time PCR (qRT-PCR) using the QuantStudio Flex 7 real time PCR system, was used to analyze gene expression. For detection of target gene expression

SYBR Green Master Mix was mixed with primers and cDNA as follows: 10 µl SYBR Green Mix, 0.5 µl forward primer (10 pmol/µl), 0.5 µl reverse primer (10 pmol/µl), 9 µl nuclease-free $H_2O$. Master Mix was added to 1 µl cDNA, which was diluted 1:10 in a MicroAMP™ optical reaction plate. To normalize the generated data sets, we used the house-keeping gene 28S RNA. Quantitative RT-PCR reaction was performed for 50 cycles (start heating phase: 95 °C 10 min, cycle phase: 95°C 15 s; 60°C 1 min). To control specificity of primers melting curves of amplified products as well as water controls were analyzed.The relative expression of the requested gene transcript and reference gene transcript was computed by ΔΔCt method.

### 4.2.7 Other assays

#### 4.2.7.1 Caspase activity assay

For detection of caspase-3/-7 activity, cells were seeded and treated as described in 4.2.1.3 in the presence of 1 µM CellEvent® Caspase-3/-7 green detection reagent. After treatment cells were counterstained with 1 µg/ml Hoechst and caspase activation was assessed by fluorescence microscopy using the ImageXpress Micro XLS Widefield High-Content fluorescence microscope and analyzed by MetaXpress Software.

#### 4.2.7.2 Proteasome activity assay

For detection of proteasome activity cell were seeded and treated as described in 4.2.1.3 for 4 hours. Afterwards, cells were pelleted (5 min, 1800 rpm, RT) and lysed with Triton-X buffer a described in 4.2.4.1. Protein concentration of the collected supernatant was determined by Pierce™ BCA protein assay kit according to manufacturer's instructions. Proteasome activity was analyzed using the 20S Proteasome Activity Assay Kit following the manufacturer's instructions using 5 µg protein. Proteasomal activity was assessed by the detection of the fluorophore 7-Amino-4-methylcoumarin (AMC) after cleavage from the labeled substrate LLVY-AMC using the Microplate Reader: Infinite M1000.

### 4.2.8 Statistical analysis

4.2.8.1 Statistical analysis

Statistical analysis was performed with SigmaPlot (v12.5). Statistical significance of different groups was assessed by ANOVA with post-hoc Tukey test. P values were interpreted as follows: $*p < 0.05$; $**p \leq 0.01$; $***p \leq 0.001$. Calculation of IC50 values was performed with GraphPad Prism (v7).

4.2.8.2 Synergistic drug interaction

Combination index (CI) based on the description of Chou[183] using CalcuSyn software, was used to analyze drug interaction. Combination index was interpreted as follows: CI<0.9 synergism, CI 0.9–1.1 additivity, CI >1.1 antagonism. Synergistic interaction was also analyzed by calculation of Bliss scores using the web application created by Aleksandr Ianevski [184]. Bliss score >0 indicates a synergistic interaction between two drugs.

# 5 Results

## 5.1 Smac mimetic and proteasome inhibitors cooperate to induce cell death in DLBCL cell lines

### 5.1.1 DLBCL cell lines are sensitive to BV6 or CFZ single treatment in a dose-dependent manner

To evaluate the potential role of the Smac mimetic BV6 and the proteasome inhibitor CFZ as single agents in DLBCL, we initially treated a panel of DLBCL cell lines of different subtypes (ABC, GCB, PMBL) with increasing concentrations of either BV6 or CFZ. We observed a dose-dependent decrease in cell viability upon treatment with BV6 or CFZ in all tested DLBCL cell lines, however, three cell lines of the GCB subtype (RCK8, OCI-LY1, U2946) were less sensitive towards BV6 treatment (Figure 5). Calculation of the IC50 values clarified the differences in sensitivity between the tested cell lines (Table 21).

**A**
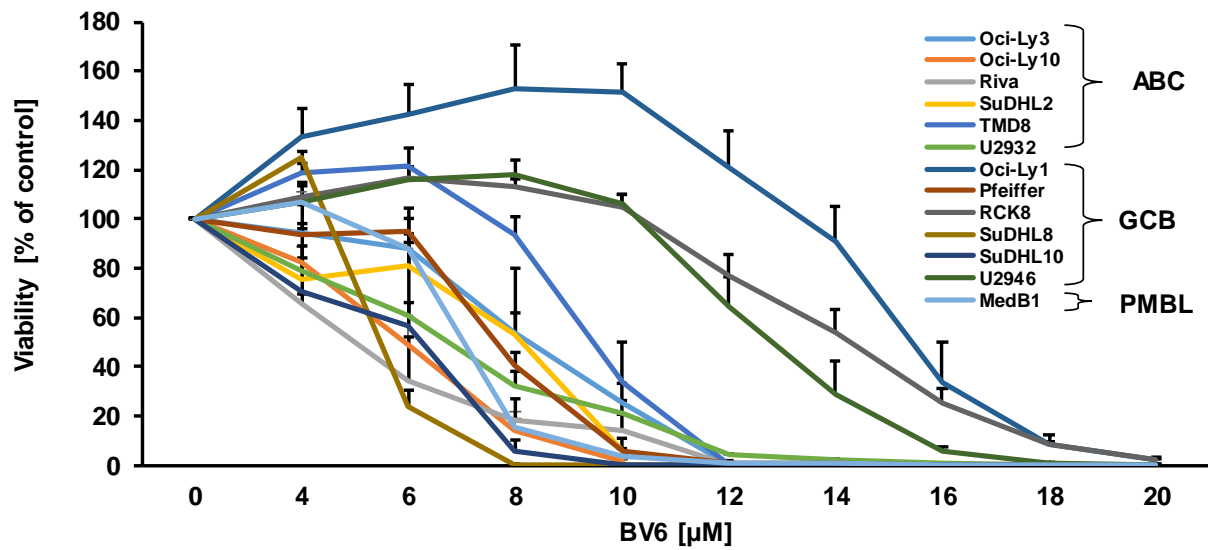


**B**
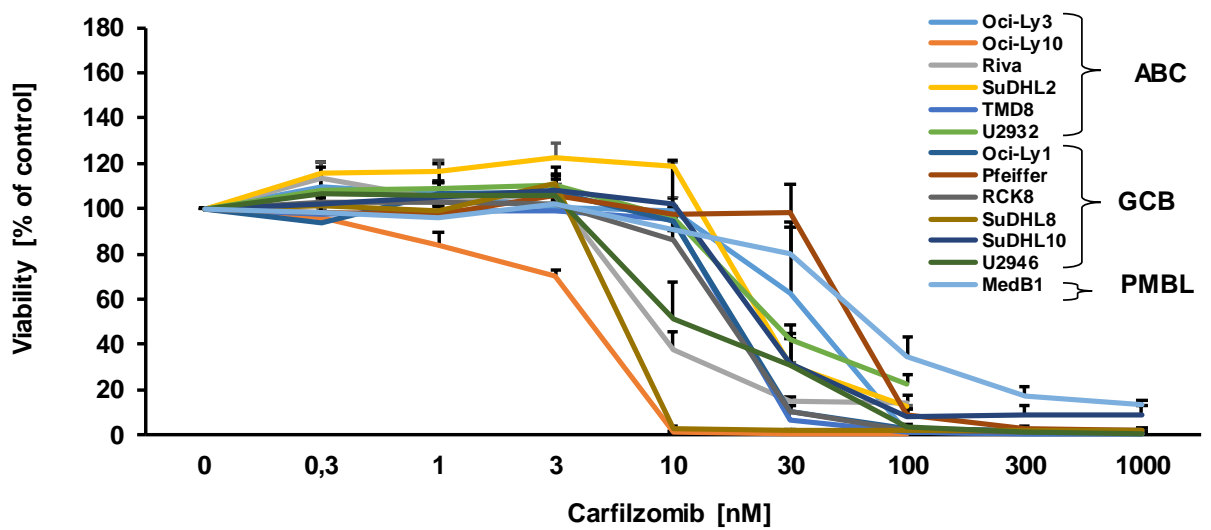


**Figure 5: BV6 and CFZ dose response in different DLBCL cell lines**

Different DLBCL cell lines were treated with indicated concentrations of (**A**) BV6 or (**B**) CFZ for 48 hours. Cell viability was assed via the CellTiterGlo Assay. Data are shown as mean and SEM of three independent experiments performed in triplicates.

**Table 21: IC50 values of BV6 or CFZ single treatment**

| Cell line | Sub-type | IC50 BV6 [µM] | IC50 CFZ [nM] |
|---|---|---|---|
| RIVA | ABC | 5,47 | 7,91 |
| SUDHL8 | GCB | 5,49 | 8,43 |
| OCI-LY10 | ABC | 6,26 | 4,04 |
| SUDHL10 | GCB | 6,66 | 23,98 |
| MedB1 | PMBL | 6,85 | 74,1 |
| U2932 | ABC | 7,46 | 26,1 |
| Pfeiffer | GCB | 7,83 | 64,32 |
| OCI-LY3 | ABC | 8,39 | 33,81 |
| SUDHL2 | ABC | 8,42 | 24,59 |
| TMD8 | ABC | 9,06 | 18,29 |
| U2946 | GCB | 12,42 | 11,41 |
| RCK8 | GCB | 13,55 | 16,03 |
| OCI-LY1 | GCB | 14,49 | 17,73 |

### 5.1.2 BV6 and CFZ synergize to decrease cell viability in DLBCL cell lines

To investigate whether BV6 sensitizes DLBCL cells to proteasome inhibitors, we next tested BV6 together with CFZ, a second-generation proteasome inhibitor. Subtoxic concentrations of both BV6 and CFZ acted in concert to decrease cell viability in a panel of DLBCL cell lines (Figure 6).
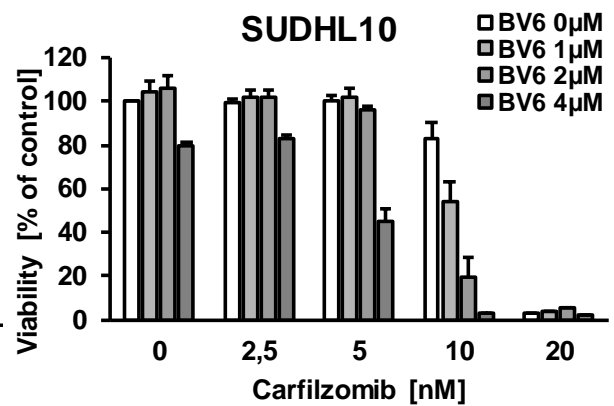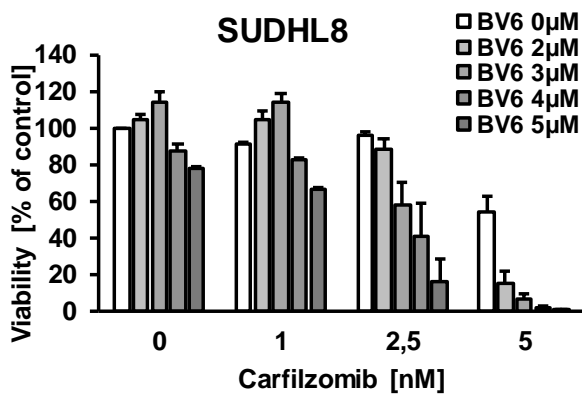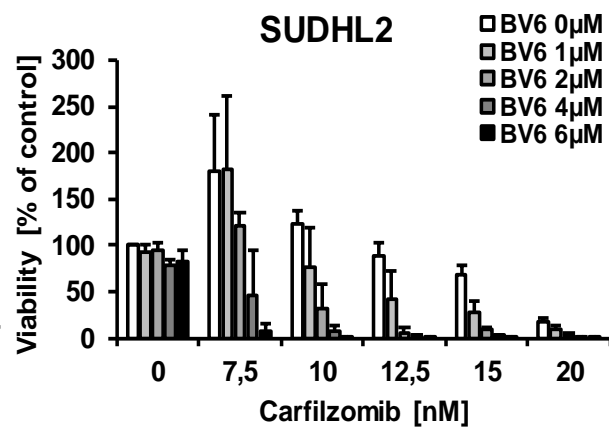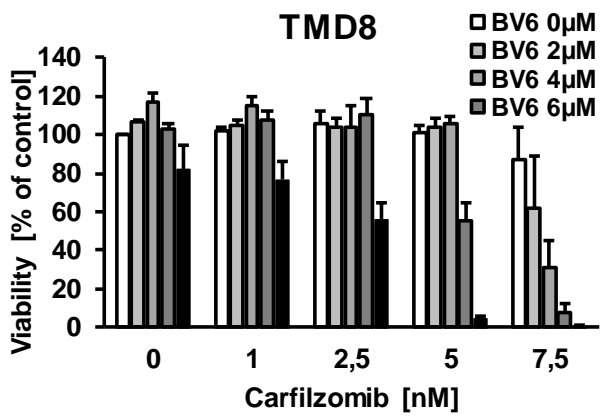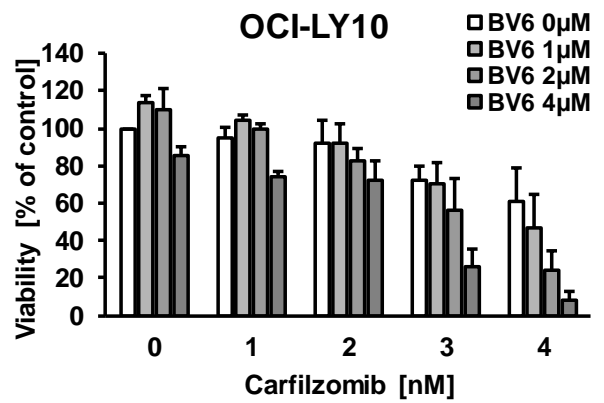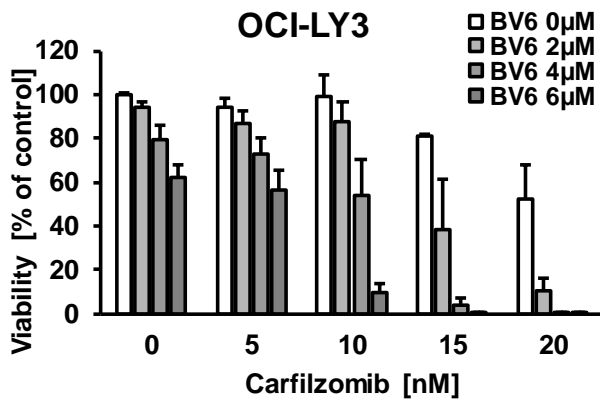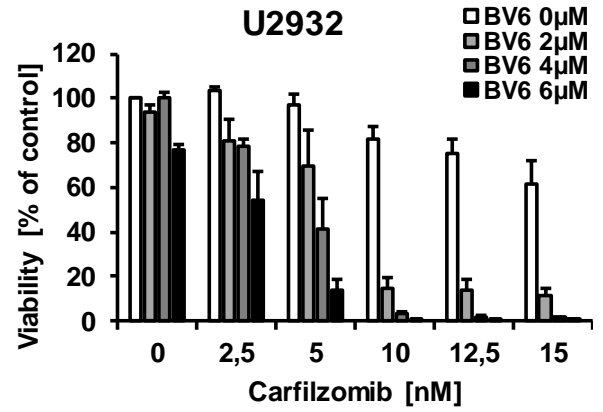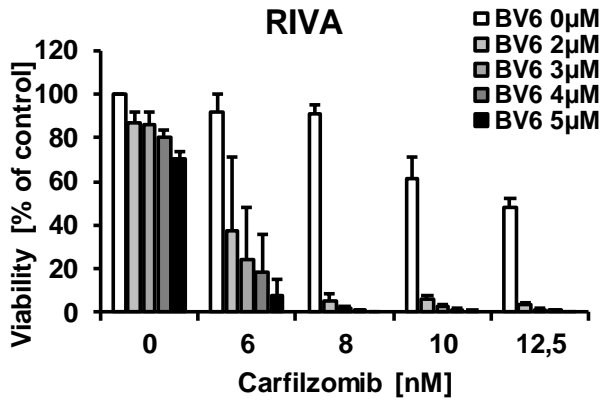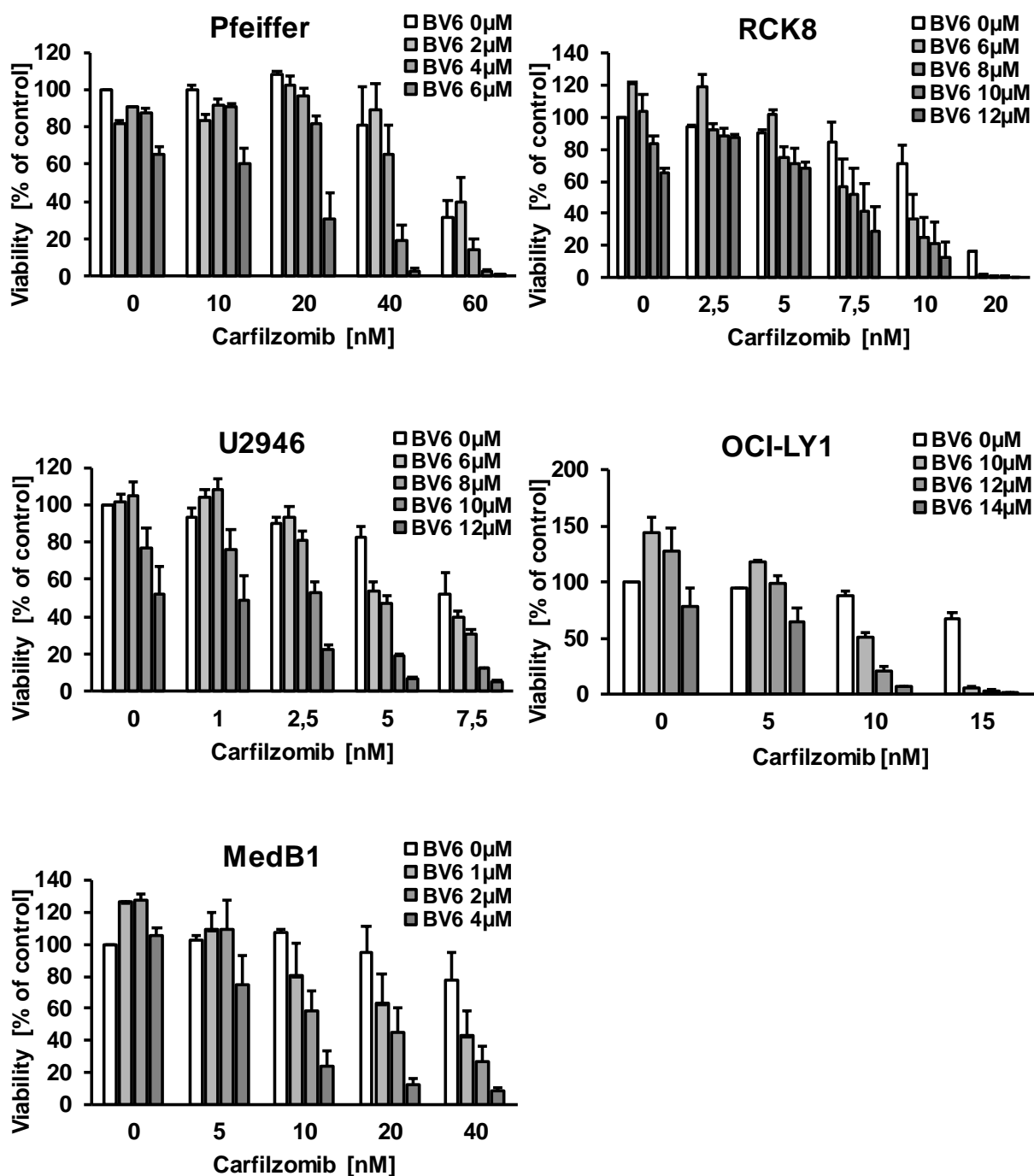
**Figure 6: BV6 and CFZ cooperate to induce cell death in different DLBCL cell lines**

DLBCL cell lines were treated with BV6 and CFZ as indicated for 48 hours. Cell viability was analyzed via the CellTiterGlo Assay. Data are shown as mean and SEM of three independent experiments performed in triplicates.

Calculation of the Combination Index (CI) as well as the Bliss score confirmed synergistic drug interaction of BV6 and CFZ (Table 22) indicated by CI < 0.9 and Bliss Scores > 0. Calculation of synergism demonstrated that BV6 in combination with CFZ is more effective than either substance alone.

**Table 22: Synergistic drug interaction of BV6 and CFZ analyzed by CI values and Bliss Score.**

| Cell line | Sub-type | Median CI value | Bliss Score |
|---|---|---|---|
| RIVA | ABC | 0,32 | 65,86 |
| U2932 | ABC | 0,31 | 49,80 |
| OCI-LY3 | ABC | 0,47 | 33,27 |
| MedB1 | PMBL | 0,41 | 29,83 |
| OCI-LY1 | GCB | 0,91 | 29,79 |
| SUDHL8 | GCB | 0,86 | 24,87 |
| U2946 | GCB | 0,99 | 18,11 |
| SUDHL2 | ABC | 0,61 | 16,87 |
| SUDHL10 | GCB | 0,95 | 15,88 |
| Pfeiffer | GCB | 0,76 | 13,65 |
| OCI-LY10 | ABC | 1,56 | 13,19 |
| RCK8 | GCB | 1,20 | 12,00 |
| TMD8 | ABC | 0,90 | 11,91 |

| Synergistic | Additive | Antagonistic |
|---|---|---|

To further investigate the mechanism of cell death induction, we focused our subsequent studies on two ABC DLBCL cell lines (RIVA, U2932), as they exhibited the lowest CI values and the highest Bliss Scores among the tested DLBCL cell lines, indicating strong synergistic interaction of BV6 and CFZ.

To determine the onset of cell death, we performed a kinetic upon BV6 and CFZ treatment in RIVA and U2932 cells. The experiments displayed that induction of cell death starts after approximately 12 hours in both cell lines (Figure 7).
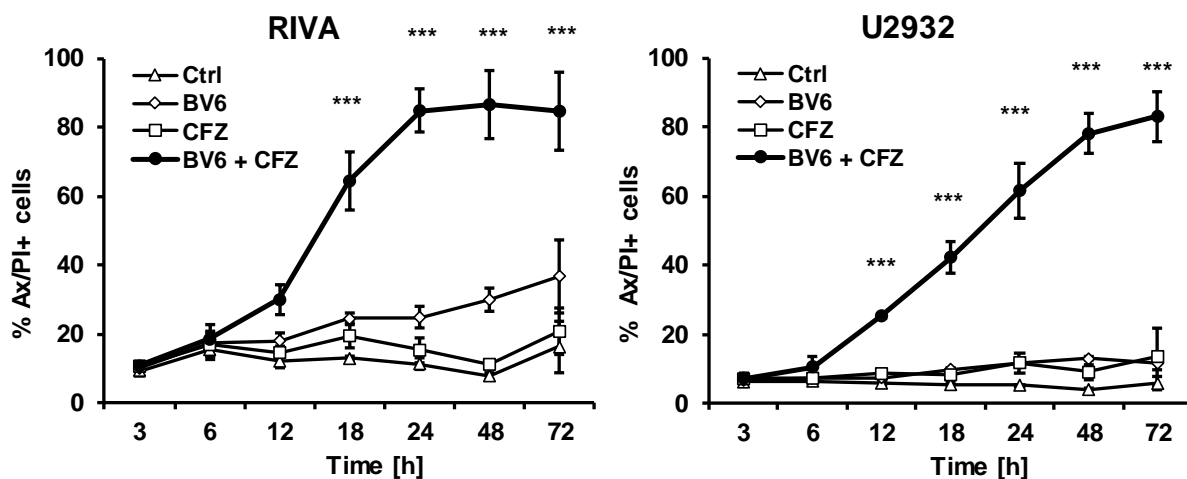
**Figure 7: Cell death kinetic upon BV6 and CFZ treatment**

RIVA cells were treated with 3 µM of BV6 and 8 nM CFZ and U2932 cells were treated with 2 µM BV6 and 5 nM CFZ for indicated time points. Cell death was assessed by Annexin V-FITC/PI double staining and flow cytometry. Data are shown as mean ± SEM of three independent experiments performed in triplicates. Significances are calculated against BV6 single treatment. * $p < 0.05$, ** $p < 0.01$, *** $p < 0.001$.

### 5.1.3 BV6 also cooperate to induce cell death with ixazomib and oprozomib

To test weather this synergistic cell death induction with BV6 and CFZ is specific for CFZ or a broader phenome, two other proteasome inhibitors called ixazomib (IXA) and oprozomib (OPR) were tested. These experiments showed that BV6 also synergized with IXA and OPR to reduce cell viability of RIVA and U2932 cells (Figure 8), which was also confirmed by calculation of the CI and Bliss Score (Table 23,Table 24).

These data indicate a high potency of the combined treatment of BV6 and proteasome inhibitors to induce cell death in DLBCL cell lines.

**A**
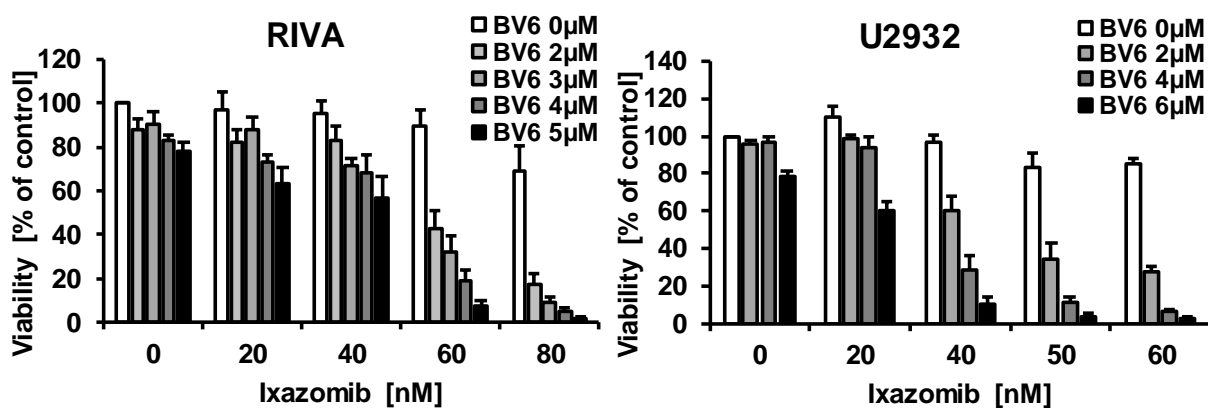


**B**
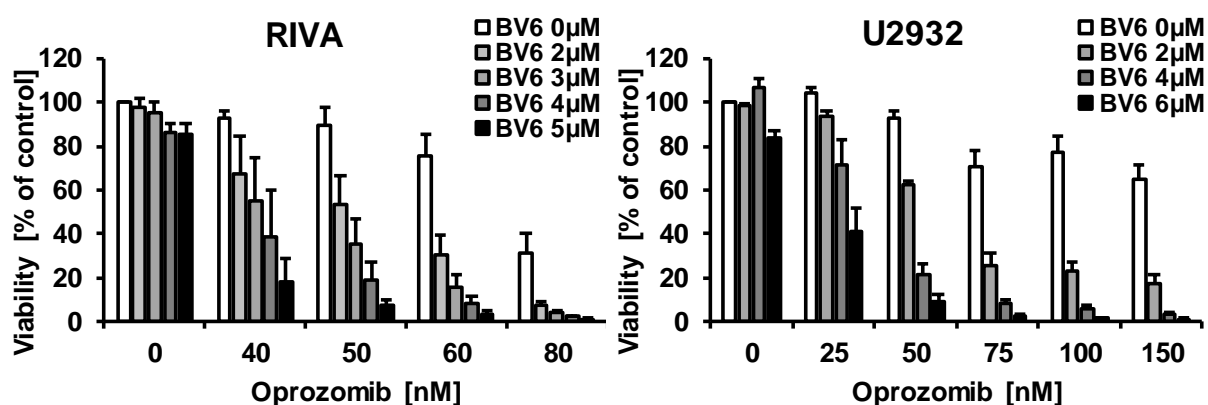


**Figure 8: BV6 cooperate with ixazomib and oprozomib to induce cell death in RIVA and U2932**

RIVA and U2932 cells were treated with BV6 and (**A**) ixazomib or (**B**) oprozomib as indicated for 48 hours. Cell viability was analyzed via the CellTiterGlo Assay. Data are shown as mean and SEM of three independent experiments performed in triplicates.

**Table 23: Synergistic drug interaction of BV6 and IXA analyzed by CI values and Bliss Score**

| Cell line | Sub-type | Median CI value | Bliss Score |
|---|---|---|---|
| RIVA | ABC | 0,462 | 35,38 |
| U2932 | ABC | 0,658 | 46,80 |

**Table 24: Synergistic drug interaction of BV6 and IXA analyzed by CI values and Bliss Score**

| Cell line | Sub-type | Median CI value | Bliss Score |
|---|---|---|---|
| RIVA | ABC | 0,730 | 49,63 |
| U2932 | ABC | 0,423 | 48,79 |

## 5.2 BV6/ CFZ combination treatment leads to cIAP degradation and NOXA accumulation

### 5.2.1 BV6/ CFZ treatment reduces cIAP protein levels and increases NOXA protein levels

Treatment with a Smac mimetic like BV6 leads to a degradation of cIAP1 and cIAP2 based on their autophosphorylation and subsequent proteasomal degradation [70, 83]. As Smac mimetics induce cell death by promoting degradation of IAPs, we analyzed whether there is a correlation between endogenous IAP expression and BV6 sensitivity. However, comparison of cIAP1, cIAP2 and XIAP expression levels in different DLBCL cell lines revealed no correlation between IAP expression and BV6 sensitivity (Figure 5 & Figure 9).
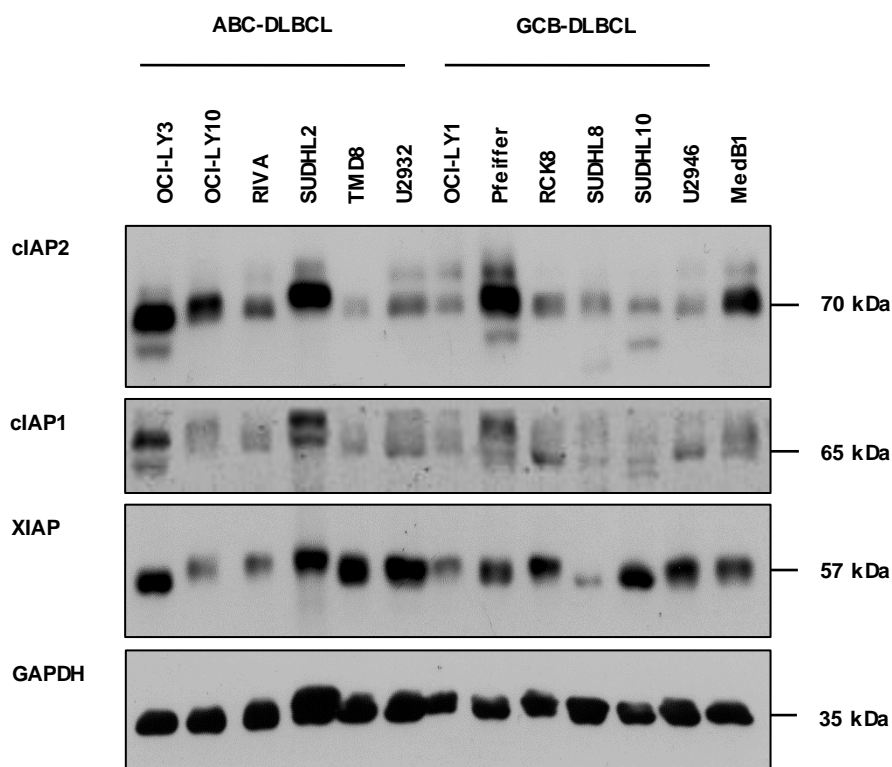
**Figure 9: Basal level of IAP proteins in different DLBCL cell lines**

Basal level of IAP proteins (cIAP1, cIAP2, XIAP) of different DLBCL cell lines was analyzed by Western blot. GAPDH served as loading control. Representative blots of two independent experiments are shown.

To explore whether inhibition of the proteasome prevents degradation of cIAPs, we examined protein expression levels of cIAP1/2 upon BV6/CFZ combination treatment. The experiments revealed that cIAP1 and cIAP2 were rapidly degraded within 0.5 hours after BV6/CFZ treatment, whereas expression levels of XIAP remained largely unchanged in both cell lines (Figure 10). In contrast, accumulation of the short-lived protein NOXA, a pro-apoptotic BH3-only protein known to be degraded by the proteasome, started around 4 hours after the addition of BV6/CFZ (Figure 10).
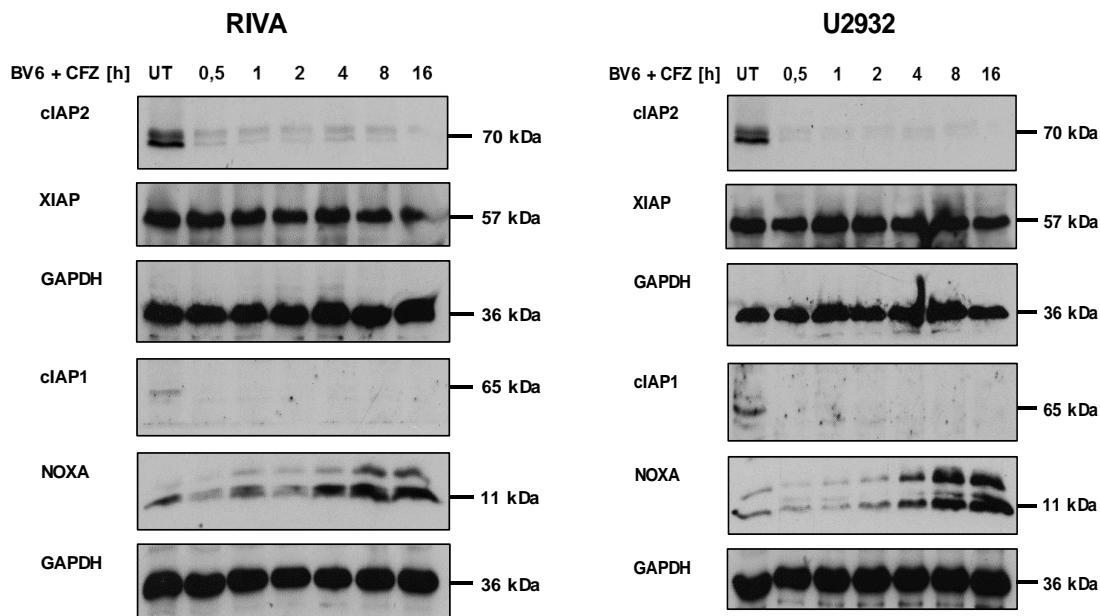
**Figure 10: Time dependent cIAP degradation and NOXA accumulation after BV6+CFZ treatment**

RIVA cells were treated with 2 μM BV6 and 8 nM CFZ, U2932 cells with 2 μM BV6 and 5 nM CFZ for indicated time points. Degradation of cellular inhibitor of apoptosis proteins and accumulation of NOXA were monitored by Western blot. GAPDH served as loading control. Representative blots of two independent experiments are shown.

## 5.2.2    CFZ and BV6/CFZ combination treatment reduce proteasome activity

To further prove that the proteasome is effectively inhibited upon treatment with CFZ alone and in combination with BV6 we directly assessed proteasomal activity. Proteasome activity was significant reduced after 4 hours of CFZ or BV6/CFZ combination treatment in both cell lines, whereas BV6 alone, had no effect on proteasome activity (Figure 11).
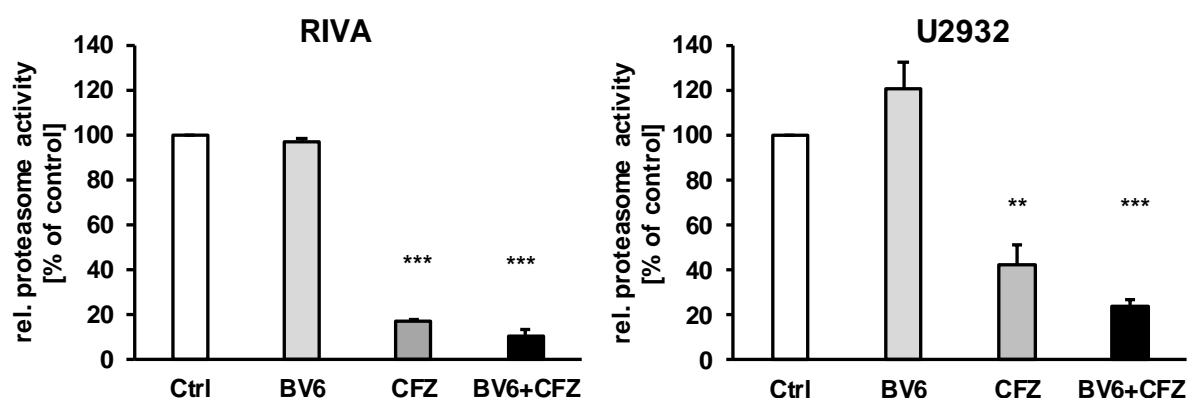
**Figure 11: Proteasome activity after BV6 and CFZ treatment**

RIVA cells were treated with 2 µM BV6 and/or 8 nM CFZ, U2932 cells with 2 µM BV6 and/or 5 nM CFZ for 4 hours. Proteasome activity was assessed by 20S Proteasome Activity Assay Kit from Chemicon. Data are shown as mean and SEM of three independent experiments. Significances are calculated against untreated control cells. ** $p < 0.01$, *** $p < 0.001$.

Taken together, these results revealed that BV6/CFZ treatment causes rapid degradation of cIAP1/2 proteins within 0.5 hours, before the proteasome is completely blocked. Furthermore, accumulation of the BH3-only protein NOXA started around 4 hours of treatment, in line with the proteasome activity assay, which showed a reduction in proteasome activity after 4 hours of CFZ or CFZ/BV6 treatment.

## 5.3 BV6/CFZ- mediated cell death is independent of non-canonical NF-κB and TNFα signaling

### 5.3.1 Activation of canonical and non-canonical NF-κB signaling upon BV6/CFZ treatment

Since cIAP degradation has been reported to induce an accumulation of NIK and subsequent activation of non- canonical NF-kB signaling [185], we next investigated NIK accumulation and activation of the NF-κB pathway after BV6/CFZ treatment. Indeed, we detected NIK accumulation as well as proteolytic processing of p100 to p52 upon treatment with BV6 alone and in combination with CFZ (Figure 12), indicative of

activation of non-canonical NF-κB signaling. In parallel, we detected phosphorylation of IκBα (Figure 12), suggesting an activation of canonical NF-κB signaling.
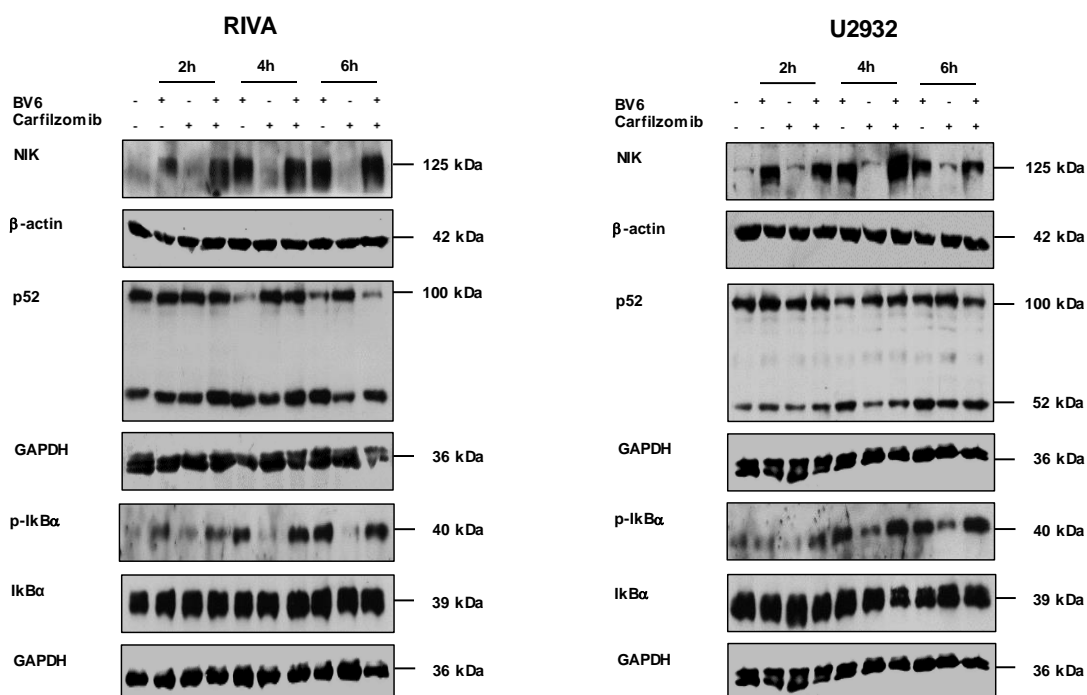


**Figure 12: Activation of canonical and non-canonical NF-κB signaling upon BV6/CFZ treatment**

RIVA cells were treated with 2 μM BV6 and 8 nM CFZ, U2932 cells with 2 μM BV6 and 5nM CFZ for indicated time points. Expression of NF-κB signaling proteins (NIK, p52, p-IκBα, IκBα) was analyzed by Western blot. GAPDH and β-actin served as loading control. Representative blots of two independent experiments are shown.

## 5.3.2 Genetic silencing of NIK did not reduce cell death induction after BV6/CFZ treatment

To examine whether NIK accumulation is important for BV6/CFZ-mediated cell death, we next performed siRNA-based gene silencing of NIK. Reduction of NIK protein level did not prevent cell death, rather, in RIVA cells, silencing of NIK revealed an increase in BV6/CFZ-induced cell death, whereas NIK knockdown seemed to have no influence on BV6/CFZ-induced cell death in U2932 cells (Figure 13). Knockdown efficiency was controlled by Western blot analysis (Figure 13).

**A**
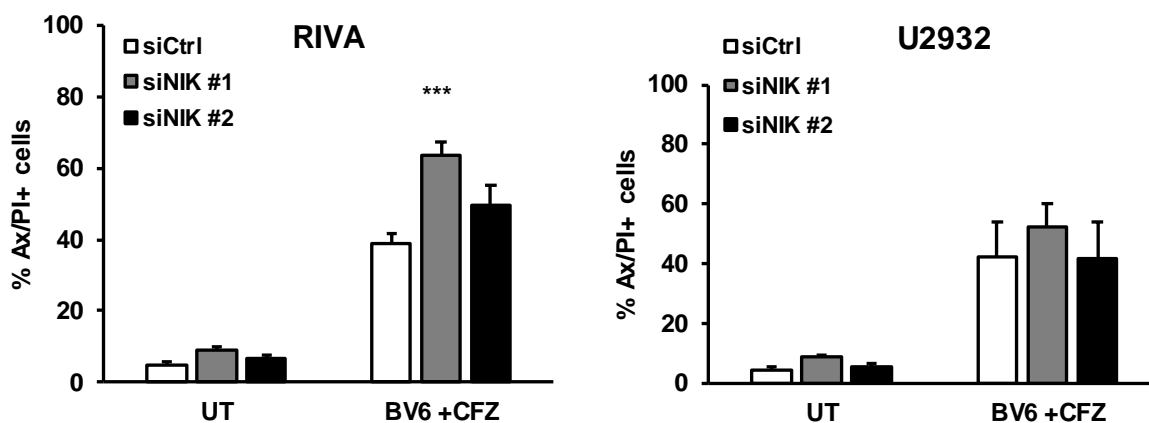


**B**
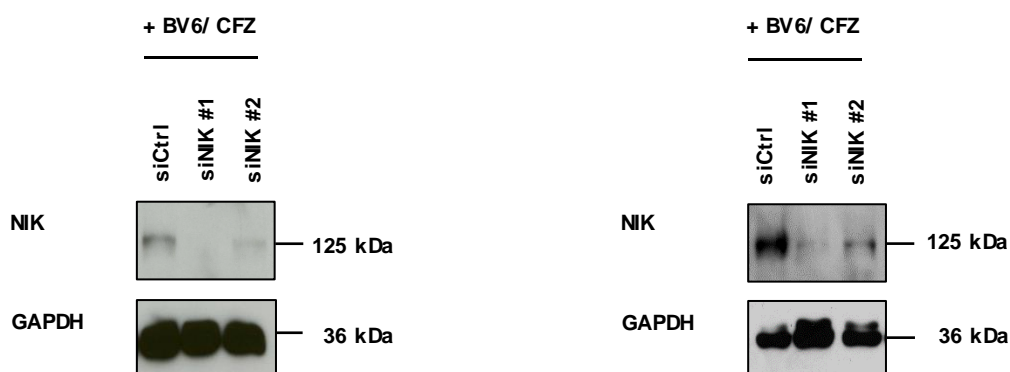


**Figure 13: Genetic silencing of NIK did not reduce cell death induction after BV6/CFZ treatment**

**A** Depletion of NIK using siRNA mediated gene silencing was performed before treatment with 3 µM BV6 and 8 nM CFZ (RIVA) for 18 hours or 2 µM BV6 and 5 nM CFZ (U2932) for 24 hours. Non-targeting siRNA (siCtrl) were used as control. Cell death was assessed by Annexin V-FITC/PI double staining and flow cytometry. Data are shown as mean and SEM of three (U2932) and six (Riva) independent experiments, respectively. Significances are calculated against treated siCtrl cells. *** $p < 0.001$. **B** Expression level of NIK after 4 hours of BV6/CFZ treatment was analyzed by Western blot and GAPDH served as loading control. Representative blots of at least three (U2932) or six (Riva) independent experiments are shown.

### 5.3.3    BV6/CFZ-mediated cell death is independent of TNFα signaling

TNFα is a well-described target gene of NF-κB signaling and could induce cell death especially in the presence of Smac mimetics via the TNFR in an autocrine/paracrine loop [70, 83, 186]. Therefore, we explored the involvement of TNFα in BV6/CFZ-mediated cell death. However, neither the addition of TNFα nor treatment with the

TNF$\alpha$ inhibitor Enbrel affected BV6/CFZ-mediated cell death in both cell lines (Figure 14). Treatment of Jurkat cells with BV6+ TNF$\alpha$ in the presence and absence of Enbrel served as positive control (Figure 15).
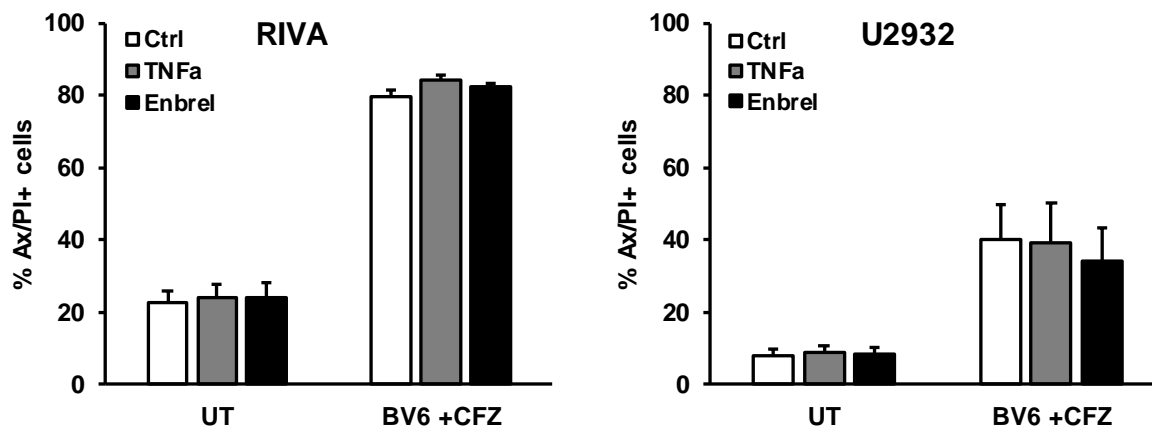


**Figure 14: BV6/ CFZ-mediated cell death is independent of TNF$\alpha$ signaling**

Cells were treated with BV6/CFZ alone (RIVA: 3 µM BV6, 8 nM CFZ; U2932: 2 µM BV6, 5 nM CFZ), BV6/CFZ + TNF (10 ng/ml) or BV6/CFZ + 1 hour Enbrel pre-treatment (50 µg/ml) for 18 hours (RIVA) and 24 hours (U2932), respectively. Cell death was assessed by Annexin V-FITC/PI double staining and flow cytometry. Data are shown as mean and SEM of three independent experiments performed in triplicates.
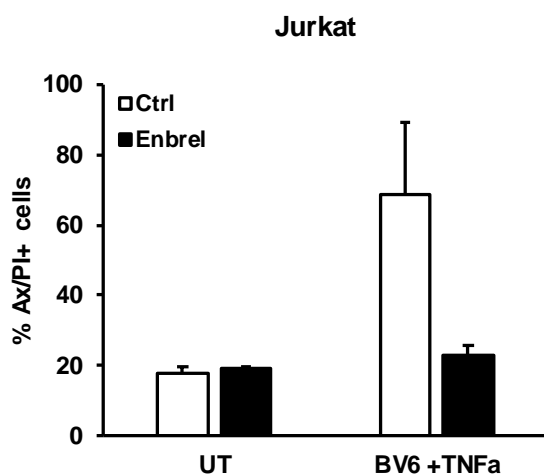


**Figure 15: Enbrel could reduce BV6 and TNF$\alpha$ -mediated cell death in Jurkat cells**

Jurkat cells were treated with 1 µM BV6 and 1 ng/ml TNF$\alpha$ or with BV6, TNF$\alpha$ and 1 hour of Enbrel pre-treatment (50 µg/ml) for 18 hours. Cell death was assessed by Annexin V-FITC/PI double staining and flow cytometry. Data are shown as mean and SEM of two independent experiments performed in triplicates.

Together, these experiments indicate that BV6/CFZ-induced cell death occurs independent of non-canonical NF-κB signaling and TNFR-mediated cell death.

## 5.4 BV6/CFZ combination treatment induces caspase dependent cell death

### 5.4.1 BV6/CFZ treatment induces activation of caspases

To gain insight into the underlying mechanism of the synergistic interaction of BV6 and CFZ, we next investigated the role of caspases, as key effectors of apoptotic cell death [28]. Cleavage of procaspases to their active, cleaved forms is required for mediating apoptotic signaling [187].

Western blot analysis revealed that BV6 and CFZ cooperated to activate caspase-3, -8 and -9 in RIVA and U2932 cells after 6 hours and more pronounced after 12 and 15 hours, as indicated by the generation of active caspase cleavage products (Figure 16). Furthermore, we observed cleavage of effector caspases-3 and -7 after BV6/CFZ treatment, which was analyzed by the caspase activity assay and gave a strong signal for caspase-3/-7 positive cells in the fluorescence microscope (Figure 17). The number of caspase-3/-7 positive cells was significantly decreased by adding the pan-caspase inhibitor zVAD.fmk (Figure 17).
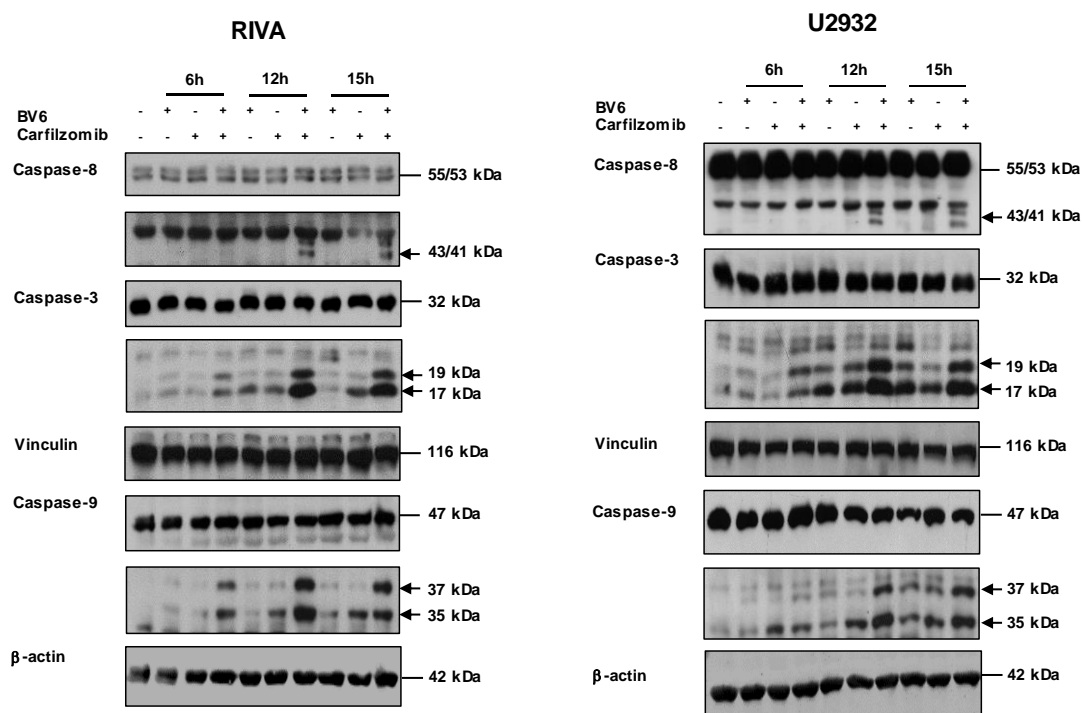
**Figure 16: BV6/CFZ treatment induces cleavage and activation of caspases**

RIVA cells were treated with 2 μM BV6 and/or 8 nM CFZ, U2932 cells with 2 μM BV6 and/or 5 nM CFZ for indicated times. Activation of caspase-8, -3 and -9 was analyzed by Western blotting. Arrowheads indicate active cleavage fragments and β-actin as well as Vinculin served as loading control. Representative blots of two independent experiments are shown.
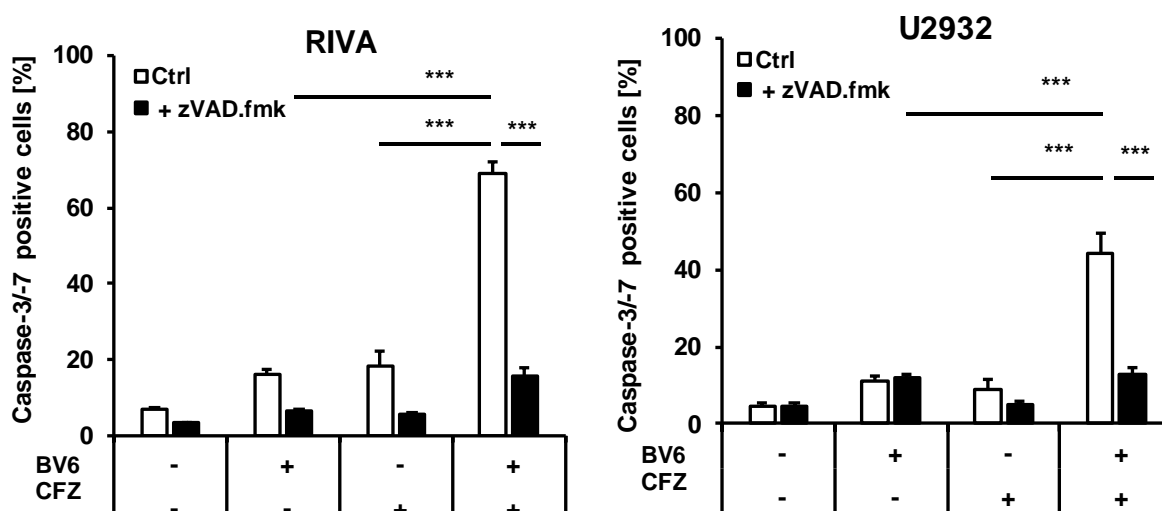


**Figure 17: BV6/CFZ treatment induces activation of caspase-3/-7**

RIVA cells were treated with 2 μM BV6 and/or 8 nM CFZ, U2932 cells with 2 μM BV6 and/or 5 nM CFZ in the presence or absence of zVAD.fmk for 24 hours. Caspase activity was measured by Caspase-3/-7 Green Detection Reagent and Hoechst counterstaining using high-content fluorescence microscopy. Data are shown as mean and SEM of three independent experiments performed in triplicates. *** $p < 0.001$.

### 5.4.2 BV6/CFZ treatment induces caspase-dependent cell death

After caspase activation, we further analyzed if this activation is crucial for BV6/CFZ-mediated cell death induction. Therefore, we pre-treated RIVA and U2932 cells with the pan-caspase inhibitor zVAD.fmk before BV6/CFZ treatment. These experiments revealed that zVAD.fmk significantly reduced BV6/CFZ-induced cell death in both cell lines, indicating a caspase-dependent cell death (Figure 18).
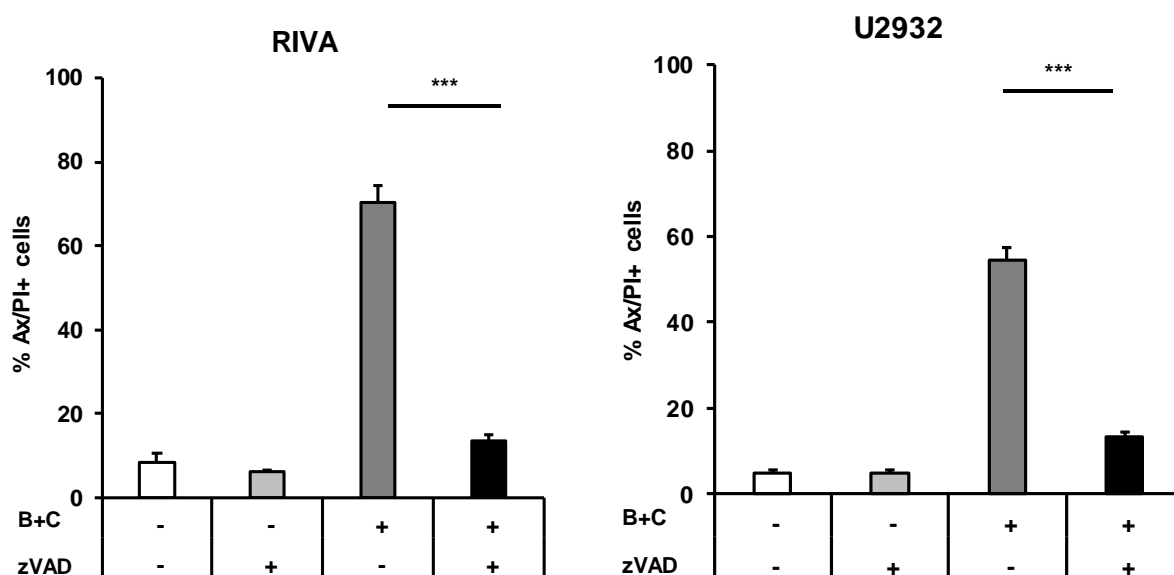


**Figure 18:BV6/CFZ-induced cell death is caspase-dependent**

RIVA cells were treated with 2 µM BV6 and/or 8 nM CFZ, U2932 cells with 2 µM BV6 and/or 5 nM CFZ in the presence or absence of zVAD.fmk for 18 hours (RIVA) and 24 hours (U2932), respectively. Cell death was assessed by Annexin V-FITC/PI double staining and flow cytometry. Data are shown as mean and SEM of three independent experiments performed in triplicates. *** p < 0.001.

These data indicate that the combination of BV6 and CFZ induces the activation of initiator and effector caspases, which finally lead to caspase-dependent apoptosis in RIVA and U2932 cells.

## 5.5 BV6 and CFZ cooperate to induce BAX/BAK activation and loss of MMP

### 5.5.1 BV6 and CFZ induce activation of BAX and BAK

Since we found an activation of different initiator and effector caspases after treatment with BV6 and CFZ, we next investigated the involvement of the two pro-apoptotic effector proteins BAX and BAK, which are key mediators of the intrinsic apoptotic pathway. BAX and BAK have been described to undergo a conformational change upon activation, which leads to an oligomerization of the two proteins [188]. The resulting homodimers are able to pierce in the mitochondrial outer membrane, which leads to the release of cytochrome c and mediates apoptotic cell death [188]. To detect an activation of BAX and BAX we used conformation-specific antibodies, which detect the active conformation and afterwards immunoprecipitated BAX and BAK [189, 190]. Combination treatment with BV6 and CFZ resulted in enhanced activation of BAX and BAK as compared to untreated cells or BV6/CFZ single treatment (Figure 19).
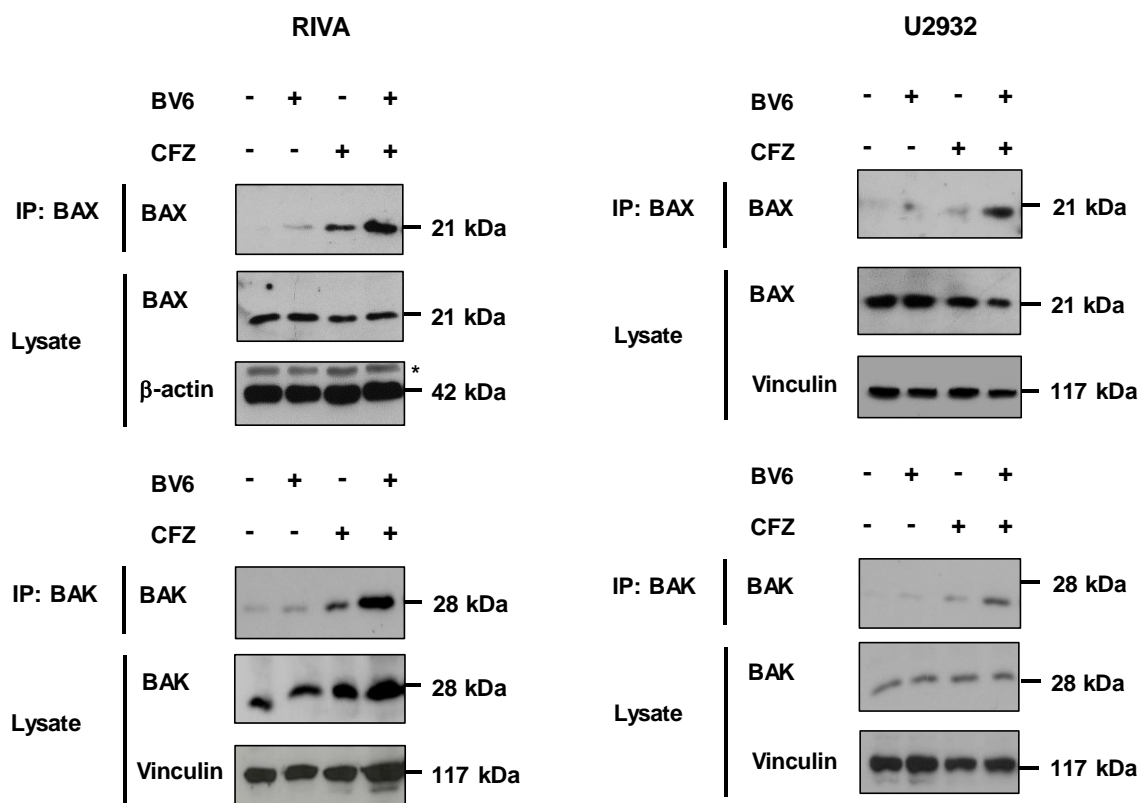
**Figure 19: BV6/CFZ treatment lead to activation of BAX and BAK**

RIVA cells were treated with 2 µM BV6 and/or 8 nM CFZ for 15 hours and U2932 cells with 2 µM BV6 and/or 5 nM CFZ for 18 hours. Activation of BAX or BAK was assessed by immunoprecipitation of activated BAX or BAK using an active conformation-specific antibody. Expression of β-actin or Vinculin served as loading control. Results are shown as representative blots of at least two to four independent experiments.

It is described that the activation of BAX and BAK lead to loss of mitochondrial membrane potential [49]. Therefore, we next investigated whether the mitochondrial pathway is affected by BV6/CFZ treatment by measurement of loss of MMP. In fact, treatment with either BV6 or CFZ led to a slight loss of MMP, which further increased in the combination treatment (Figure 20).

62
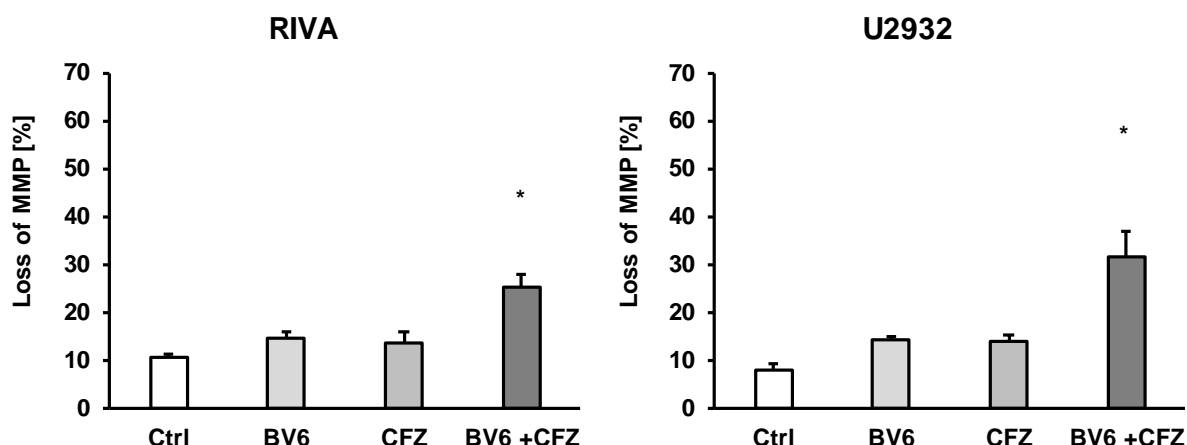
**Figure 20: BV6/CFZ treatment induce loss of mitochondrial membrane potential**

RIVA cells were treated with 2 µM BV6 and/or 8 nM CFZ for 15 hours and U2932 cells with 2 µM BV6 and/or 5 nM CFZ for 18 hours. Loss of mitochondrial membrane potential was assessed by TMRM staining of the whole cell population and flow cytometry. Data are shown as mean and SEM of three independent experiments. Significances are calculated against untreated control cells. * p < 0.05.

Taken together, these results prove that combination treatment with BV6 and CFZ triggers activation of BAX and BAK, as well as mitochondrial perturbation indicated by loss of MMP.

## 5.5.2 BV6/CFZ-mediated cell death depend on BAX and BAK

In the next step, we analyzed if BAX and BAK are required for BV6/CFZ-induced cell death. Therefore, we reduced BAX and BAK protein expression by using siRNA-mediated knockdown. Interestingly, single knockdown of either BAX or BAK reduced BV6/CFZ-mediated cell death in RIVA and U2932 cells (Figure 21). Moreover, simultaneous gene silencing of BAX and BAK, further decreased cell death compared to BAX and BAK single knockdowns (Figure 22), indicating that both BAX and BAK are required for the induction of apoptosis.

**A**
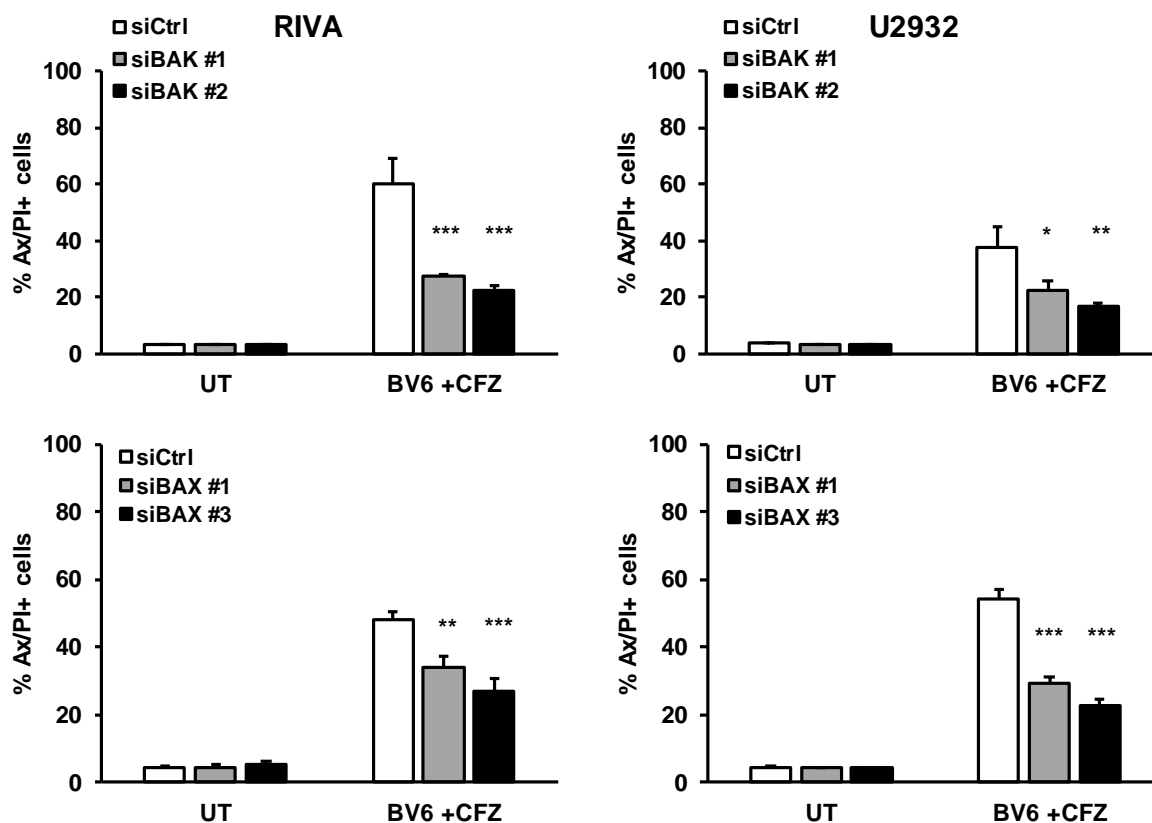


**B**



**Figure 21: BAX or BAK knockdown reduces BV6/CFZ-mediated cell death**

**A** Depletion of BAX or BAK using siRNA mediated gene silencing was performed before treatment with 3 μM BV6 and 8 nM CFZ (RIVA) for 18 hours or 2 μM BV6 and 5 nM CFZ (U2932) for 24 hours. Non-targeting siRNA (siCtrl) were used as controls. Cell death was assessed by Annexin V-FITC/PI double staining and flow cytometry. Data are shown as mean and SEM of three independent experiments performed in triplicates. Significances are calculated against treated siCtrl cells. * $p < 0.05$, ** $p < 0.01$, *** $p < 0.001$. **B** Expression level of BAX and BAK were analyzed by Western blotting and β-actin or GAPDH served as loading control. Representative blots of at least three independent experiments are shown.

**A**
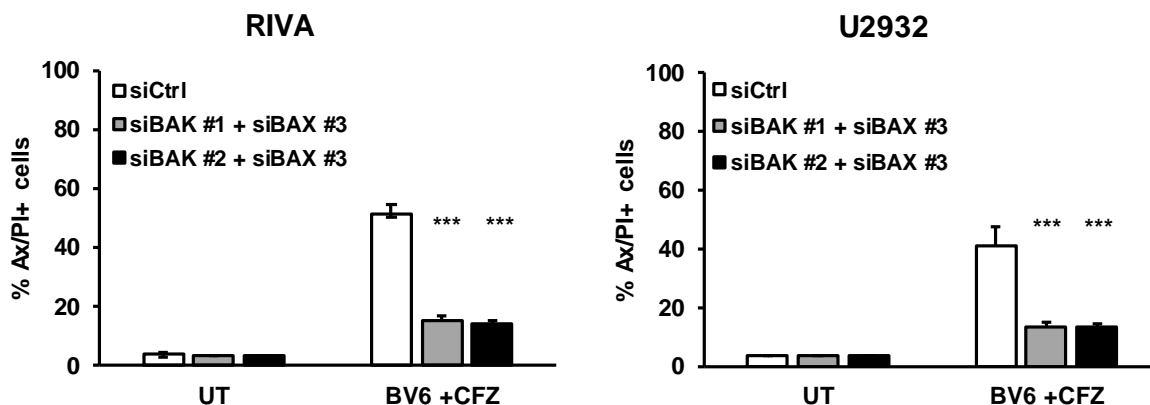


**B**



**Figure 22: BAX/BAK double knockdown rescues BV6/CFZ-induced cell death**

**A** Simultaneous depletion of BAX and BAK using siRNA mediated gene silencing was assessed by combination of one construct targeting BAX (siBAX #3) and one construct targeting BAK (siBAK #1 or siBAK #2). RIVA cells were treated with 3 µM BV6 and 8 nM CFZ for 18 hours and U2932 cells were treated with 2 µM BV6 and 5 nM CFZ for 24 hours. Cell death was assessed by Annexin V-FITC/PI double staining and flow cytometry. Data are shown as mean and SEM of three independent experiments performed in triplicates. Significances are calculated against treated siCtrl cells. *** $p < 0.001$. **B** Expression level of BAX and BAK were analyzed by Western blotting and β-actin served as loading control. Representative blots of at least three independent experiments are shown.

These experiments confirm that CFZ/BV6 induced apoptosis is mediated via the intrinsic apoptotic signaling pathway with BAX and BAK playing a critical role in executing BV6/CFZ-induced cell death.

## 5.6 Involvement of BCL-2 proteins in BV6/CFZ-mediated cell death

### 5.6.1 Expression levels of BCL-2 proteins after BV6/CFZ treatment

After demonstrating that BAX and BAK play an important role for BV6/CFZ-mediated cell death, we next investigated the expression of different pro-and anti-apoptotic BCL-2 proteins after treatment with BV6/CFZ, in order to gain further insight into the molecular mechanism. Proteins of the BCL-2 family are important for BAX/BAK activation and therefore for the induction of cell death via the mitochondrial pathway [39].

Interestingly, treatment with BV6/CFZ led to a strong accumulation of NOXA in both cell lines and an induction of the short isoform of BIM (BIMs) in RIVA cells (Figure 23). Furthermore, we could detect the caspase cleavage product of BID called truncated BID (tBID) after treatment with BV6/CFZ, indicating a crosstalk between extrinsic and intrinsic apoptotic signaling pathways. Cleavage of BID however was abrogated after addition of the caspase inhibitor zVAD.fmk (Figure 23). Interestingly, we found that BMF is cleaved by caspases in RIVA cells, indicated by a small BMF product (~15kDa) appearing after BV6/CFZ treatment, which disappeared again after addition of zVAD.fmk. Of note, analysis of the anti-apoptotic proteins BCL-2 and MCL-1 did not show any changes in protein expression after combination treatment (Figure 23).
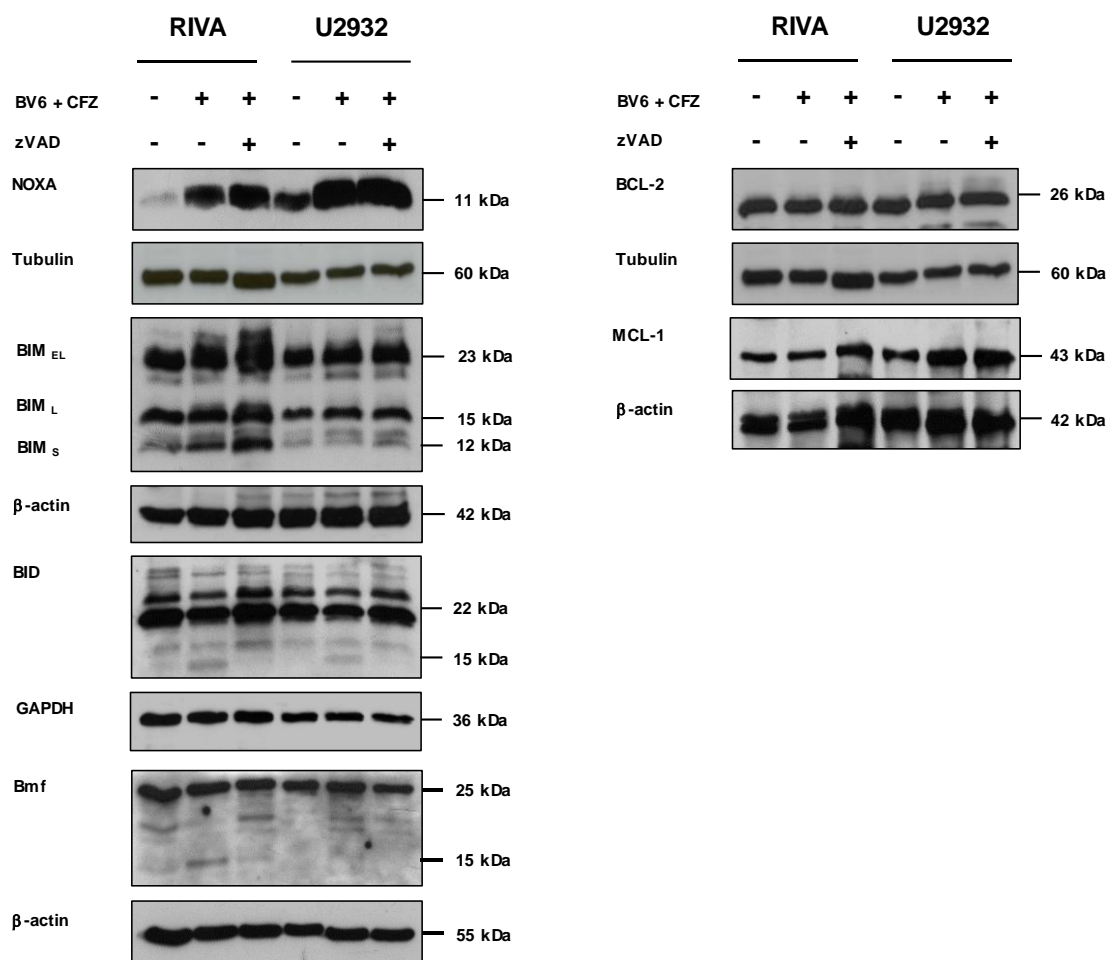
**Figure 23: Expression of BCL-2 proteins after BV6/CFZ treatment**

Cells were treated for 15 hours with BV6/CFZ (RIVA: 3 µM BV6, 8 nM CFZ; U2932: 2 µM BV6, 5 nM CFZ) or BV6/CFZ + 1 hour zVAD.fmk pre-treatment. Expression of BCL-2 proteins was analyzed by Western blot. Tubulin and β-actin served as loading control. Representative blots of 2-3 independent experiments are shown.

## 5.6.2 Accumulation of NOXA after BV6/CFZ treatment plays an important role for cell death induction

To verify if the marked increase in NOXA protein is due to accumulation of the protein and not due to protein expression, we analyzed NOXA mRNA levels via RT-qPCR. NOXA mRNA expression slightly increased upon BV6/CFZ single or combination treatment, but NOXA mRNA increase was statistically not significant (Figure 24). These result confirmed that the increased amount of NOXA protein is due to NOXA protein accumulation and not due to protein expression.
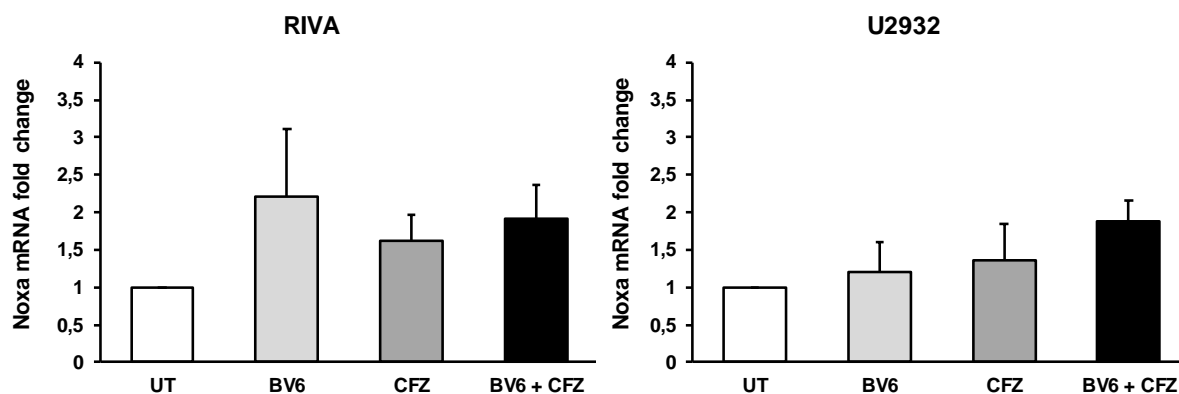
**Figure 24: NOXA mRNA expression after BV6/CFZ treatment**

RIVA cells were treated with 3 µM BV6 and/or 8 nM CFZ and U2932 cells with 2 µM BV6 and/or 5 nM CFZ for 6 hours. Expression of NOXA mRNA was analyzed by RT-qPCR. Data are shown as mean and SEM of three independent experiments performed in triplicates.

We next investigated, if the accumulation of NOXA protein level has a functional role for BV6/CFZ-induced cell death. Therefore, siRNA-based knockdown experiments to diminish protein expression of NOXA were performed. Intriguingly, reduction of NOXA protein level correlated with a significant reduction in BV6/CFZ-mediated cell death in RIVA and U2932 cells (Figure 25).

**A**
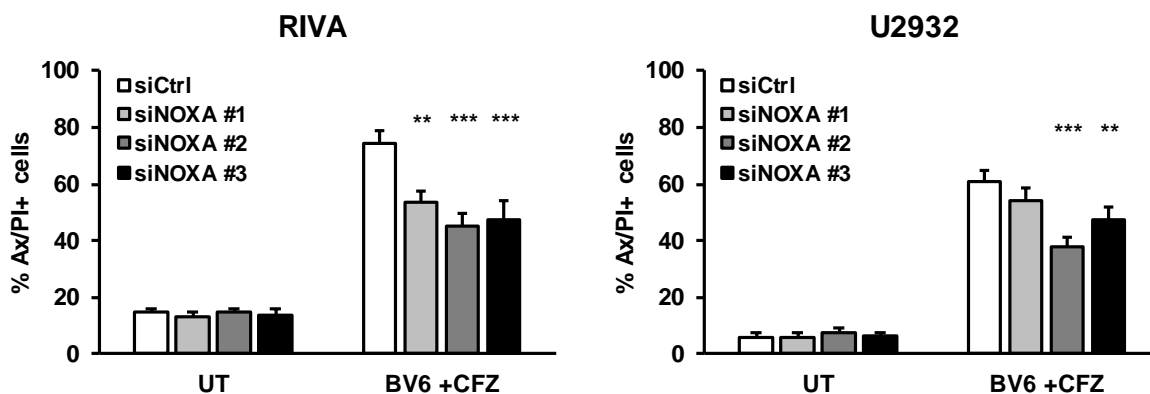
**B**
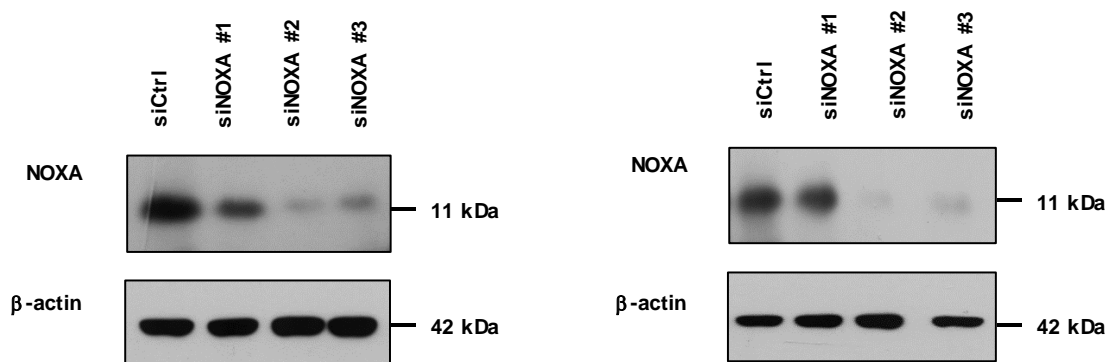


**Figure 25: Knockdown of NOXA protein level reduces BV6/CFZ-mediated cell death**

**A** Depletion of NOXA using siRNA mediated gene silencing was performed before treatment with 3 µM BV6 and 8 nM CFZ (RIVA) for 15 hours or 2 µM BV6 and 5 nM CFZ (U2932) for 24 hours. Non-targeting siRNA (siCtrl) were used as controls. Cell death was assessed by Annexin V-FITC/PI double staining and flow cytometry. Data are shown as mean and SEM of 3-5 independent experiments performed in triplicates. Significances are calculated against treated siCtrl cells ** $p < 0.01$, *** $p < 0.001$. **B** Expression level of NOXA was analyzed by Western blotting and β-actin served as loading control. Representative blots of at least 3-5 independent experiments are shown.

Together this set of experiments indicate an important role of the pro-apoptotic BCL-2 protein NOXA for the induction of BV6/CFZ-mediated cell death in RIVA and U2932 cells.

## 5.7 Interaction of pro- and anti-apoptotic BCL-2 proteins in BV6/CFZ-mediated cell death

Since we found that BV6/CFZ treatment mainly induces intrinsic apoptosis mediated via the mitochondria and involvement of particular BCL-2 proteins, we wanted to gain further insight into the molecular mechanism. For the induction of intrinsic apoptosis the interplay between pro- and anti-apoptotic BCL-2 proteins play an important role [191]. To gain further insight into the molecular mechanism of BV6/CFZ-induced cell death we next analyzed the interaction between pro- and anti-apoptotic BCL-2 proteins by different immunoprecipitation experiments.

### 5.7.1 Changes of BCL-2 interaction partner upon BV6/CFZ treatment

The anti-apoptotic BCL-2 protein is highly expressed in RIVA and U2932 cells [192], therefore we started our immunoprecipitation experiments with BCL-2, to investigate if there are changes in BCL-2 binding partners upon BV6/CFZ treatment. Indeed, we could detect increased binding of a specific BMF isoform to BCL-2 as well as slightly decreased binding of BAX to BCL-2 after combination treatment (Figure 26). Binding of other BH3-only proteins like BIM or PUMA to BCL-2 were not affected by BV6/CFZ treatment. Furthermore, the BH3-only protein BAD is not bound to BCL-2 in RIVA cells (Figure 26).
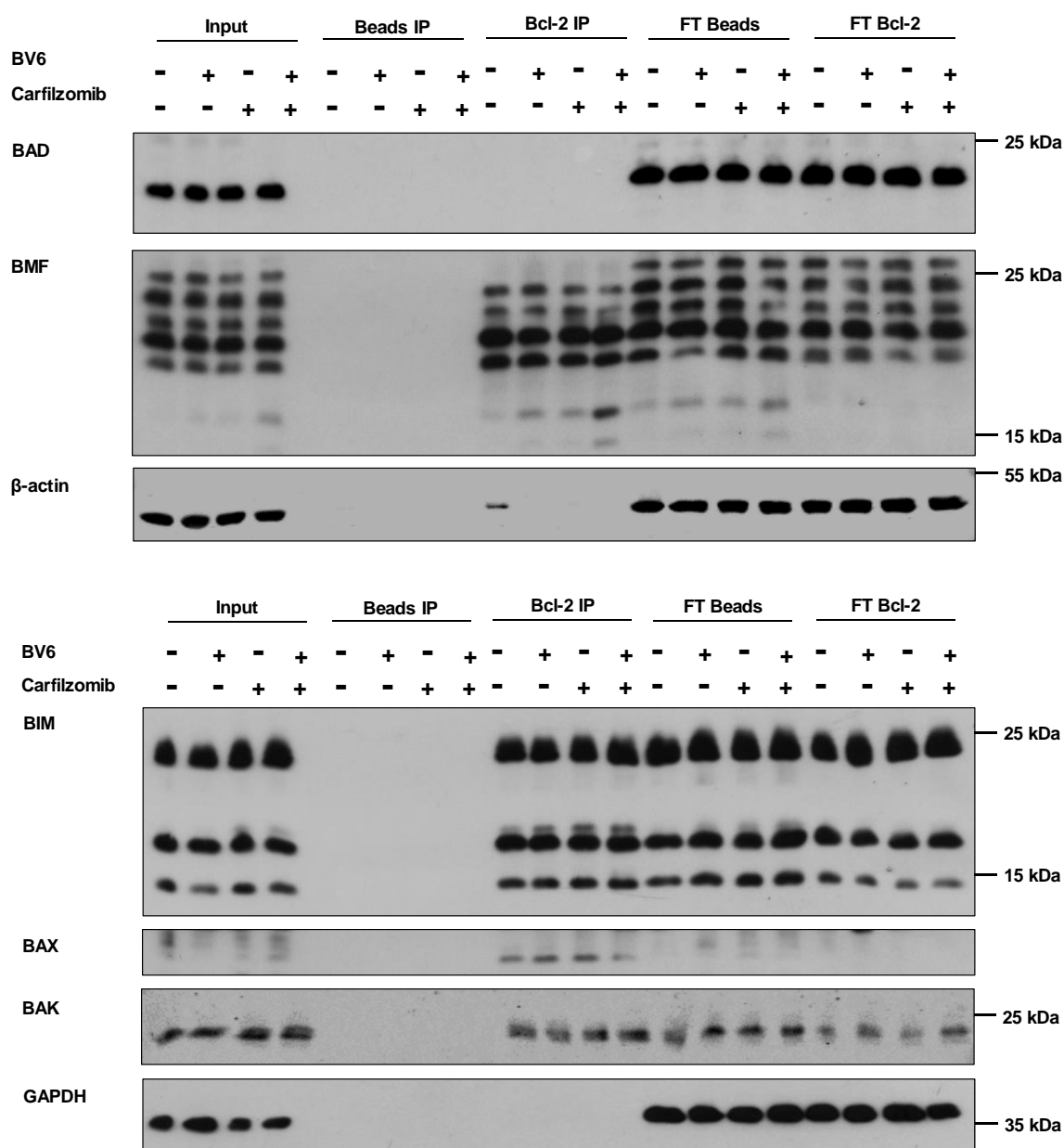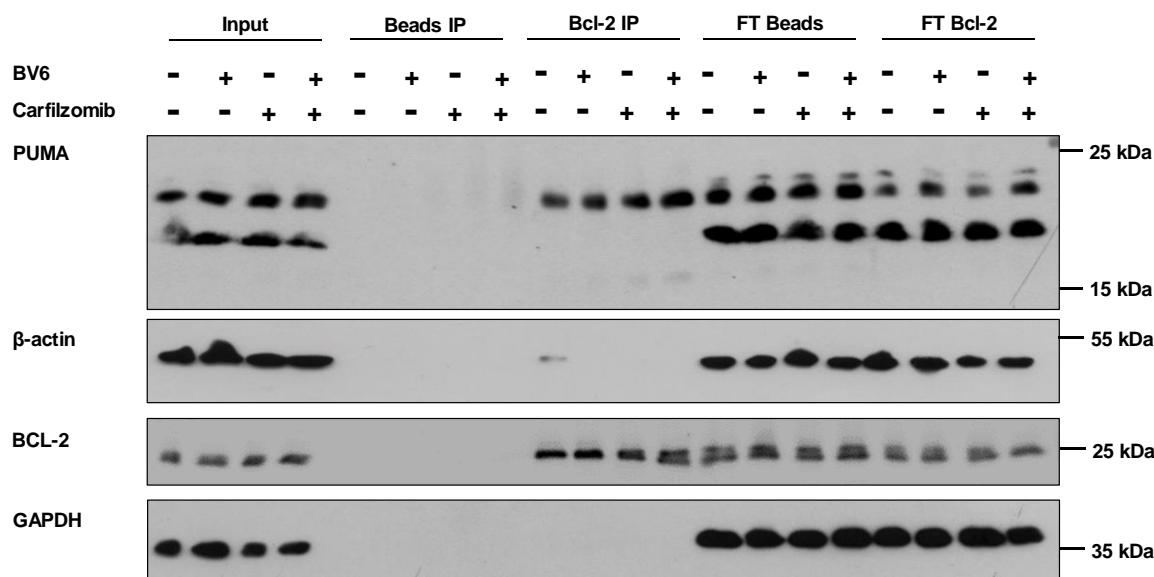
**Figure 26: Changes of BCL-2 interaction partner upon BV6/CFZ treatment in RIVA cells**

RIVA cells were treated for 18 hours with BV6 and/ or CFZ (3 µM BV6, 8 nM CFZ).Interaction partner of BCL-2 were identified by BCL-2 immunoprecipitation using anti-BCL-2 antibody. Detection of indicated proteins was carried out by Western blotting. GAPDH and β-actin served as loading control. Membrane was stripped.

In the U2932 cell line we observed the same results as for the RIVA cells. BMF was more bound to BCL-2 after BV6/CFZ combination treatment and BAX was less bound to BCL-2 (Figure 27). Furthermore, binding of BIM or PUMA was unaffected by BV6/CFZ treatment (Figure 27) and BAD did not bind to BCL-2 in the U2932 cells.



71
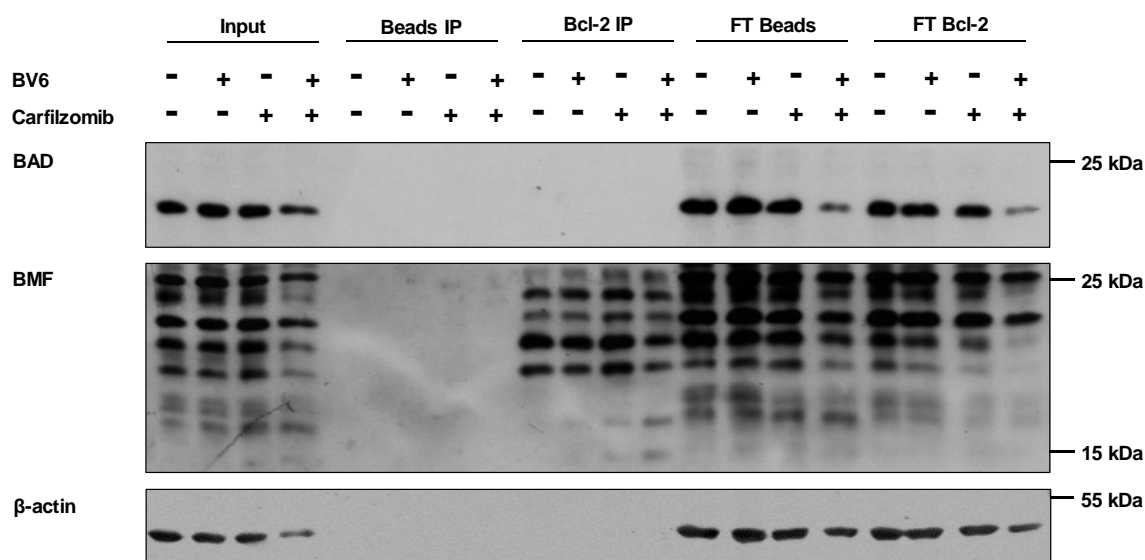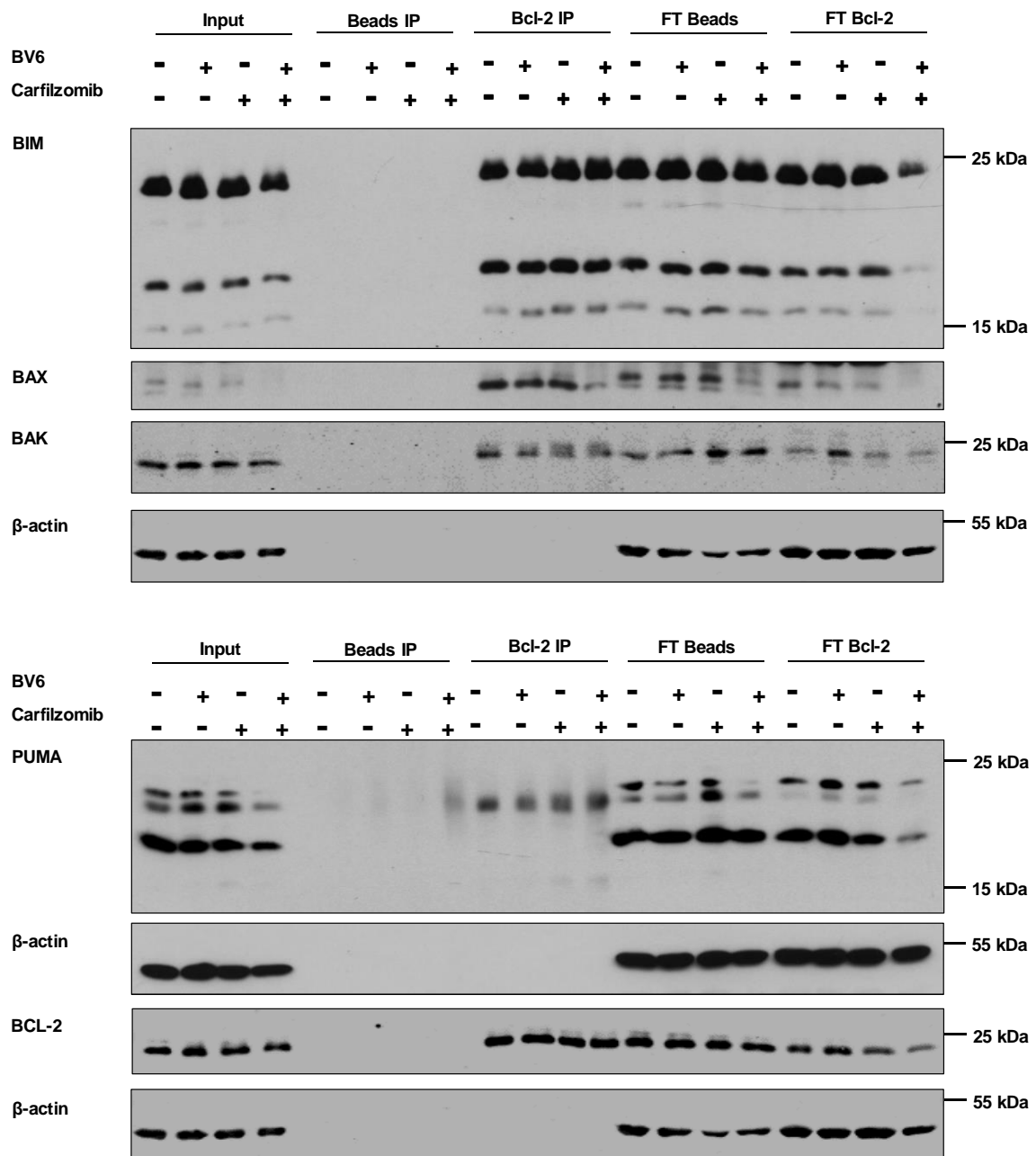
**Figure 27: Changes of BCL-2 interaction partner upon BV6/CFZ treatment in U2932 cells**

U2932 cells were treated for 18 hours with BV6 and/ or CFZ (2 µM BV6, 5 nM CFZ). Interaction partner of BCL-2 were identified by BCL-2 immunoprecipitation using anti-BCL-2 antibody. Detection of indicated proteins was carried out by Western blotting. GAPDH and β-actin served as loading control. Membrane was stripped.

Together, this set of experiments revealed changes in BCL-2 binding partners (BMF and BAX) upon BV6/CFZ treatment, which could play a role in the induction of cell death.

## 5.7.2    Changes of MCL-1 interaction partner upon BV6/CFZ treatment

Because of strong accumulation of NOXA and its functional role for BV6/CFZ-mediated cell death, we next investigated changes of MCL-1 binding to NOXA. MCL-1 immunoprecipitation studies revealed an increased binding of NOXA to MCL-1 upon BV6/CFZ treatment in both cell lines (Figure 28). We also detected a lot of NOXA which is not bound to MCL-1 in the MCL-1 immunoprecipitation flow through. Furthermore, an interaction of BAK with MCL-1 could not clearly be identified (Figure 28).

**A**
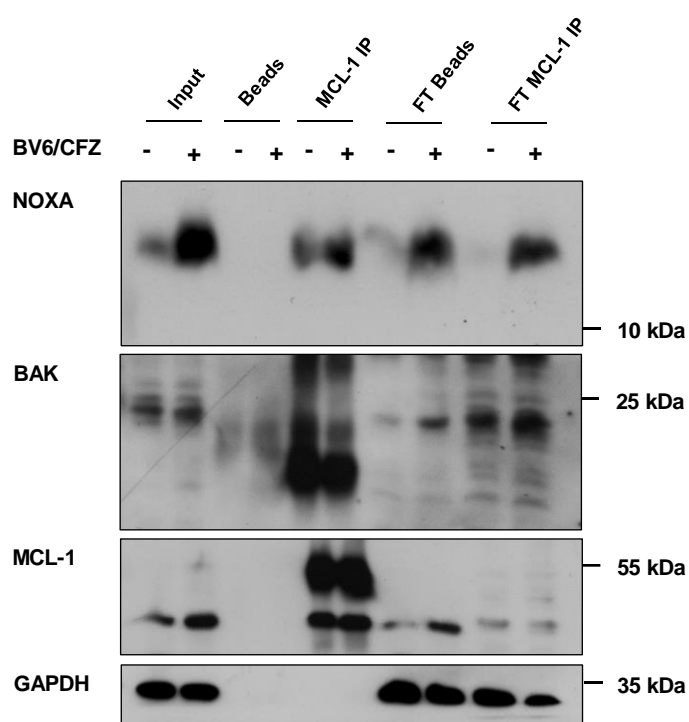
**B**
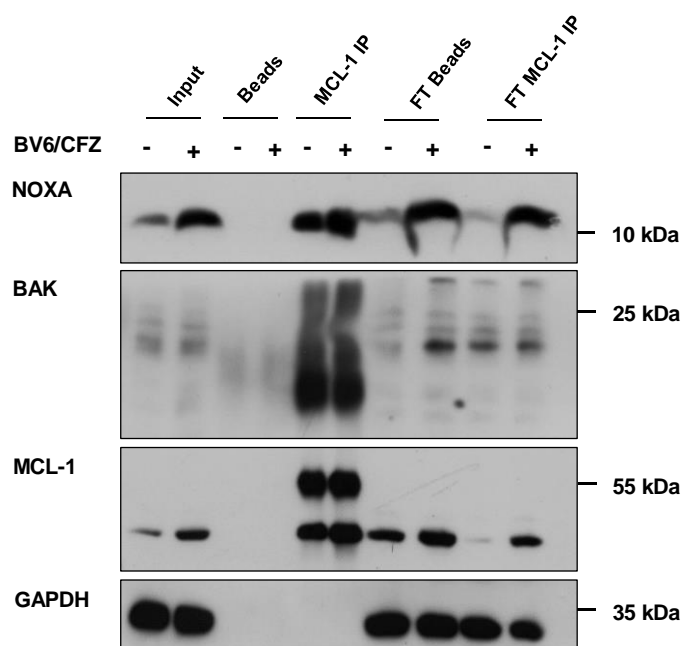


**Figure 28: Changes in MCL-1 interaction partner upon BV6/CFZ treatment in RIVA and U2932 cells**

**A** RIVA cells were treated for 12 hours with BV6 and CFZ (3 µM BV6, 8 nM CFZ) and **B** U2932 cells were treated for 18 hours with BV6 and CFZ (2 µM BV6, 5 nM CFZ). Interaction partner of MCL-1 were identified by MCL-1 immunoprecipitation using anti-MCL-1 antibody. Detection of indicated proteins was carried out by Western blotting. GAPDH served as loading control.

### 5.7.3    Changes in NOXA interaction partner upon BV6/CFZ treatment

The pro-apoptotic protein NOXA mostly binds to its anti-apoptotic partner MCL-1, but it has been reported that NOXA can also bind to BCL-2 or BCL-xL [193, 194]. Furthermore, it is described that NOXA can directly interact with BAX and BAK during induction of apoptosis [195, 196]. Therefore, we investigated if the unbound NOXA that we detected in the MCL-1 immunoprecipitation, may interact with other anti-apoptotic BCL-2 proteins or with BAX and BAK. In RIVA cells we could not detect any interaction between NOXA and BAK (Figure 29). In the U2932 cells we observed a slight interaction of NOXA and BAK, which increased upon BV6/CFZ treatment (Figure 29). However, there was no interaction of NOXA with BCL-2 or BCL-xL in the U2932 cells (Figure 29).

NOXA seems to play an important role for BV6/CFZ-induced cell death, but the molecular mechanism how NOXA contributes to BAX and BAK activation requires further characterization.

**A**
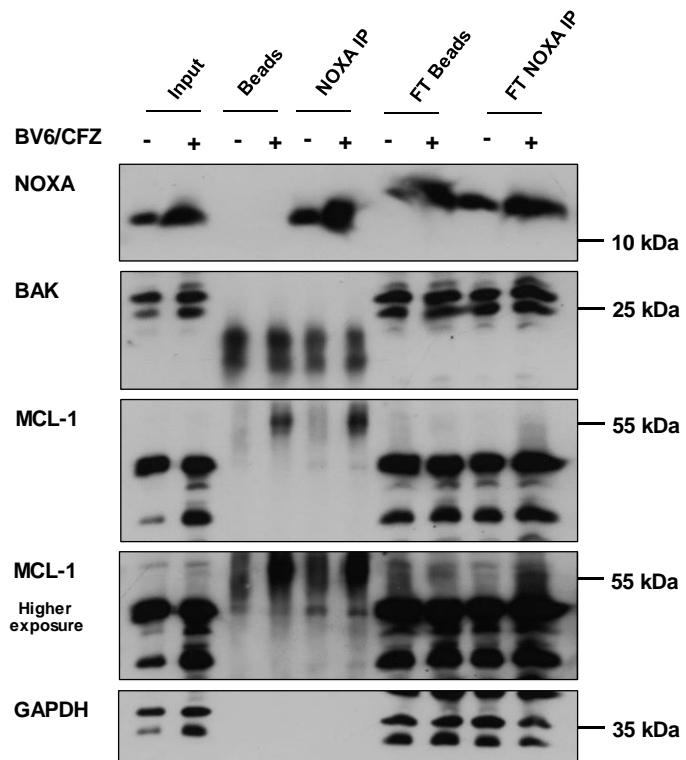
**B**
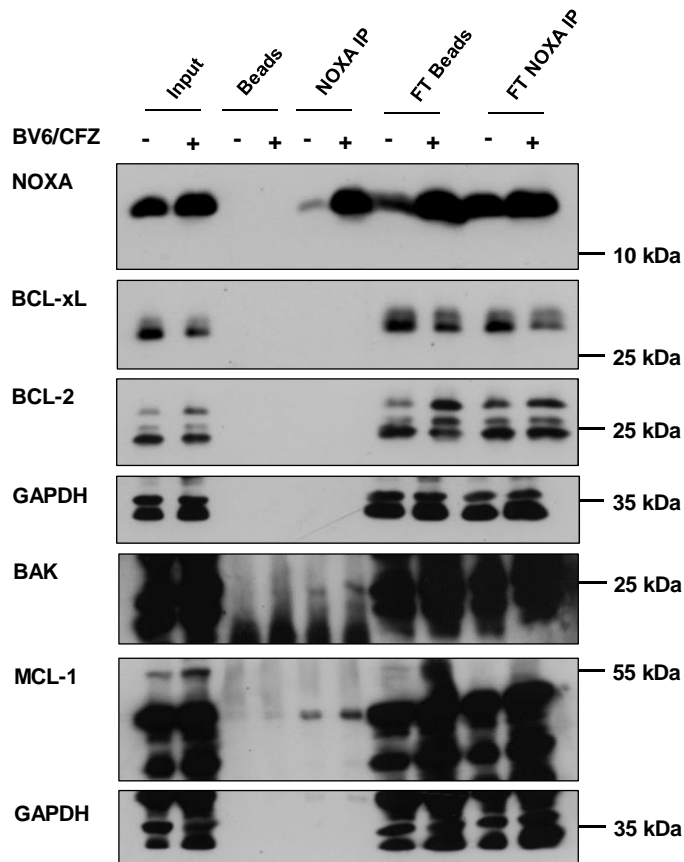


**Figure 29: Changes in NOXA interaction partner upon BV6/CFZ treatment in RIVA and U2932 cells**

**A** RIVA cells were treated for 12 hours with BV6 and CFZ (3 μM BV6, 8 nM CFZ) and **B** U2932 cells were treated for 18 hours with BV6 and CFZ (2 μM BV6, 5 nM CFZ). Interaction partner of NOXA were identified by NOXA immunoprecipitation using anti-NOXA antibody. Detection of indicated proteins was carried out by Western blotting. GAPDH served as loading control.

## 5.8    Involvement of IAPs and caspase-8 in BV6/CFZ-mediated cell death

### 5.8.1    Role of cIAP1/2 and XIAP for BV6/CFZ-mediated cell death

To further elucidate the role of BV6 in BV6/CFZ-mediated cell death, we analyzed the involvement of XIAP inhibition, which could also play an important role for Smac mimetic-mediated cell death induction [103]. Therefore, we next investigated the role

of XIAP inhibition in our system by genetic silencing of XIAP followed by CFZ treatment. Knockdown of XIAP followed by CFZ treatment could mimic BV6/CFZ treatment in U2932 cells, whereas it had no effect on cell death in RIVA cells (Figure 30).

**A**
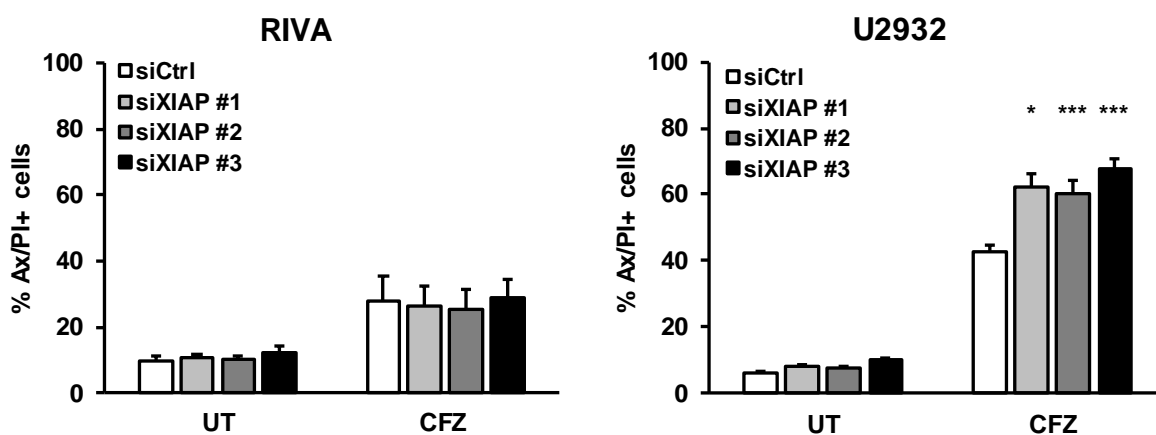


**B**
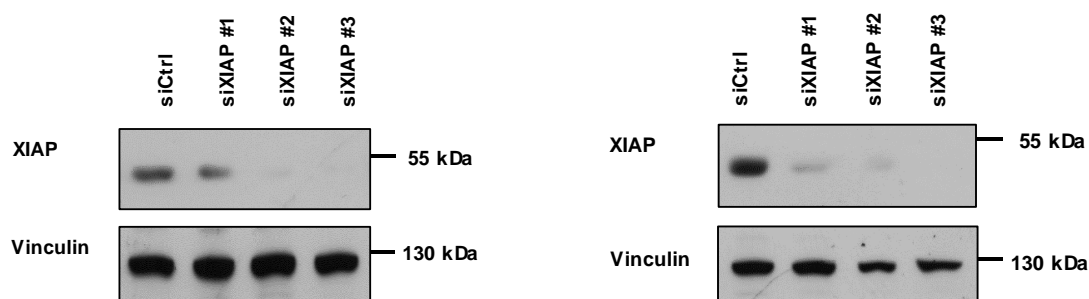


**Figure 30: XIAP is important for BV6/CFZ-mediated cell death in U2932 cells**

**A** Depletion of XIAP using siRNA-mediated gene silencing was performed prior to treatment with 8 nM CFZ (RIVA) for 18 hours or 10 nM CFZ (U2932) for 24 hours. Non-targeting siRNA (siCtrl) were used as control. Cell death was assessed by Annexin V-FITC/PI double staining and flow cytometry. Data are shown as mean and SEM of three independent experiments performed in triplicates. Significances are calculated against CFZ treated siCtrl cells. * $p < 0.05$, *** $p < 0.001$. **B** Expression level of XIAP was analyzed by Western blotting and Vinculin served as loading control. Representative blots of at least three independent experiments are shown.

To elucidate the role of cIAP1 and 2 for BV6/CFZ-mediated cell death, we performed siRNA-based double knockdown experiments to diminish protein expression. Reduction of the level of both cIAP proteins and subsequent treatment with CFZ could mimic BV6/CFZ treatment in RIVA cells in one siRNA combination (Figure 31). In

U2932 cells double knockdown of cIAP1/2 could not mimic BV6/CFZ treatment, however, genetic silencing of cIAP proteins was not successful in this cell line (Figure 31). Together, this set of experiments indicate that different IAPs play a role in BV6/CFZ-mediated cell death dependent on the different cell line.

**A**
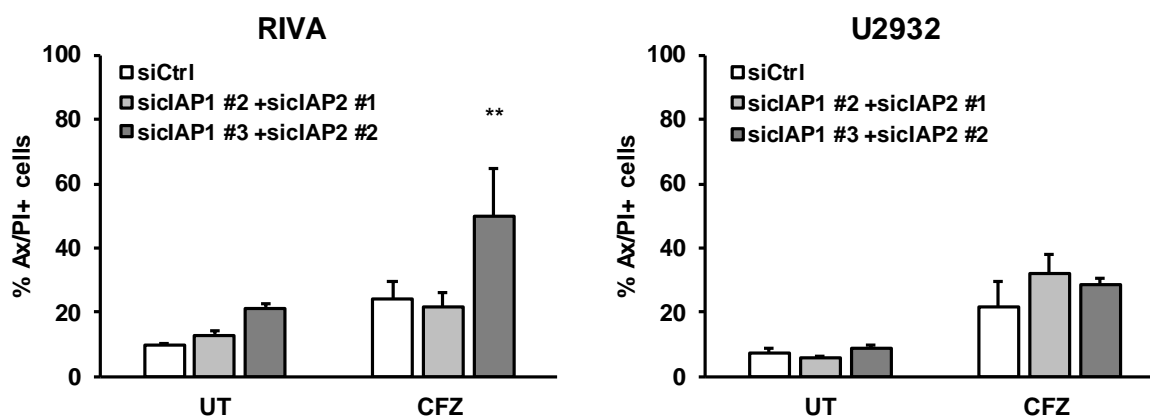


**B**
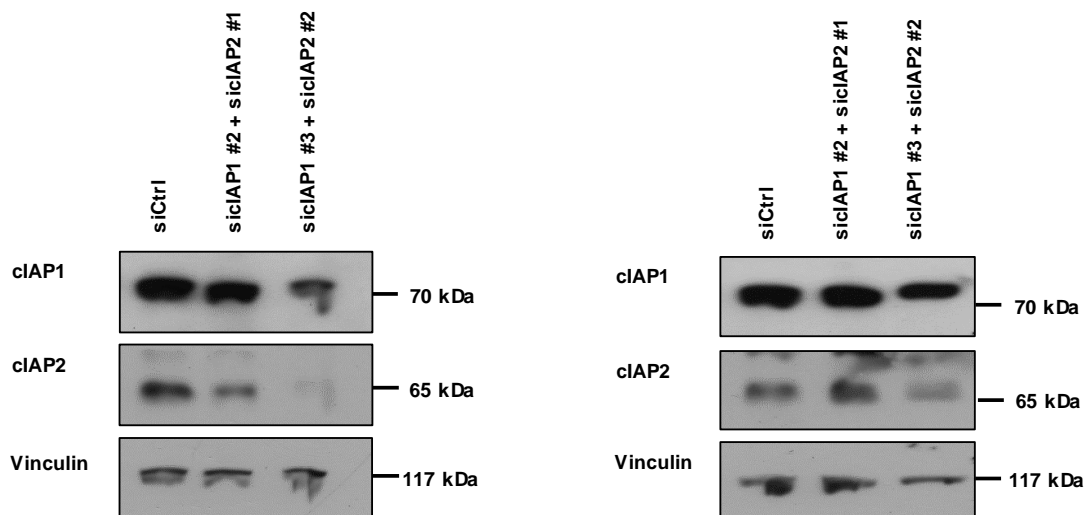


**Figure 31: cIAP1/2 seems to be important for BV6/CFZ-mediated cell death in RIVA cells**

**A** Depletion of cIAP1/2 using siRNA-mediated gene silencing was performed prior to treatment with 8 nM CFZ (RIVA) for 18 hours or 10 nM CFZ (U2932) for 24 hours. Non-targeting siRNA (siCtrl) were used as controls. Cell death was assessed by Annexin V-FITC/PI double staining and flow cytometry. Data are shown as mean and SEM of three independent experiments performed in triplicates. Significances are calculated against CFZ treated siCtrl cells. ** $p < 0.01$. **B** Expression level of cIAP1/2 was analyzed by Western blotting and Vinculin served as loading control. Representative blots of at least three independent experiments are shown.

### 5.8.2    Role of caspase-8 for BV6/CFZ-mediated cell death

After we could detect different roles of IAPs for BV6/CFZ-induced cell death, we next analyzed if caspase-8 is important for the induction of cell death as cIAP depletion can promote formation of the ripoptosome comprising of RIPK1, RIPK3, FADD, FLIP$_L$ and caspase-8 and leading to the induction of cell death [68-70]. Indeed, reduction of caspase-8 protein level by genetic silencing diminished BV6/CFZ-induced cell death in RIVA cells (Figure 32). Reduction of cell death only occurred with siRNA construct #3, which correlated with knockdown efficiency (Figure 32). In U2932 cells we detected no significant reduction in BV6/CFZ-mediated cell death upon genetic silencing of caspase-8 (Figure 32). These experiments indicate that caspase-8 has a functional role for BV6/CFZ-mediated cell death, at least in the RIVA cell line.

**A**
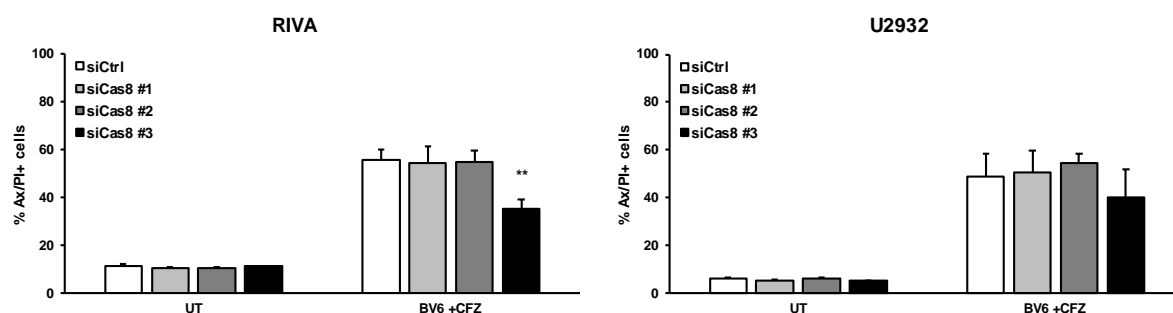


**B**
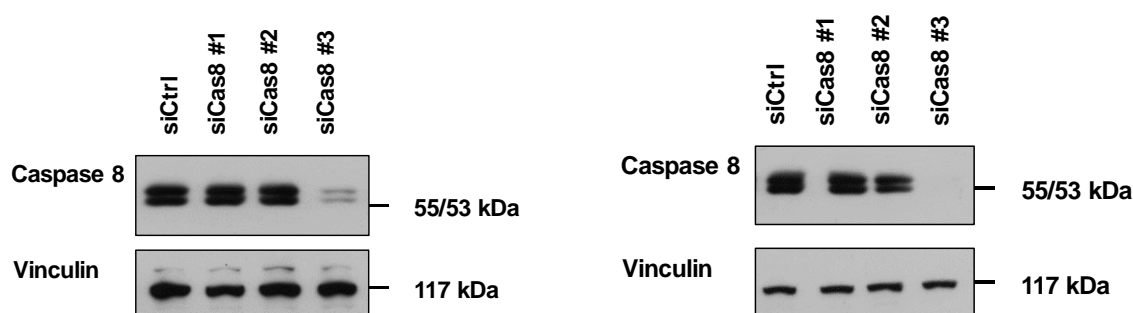


**Figure 32: Caspase-8 is important for BV6/CFZ-mediated cell death in RIVA cells**

**A** Depletion of caspase-8 using siRNA-mediated gene silencing was performed prior to treatment with 3 µM BV6+ 8 nM CFZ (RIVA) for 18 hours or 2 µM BV6 +5 nM CFZ (U2932) for 24 hours. Non-targeting siRNA (siCtrl) were used as control. Cell death was assessed by Annexin V-FITC/PI double staining and flow cytometry. Data are shown as mean and SEM of three independent experiments performed in triplicates. Significances are calculated against BV6+CFZ treated siCtrl cells. ** $p < 0.01$. **B** Expression level of caspase-8 was analyzed by Western blotting and Vinculin served as loading control. Representative blots of at least three independent experiments are shown.

## 5.9 Involvement of ROS in BV6/CFZ-mediated cell death

### 5.9.1 BV6/CFZ treatment induces ROS production prior to cell death

Since proteasome inhibitors are reported to induce the generation of ROS [127, 197], we next investigated if BV6/CFZ treatment induce ROS production. Mitochondrial ROS was measured by the fluorescent dye Mitosox and overall ROS by DCF and CellRox staining followed by flow cytometry analysis. To ensure that ROS production was prior to cell death, ROS measurement was performed before cell death induction (cell death

< 25%) (Figure 33). Interestingly, staining for mitochondrial ROS by Mitosox revealed a significant increase in ROS production after treatment with BV6 and CFZ in both cell lines (Figure 33). Furthermore, CellROX staining also showed a significant increase after BV6/CFZ treatment in both cell lines, indicating ROS production prior to cell death (Figure 33). In summary, these data indicate that BV6/CFZ treatment induced ROS production in RIVA and U2932 cells prior to cell death.

**A**
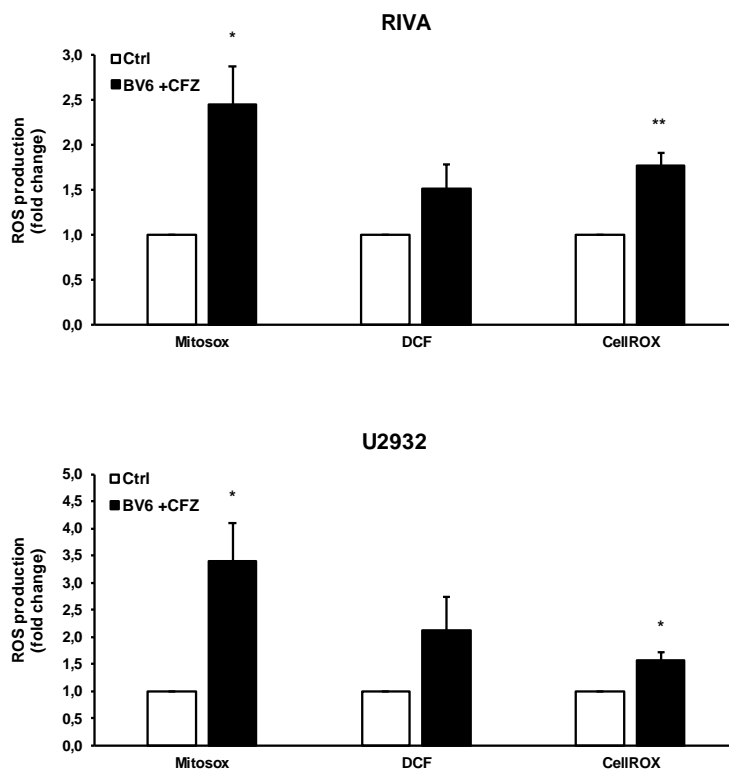
**B**
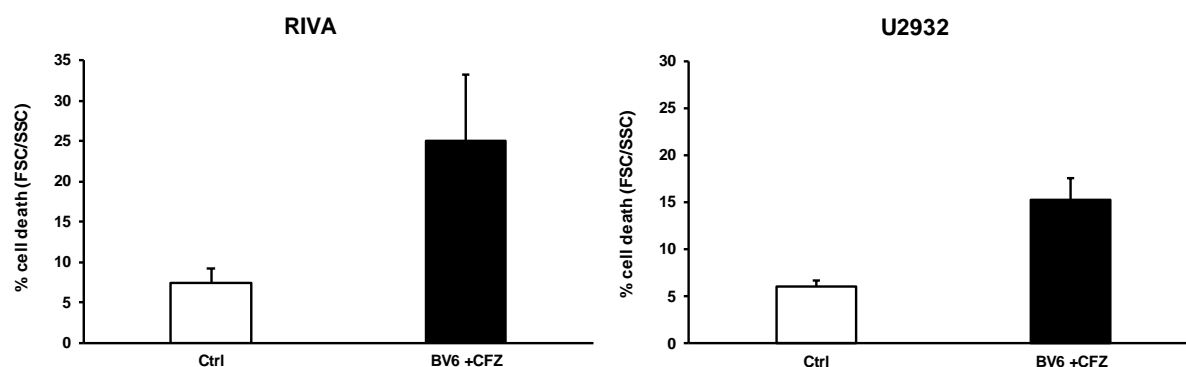


**Figure 33: ROS production after BV6/CFZ treatment occurs prior to cell death**

RIVA and U2932 cells were treated for 15 hours with BV6 and CFZ (RIVA: 3 µM BV6, 8 nM CFZ, U2932: 2 µM BV6, 5 nM CFZ). **A** ROS production was determined by flow cytometry in the living cell population by FSC/SSC analysis and the fluorescent dyes Mitosox, DCF or CellROX. **B** Cell death was assessed by FSC/SSC analysis. Results are shown as fold changes to Ctrl as mean and SEM of three independent experiments performed in triplicates. * $p < 0.05$, ** $p < 0.01$.

## 5.9.2    ROS production contributes to BV6/CFZ-induced cell death

Since, we detected an increase in ROS levels after BV6/CFZ treatment, we further analyzed if this increase in ROS production contributes to cell death induction. Therefore, we pre-treated RIVA and U2932 cells with different ROS scavengers (MnTBAP, GSH, α-Toc, NAC) before BV6/CFZ treatment. To confirm that the ROS scavengers are functional, we used RSL3 treatment as positive control, which is described to induce ROS dependent cell death by inhibiting GPX4, an antioxidant enzyme.[198]. Indeed, we detected a reduction of cell death upon MnTBAP pre-treatment in RIVA and U2932 cells (Figure 34), which is in line with the high induction of mitochondrial ROS (Figure 33), because MnTBAP is a manganese superoxide dismutase (MnSOD) mimetic and MnSOD an antioxidant enzyme, which is localized in the mitochondrial matrix [199]. Furthermore, we revealed a reduction of cell death after α-Toc pre-treatment followed by BV6/CFZ treatment in the U2932 cell line (Figure 34). RSL3 induced cell death could be rescued with GSH, α-Toc and NAC in both cell lines and confirmed efficiency of ROS scavengers (Figure 34).

**A**
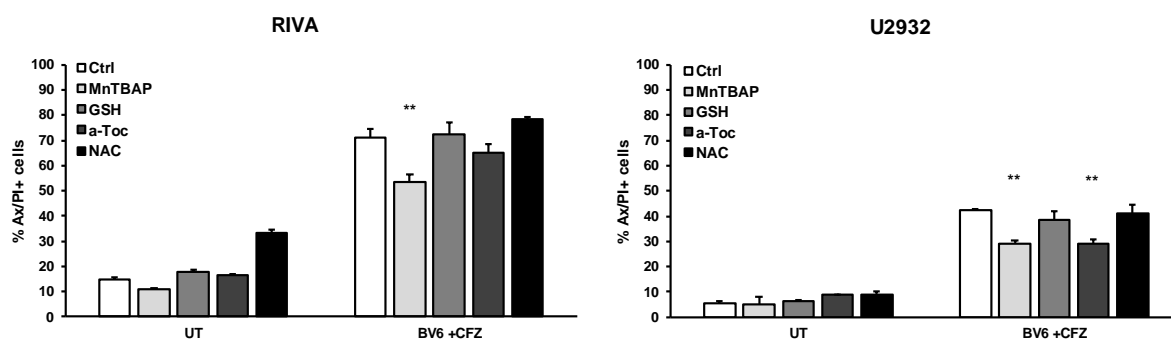


**B**
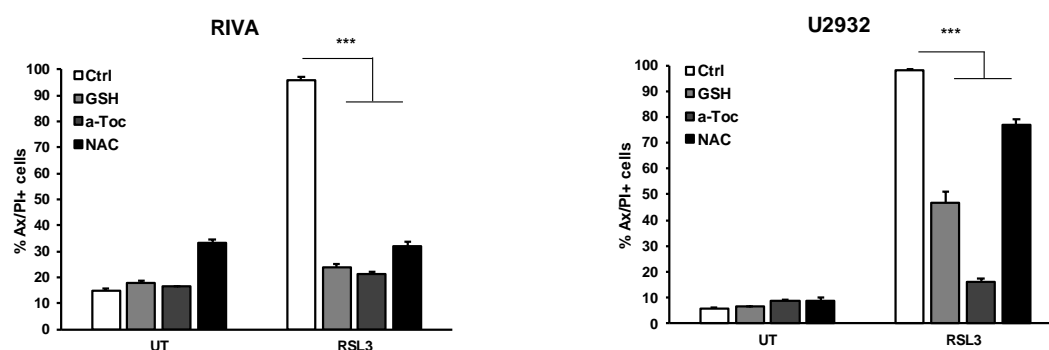


**Figure 34: ROS scavengers partially rescue BV6/CFZ-induced cell death**

RIVA and U2932 cells were 1 hour pre-treated 150 µM MntBAP, 10 mM NAC, 2,5 mM GSH or 25 µM (U2932)/ 50 µM (RIVA) α-Tocopherol. **A** After pre-treatment RIVA cells were treated with 3 µM BV6 and 8 nM CFZ and U2932 cells were treated with 2 µM BV6 and 5 nM CFZ for 18 hours. **B** After pre-treatment RIVA cells were treated with 75nM and U2932 cells with 1µM RSL3 for 18 hours. Cell death was assessed by Annexin V-FITC/PI double staining and flow cytometry. Data are shown as mean and SEM of 2-4 independent experiments. ** $p < 0.01$, *** $p < 0.001$.

These experiments indicate that mitochondrial ROS may play a role in BV6/CFZ-induced cell death in RIVA and U2932 cells, but overall ROS production only plays a minor role and is not required for BV6/CFZ-mediated cell death.

# 6        Discussion

## 6.1       BV6/CFZ treatment induced cell death in a panel of DLBCL cell lines

### 6.1.1      Smac mimetic-mediated reduction of cell viability in DLBCL

IAPs play an important role for the development and treatment of DLBCL as copy number gains of cIAP1/2 as well as increased expression levels of cIAP1/2 were identified in DLBCL [93]. Furthermore, high expression of XIAP correlates with poor outcome in DLBCL patients [176]. Therefore, targeting IAPs with Smac mimetics provide a possible treatment strategy for DLBCL. Here we show that the Smac mimetic BV6 was efficient in reducing cell viability in different subtypes of DLBCL. These results were in line with other studies, which also reported a cytotoxic effect of Smac mimetics on different tumor cells including DLBCL cell lines and cultured lymphoma cells of patients with DLBCL [180, 200-202]. Chauhan et al. showed effective induction of cell death in multiple myeloma cell lines as well as in primary patient samples with the Smac mimetic LBW242 [180]. Another study performed by Ward and colleagues used the DLBCL cell line WSU-DLCL2, which has a high basal cIAP2 expression, to demonstrate the effectiveness of the Smac mimetic ASTX660 to antagonize cIAP1 and cIAP2 and showed reducing effects on cell viability in melanoma cell lines [201]. Cillessen et al. treated DLBCL patient samples with a XIAP antagonist (1396-12) and showed induction of apoptosis in 16 of 20 tested samples [200]. Runckel and colleagues demonstrated single toxicity of the Smac mimetic LCL-161, which antagonize cIAP1/2 and XIAP, at mircomolar concentrations in ABC and GCB DLBCL [202]. Furthermore, Yang and colleagues reported a selective toxicity of the Smac mimetic Birinapant for ABC DLBCL cell lines compared to GCB cell lines [93]. In our study, three out of six GCB cell lines (OCI-LY1, RCK8, U2946) were less sensitive to BV6 treatment, but comparison of the IC50 values showed no significant difference in

BV6 sensitivity between ABC and GCB, which is in contrast to the results reported by Yang et al.

### 6.1.2 Reduction of cell viability by proteasome inhibition in DLBCL

The proteasome plays an important role for malignant cells as they are highly proliferating cells with high protein expression and protein turnover [118-120]. In line with this property pre-clinical studies could show that cancer cells were more vulnerable to proteasome inhibition than non-malignant cells. Masdehors et al. demonstrated that the proteasome inhibitor lactacystin induces apoptosis in human chronic lymphocytic leukemia (CLL) cells but had no effect on normal lymphocytes [121] and Hideshima and colleagues observed that multiple myeloma cells were more sensitive to the proteasome inhibitor BTZ than normal PBMCs [122]. In our system, treatment with the second generation proteasome inhibitor CFZ dose-dependently decreased cell viability in all tested DLBCL cell lines at nanomolar concentrations. These results were supported by other studies, which also showed a sensitivity of lymphoma lines as well as primary patient samples towards CFZ [140, 141, 202].

### 6.1.3 Smac mimetics and proteasome inhibitors cooperated to induce cell death in DLBCL

Combination of the Smac mimetic BV6 with the proteasome inhibitor CFZ resulted in a synergistic reduction of cell viability in all tested DLBCL cell lines and cooperated to induce cell death in two exemplary cell lines (RIVA, U2932). This synergistic drug interaction was confirmed by calculation of CI value as well as Bliss score. Synergistic reduction of cell viability was also observed with BV6 in combination with two other proteasome inhibitors IXA and OPR. These experiments show that the observed effect is not limited to one compound and highlights the general efficiency of Smac mimetics with proteasome inhibitors to reduce cell viability in DLBCL.

The potential of Smac mimetics in combination with chemotherapeutic agents or targeted drugs aiming to improve their clinical application has already been shown in pre-clinical studies in different types of cancer [177, 178, 203-208]. Beside pre-clinical studies also clinical trials evaluate the potential of Smac mimetic combination

treatment in several types of cancer including lymphomas and solid tumors. Moreover, different studies demonstrated synergistic interaction of CFZ with BCL-2 inhibitors or HDAC inhibitors in DLBCL cells [142, 143]. The rationale behind CFZ combination treatment is strengthen by further preclinical studies demonstrating a synergistic interaction with chemotherapeutic agents [144] as well as with a panel of different cytotoxic substance including BCL-2 inhibitors [145-149], CDK inhibitors [150], histone deacetylase inhibitors [151-155], heat shock protein inhibitors [156] and TRAIL [157-159]. Certain clinical trials already demonstrated a promising activity of BTZ in relapsed/refractory DLBCL patients [5, 209, 210] and combination treatment of CFZ with chemotherapeutic agents or targeted drugs are currently under evaluation in phase I and II clinical trials in DLBCL, underlining the clinical relevance of proteasome inhibitor treatment in DLBCL. These previous studies highlight the potential of combination treatment of Smac mimetics and proteasome inhibitors. Until now, the combined treatment of Smac mimetics with proteasome inhibitors has been investigated only in selected cases e.g. in multiple myeloma [180], melanoma [181] or non-Hodgkin lymphomas [179, 202]. All these pre-clinical studies demonstrated cooperative effects of Smac mimetics with proteasome inhibitors in multiple myeloma, melanoma or NHL, which is in line with our results in DLBCL, but they did not go further into detail for the underling mechanism behind this combinatory effect. Only the previous study of our lab from Bhatti et al. demonstrated a necroptotic cell death mechanism after treatment with BV6 and BTZ in Burkitt's lymphoma [179].

## 6.2 Induction of apoptotic cell death is mediated via the mitochondria

### 6.2.1 BV6/CFZ combination treatment induced caspase-dependent cell death

At the level of cell death execution, we detected cleavage of caspase-3 and -9 as well as of caspase-8 after BV6/CFZ co-treatment, while both single agents only had minor or no effects on caspase activation. Caspase activation assay, as a second readout, revealed activation of caspase-3 and -7 after BV6/CFZ combination treatment and only minor caspase activation upon BV6 and CFZ single treatment. To confirm the

importance of caspase cleavage as the major executive apoptotic feature, we used the pan-caspase inhibitor zVAD.fmk. Inhibition of caspases resulted in a complete reduction of BV6/CFZ-induced cell death in both cell lines. These experiments clearly showed that the combination of BV6 and CFZ induced caspase activation and caspase-dependent apoptotic cell death in DLBCL cells.

## 6.2.2    BV6/CFZ co-treatment induced BAX/ BAK activation and loss of MMP

Caspase-3,-7 and -9 are usually activated downstream of mitochondrial signaling initiated by the release of mitochondrial intermembrane space proteins such as cytochrome c or Smac into the cytosol [38, 51]. The release of intermembrane space proteins involves pore formation of the outer mitochondrial membrane and loss of MMP [50]. Upon BV6/CFZ co-treatment we detected an activation of the two pore forming proteins BAX and BAK, which are key mediators of the intrinsic apoptotic pathway. In line with BAX and BAK activation we revealed loss of MMP after BV6/CFZ combination treatment.

Loss of MMP is another typical feature of intrinsic apoptosis and tightly controlled by the balance between pro- and anti-apoptotic BCL-2 proteins [40]. If the balance of pro- and anti-apoptotic proteins shifts towards the pro-apoptotic side, the pro-apoptotic multidomain proteins BAX and BAK mediate disruption of the mitochondrial membrane integrity resulting in loss of MMP [40]. Other studies could also demonstrate that treatment with proteasome inhibitors induced changes in mitochondria membrane potential manifested by a decrease in MMP [211] and dissipation of MMP [169, 171]. Furthermore, Gu and colleagues showed an upregulation of BAK upon CFZ exposure in Burkitt's lymphoma cell lines[141]. Moreover, in MCL cell lines treatment with BTZ also led to an activation of BAX and BAK indicated by their conformational changes [146]. These findings strengthen our assumption of mitochondria mediated apoptosis upon BV6/CFZ treatment.

## 6.2.3    BAX and BAK are important factors for BV6/CFZ-mediated apoptosis

Since we detected activation of BAX and BAK as well as loss of MMP, we further analyzed the functional role of BAX and BAK by genetic silencing of those two key

proteins of the intrinsic apoptosis pathway. Single knockdown of either BAX or BAK significantly reduced BV6/CFZ-mediated cell death in RIVA and U2932 cells. Simultaneous knockdown of BAX and BAK further decreased BV6/CFZ-induced cell death, indicating that RIVA and U2932 cells depend on both proteins for cell death induction. These results are confirmed by others, which showed a reduction of BTZ-mediated cytotoxicity upon BAX, BAK depletion [211]. In summary, BV6/CFZ-induced cell death requires mitochondrial apoptotic signaling mediated via BAX and BAK.

## 6.2.4    Role of BCL-2 proteins for BV6/CFZ-induced cell death

Mitochondria-mediated apoptosis is controlled by the distribution and interaction of pro- and anti-apoptotic BCL-2 proteins [39]. Since we found an apoptotic cell death that is mediated via the mitochondria, we hypothesized that BV6 and CFZ interfere with this distribution. Indeed, we detected a strong accumulation of the pro-apoptotic protein NOXA upon BV6/CFZ treatment in both cell lines, which is mostly attributed to the proteasome inhibitor, as NOXA belongs to the group of short lived proteins, which are normally degraded via the proteasome [212]. Besides NOXA accumulation, we detected an increase in BIM protein level in RIVA cells. Accumulation of NOXA and BIM upon proteasome inhibitor treatment was already reported by others [146, 167, 213], indicating that these observed changes are mainly referable to CFZ. Furthermore, we detected the caspase cleavage product of BID (tBID) after treatment with BV6/CFZ in both cell lines, which could indicate a crosstalk between extrinsic and intrinsic apoptotic signaling, since tBID lead to an activation of BAX and BAK and cytochrome c release [33, 34]. However, we did not further analyzed if BID processing is an initial trigger of mitochondrial dysfunction, initiated by receptor-mediated activation of caspase-8 or downstream of LOMMP and a feedback loop of caspase activation, since activation of caspase-3 and -7 also lead to an activation of caspase-8, which then could processes BID to tBID.

Interestingly, we found that BMF is cleaved by caspases in RIVA cells, indicated by a small BMF product (~15kDa) appearing after BV6/CFZ treatment, which disappeared again after addition of zVAD.fmk. DLBCL cell lines contain high BMF protein levels compared to other tumor cell lines and more variations of BMF isoforms. The CaspDB database is an online platform to predict caspase cleavage sites of human proteins.

For the human BMF protein the CaspDB database calculated six different possible caspase cleavage sites. Two of these predicted BMF cleavage products would have a size of 16.05 and 16.94kDa, respectably, which could fit to the cleavage product detected in RIVA cells after BV6/CFZ treatment with a size around 15kDa. Of note, the BH3 binding domain of BMF would be still intact and not affected by the cleavage in the two isoforms of 16.06 and 16.96kDa. Notably, cleavage of BMF by caspases has so far not been described. Since the BCL-2 protein is highly expressed in RIVA and U2932 cells compared to other DLBCL cell lines [192], we investigated changes in BCL-2 binding partners upon BV6/CFZ single and combination treatment. Interestingly, immunoprecipitation of BCL-2 revealed increased binding of a BMF isoform/cleavage product (15kDa) in RIVA and U2932 cells after single BV6 or CFZ treatment, which was more pronounced after combination treatment. Interaction of BMF with BCL-2 was already reported by others [214] confirming our detected interaction between BCL-2 and BMF. Cytoplasmic BMF is sequestered to myosin V motors by association with dynein light chain 2 (DLC2), which leads to stabilization of the BMF protein [214]. Upon a stress stimulus BMF can translocate from DLC2 to the mitochondria and interact with BCL-2, which is located on the outer mitochondrial membrane [214-216]. This interaction of BMF with BCL-2, which we also detected in our immunoprecipitation studies, could neutralizes the anti-apoptotic action of BCL-2, by liberating activator BH3-only proteins (i.e. BID, BIM) from BCL-2 to induce cell death [217]. Moreover, BMF could displaces pre-bound BAX from BCL-2, thereby leading to apoptotic cell death induction.

To confirm the hypotheses of BMF mediated induction of cell death further BCL-2 immunoprecipitation studies are needed. Furthermore, siRNA mediated knockdown experiments of BMF could elucidate a functional role of BMF for BV6/CFZ-induced cell death.

In this study we detected changes in the distribution of pro-apoptotic proteins, which could lead to an imbalance between pro-and anti-apoptotic proteins and therefore to the induction of apoptotic cell death. The revealed induction of pro-apoptotic NOXA protein is functionally relevant as knockdown of NOXA protein level with specific siRNAs, led to a significant reduction of cell death induced by BV6 and CFZ. An increase of NOXA protein level and NOXA-dependent apoptosis was also detected in CLL cells after BTZ treatment [218] and a study of Miller et al. in melanoma cells also

demonstrated an accumulation of NOXA as well as NOXA-dependent cell death upon ABT 737 (BH3-mimetic) and MG-132 (proteasome inhibitor) treatment [219]. Another study in melanoma cells showed that BTZ treatment led to an increase in NOXA levels at early time points (3 to 6 hours) after treatment and before disruption of the MMP [213]. This confirmed our observations of early accumulation of NOXA, starting around 4 hours after BV6/CFZ treatment, followed by loss of MMP at later time points around 15 to 18 hours.

The role of upregulated NOXA gene expression has been discussed in different studies that showed transcription-dependent [220] as well as transcription-independent [218] increase of NOXA protein after BTZ treatment. However, significantly increased NOXA gene expression was not detected after BV6 and CFZ single or combination treatment, indicating that increased NOXA levels are transcription-independent and attributed to accumulation of NOXA due to proteasomal inhibition by CFZ in this setting.

To further elucidate the mechanism how BCL-2 proteins contribute to cell death induction, we performed immunoprecipitation studies. Since, NOXA preferentially binds to its anti-apoptotic binding partner MCL-1, we investigated changes in NOXA binding to MCL-1 upon BV6/CFZ treatment. These experiments revealed that upon BV6/CFZ co-treatment NOXA is more bound to MCL-1 compared to untreated control cells. Since NOXA is constitutively bound to MCL-1, RIVA and U2932 cells are initially primed to undergo apoptosis. This priming for intrinsic apoptosis is enhanced by BV6/CFZ co-treatment further increasing NOXA protein levels leading to the hypothesis that increased NOXA levels may functionally inhibit and inactivate MCL-1. The ratio between NOXA and MCL-1 has already been shown to determine cell death or cell survival and higher NOXA levels compared to MCL-1 levels lead to a more likely induction of apoptosis [221, 222]. One possibility how NOXA contribute to apoptosis could be by displacement of pre-bound BIM and disruption of preformed BIM-MCL-1 complexes. BIM is a direct activator of BAX and BAK and, when released from anti-apoptotic binding partners, could promote cell death by directly inducing a conformational change and oligomerization of BAX and BAK [223]. Furthermore, NOXA could liberate pre-bound BAX or BAK from MCL-1 thereby inducing the mitochondrial apoptotic pathway [224, 225]. This hypothesis is supported by our MCL-1 immunoprecipitation experiments, which revealed that BAK may be less bound to MCL-1 in RIVA cells after BV6/CFZ treatment. Additionally, unbound NOXA itself could

function as a direct activator of BAX and BAK, thereby promoting intrinsic apoptosis, as suggested by a previous study [196]. This assumption is supported by our MCL-1 immunoprecipitation studies, which showed a lot of unbound NOXA beside increased NOXA-MCL-1 complexes. Moreover, we detected a slight increase in NOXA binding to BAK in U2932 cells after combination treatment. However, for more detailed and profound insights into the underling mechanism immunoprecipitation of BAK as well as BAX would be needed to reveal changed interactions between MCL-1 and BAX/BAK as well as NOXA and BAX/BAK. Another opportunity to analyze these protein interactions would be the use of a proximity ligation assay.

Other studies reported that NOXA can also bind to BCL-2 or BCL-xL [193, 194] but this was not the case in our system, as we did not detect any binding of NOXA to BCL-2 or BCL-xL.

### 6.2.5    BV6/CFZ treatment involved ROS production

As part of BV6/CFZ-mediated cell death we observed changes in mitochondria properties indicated by loss of MMP, as intact MMP is an indicator of functional mitochondria. Additionally, we observed a high induction of mitochondrial ROS upon BV6/CFZ treatment as well as an increase in overall ROS production prior to cell death.

Inhibition of the proteasome leads to an accumulation of unfolded proteins, which trigger endoplasmic reticulum (ER) stress [226, 227]. Sustained ER stress can cause cell death via different pathways including increased ROS production [228] and oxidative stress has been identified as a major mediator of proteasome inhibitor induced cytotoxicity in mantle cell lymphoma and multiple myeloma [146, 226, 229, 230]. Moreover, it has been reported that ROS can lead to opening of the permeability transition pore (PTP), which resulted in opening of the inner and outer mitochondrial membrane, followed by loss of MMP, cytochrome c release and cell death [231]. Since, we detected an increase in ROS levels prior to cell death and loss of MMP in our cell system, PTP opening by ROS could also contribute to mitochondria dysfunction. Experiments with ROS scavengers demonstrated that, if ROS play a role, mainly mitochondrial ROS contribute to BV6/CFZ-mediated cell death in RIVA and U2932 cells, as pre-treatment with a mitochondrial ROS scavenger reduced BV6/CFZ-

mediated cell death. ROS scavenging substances for cytosolic ROS had no until minor effects on cell death induction.

To further analyze the role of ROS for BV6/CFZ-mediated cell death it might be interesting to test weather ROS scavengers could reduce mitochondrial changes, i.e. loss of MMP. Moreover, involvement of the ER could be tested by detection of relevant ER stress proteins like CHOP, ATF-4 and GRP-78, as increased expression levels of these proteins were detected in BTZ-mediated apoptosis [197].

## 6.3 Role of IAPs for BV6/CFZ induced cell death

### 6.3.1 BV6/CFZ-induced cell death is independent of TNFα and NF-κB signaling

In this study, we revealed a rapid degradation of cIAP1/2 upon BV6 single and BV6/CFZ combination treatment. Degradation of cIAPs was accompanied by accumulation of NIK and activation of the non-canonical NF-κB signaling. Furthermore, we detected phosphorylation of IκBα, indicating a possible activation of canonical NF-κB signaling as well. Accumulation of NIK upon Smac mimetic treatment is well described [70, 232] and CFZ further enhanced NIK accumulation by inhibiting its proteasomal degradation. Moreover, it is described that NIK not only phosphorylates IKKα but could also phosphorylate IKKβ and p65 of the canonical NF-κB signaling pathway, thereby activating both the canonical and non-canonical NF-κB pathway [233, 234]. Nevertheless, activation of canonical NF-κB signaling could not be fully confirmed, because we did not detect any changes in IκBα protein levels, which could be explained by high reproduction (turnover) of NF-κB proteins mediated by the NF-κB signaling itself. Therefore, a kinetic with shorter time periods e.g. 5-10 min, could detect IκBα protein degradation. Furthermore, CFZ as proteasome inhibitor prevents degradation of IκBα.

Since, NIK is reported to have a pro-apoptotic function in a TNFR1 dependent manner [235], we analyzed the impact of NIK on cell death induction in our cell system.

However, NIK did not contribute to cell death induction, as genetic silencing of NIK did not reduce BV6/CFZ-mediated cell death. In line with NIK knockdown experiments, BV6/CFZ-induced cell death was independent of TNF$\alpha$ signaling, as neither treatment with the TNF$\alpha$ inhibitor Enbrel reduced BV6/CFZ-induced cell death nor did additional TNF$\alpha$ enhance cell death. These results are supported by other studies, which also showed a Smac mimetic induced cell death independent of TNF$\alpha$ or non-canonical NF-$\kappa$B signaling [236-238]. CIAP depletion by Smac mimetic can also stimulate ripoptosome formation and induction of apoptotic cell death independent of TNF$\alpha$ thus providing a possible explanation for a pro-apoptotic effect of cIAP degradation [239, 240]. The core components of the ripoptosome are RIPK1, FADD and caspase-8 and are negatively regulated by cFLIP$_L$, cIAP1, cIAP2 and XIAP [240]. BTZ is reported to down regulate cFLIP [241] and Smac mimetics antagonize cIAP1, cIAP2 and XIAP [70] building a rational for co-treatment of CFZ and BV6 to promote ripoptosome formation. Moreover, cIAP1 may be able to ubiquitylate caspase-3 and -7 leading to their proteasomal degradation [71], therefore cIAP1 depletion and proteasome inhibition may lead to a stabilization of caspase-3 and -7, which could further enhance induction of apoptosis.

Besides TNF$\alpha$ other death receptor ligands like TRAIL and FasL, which are NF-kB target gens as well [242-244], could induce activation of caspase-8 and induction of the apoptotic pathway [32]. To elucidate the role of TRAIL and FasL for BV6/CFZ-induced cell death, blocking antibodies of the ligands or siRNA-mediated downregulation of their corresponding receptors would give further insights into the underlying mechanism.

### 6.3.2    Cell context-dependent role of IAPs for BV6/CFZ-mediated cell death

Besides cIAP depletion the direct inhibition of caspases by XIAP downstream of mitochondria may play an important role for Smac mimetic mediated cell death induction [103, 104]. In this study, genetic silencing of XIAP followed by CFZ treatment could mimic BV6/CFZ treatment in U2932 but not in RIVA cells, indicating an important role for XIAP inhibition by BV6 for cell death induction in U2932 cells. Inhibition of XIAP leads to a liberation of caspase-3, -7 and -9 and contributes to apoptosis induction [59, 60]. U2932 cells contain a higher basal protein level of XIAP compared to RIVA cells,

which could explain why U2932 cells are more susceptible to XIAP downregulation or inhibition, indicating a BV6 dependent mode of action determined by basal IAP expression.

Interestingly, simultaneous knockdown of cIAP1 and cIAP2 protein level with specific siRNAs followed by CFZ treatment could mimic BV6/CFZ treatment in RIVA but not in U2932 cells, indicating an important role of cIAPs for BV6/CFZ-mediated cell death in RIVA cells. In line with cIAP knockdown experiments, genetic silencing of caspase-8 could only significantly reduce BV6/CFZ-mediated cell death in RIVA cells. As discussed in section 6.3.1 cIAP depletion promotes ripoptosome formation, which requires active caspase-8. It seems that in RIVA cells BV6/CFZ-mediated cell death partially depend on cIAP depletion and ripoptosome formation including active caspase-8, while U2932 cells depend more on XIAP and its inhibitory function on caspase-3, -7, and -9.

To further support these assumptions, immunoprecipitation studies of caspase-8 to confirm ripoptosome formation after BV6/CFZ treatment as well as immunoprecipitation of XIAP to approve displacement of caspases would strengthen these findings.

## 6.4    Efficacy of the combination of Smac mimetic and proteasome inhibitors in DLBCL

Classification of DLBCL on the basis of gene expression and cell of origin studies initially revealed three different subtypes: ABC, GCB and PMBL [7-10]. However later analyses based on genomic and transcriptomic analysis revealed additional subtypes of DLBCL (MCD, BN2, N1, EZB) [25] and further highlights the heterogeneous biology of this disease. Although, all tested DLBCL cell lines tested in this study belong to different subtypes of DLBCL, all cell lines responded to the combination of Smac mimetic (BV6) and proteasome inhibitor (CFZ, IXA, OPR) with induction of cell death or decrease in cell viability. These results show that the treatment efficacy is not dependent on a specific subtype of DLBCL and maybe applicable in all cases.

The combination of Smac mimetics with proteasome inhibitors has so far only been investigated in selected cases e.g. in multiple myeloma [180], melanoma [181] or non-Hodgkin lymphomas [179, 202]. Most of these studies used the reversible first generation proteasome inhibitor BTZ in combination with Smac mimetic [179-181] and revealed caspase dependent as well as caspase independent cell death, indicating that induced cell death is context dependent. Moreover, Runckel and colleagues could show that the Smac mimetic LCL-161 enhances the cytotoxic effect of CFZ in ex vivo lymphoma biopsy samples [202]. These studies as well as our study are in line with previous evidence showing that Smac mimetics synergistically enhance chemotherapeutics, epigenetic drugs, death receptor ligands and other cytotoxic drugs [106, 178, 203, 245, 246] strengthen the assumption of Smac mimetic combination treatment as therapeutic approach.

However, the molecular mechanism behind synergistic cell death induction of Smac mimetics and proteasome inhibitors was not elucidated so far. Our study revealed that the combination of BV6 and CFZ synergistically induced caspase dependent cell death mediated primarily via the mitochondria. Accumulation of NOXA, attributed to proteasome inhibition, followed by enhanced binding of NOXA to its anti-apoptotic binding partner MCL-1, shifts the balance of anti-apoptotic towards pro-apoptotic proteins inducing BAX and BAK activation and perturbation of the MMP resulting in caspase activation. Treatment with the Smac mimetic BV6 led to a rapid degradation of cIAP1/2 and activation of caspases, which could be mediated via ripoptosome formation. Furthermore, inhibition of XIAP by BV6 may liberate caspase-3,-7 and -9 from XIAP sequestration further enhancing activation of caspases. We hypothesize that CFZ induces cell death via the mitochondrial pathway and BV6 contributes to cell death induction via ripoptosome formation and activation of caspases downstream of the mitochondria. In summary, CFZ and BV6 may act in concert to induce cell death by affecting different sections of the apoptotic cell death pathway.

# 7 Outlook

Although we already gave a comprehensive insight into the molecular mechanisms of cell death induction in DLBCL cells upon treatment with BV6 in combination with CFZ, there are some points that can be further addressed or examined in more detail. Questions or ideas for additional experiments, which arose during interpretation of the results, are listed in the following paragraphs.

Smac mimetics and proteasome inhibitors are currently under evaluation in several combination treatments in clinical trials, underlining their clinical relevance in co-treatment strategies in general. To further strengthen the potency of the combination of Smac mimetics and proteasome inhibitors, experiments with other Smac mimetics like Birinapant or ASTX660 in combination with different proteasome inhibitors (CFZ, IXA, OPR) could be conducted. Furthermore, testing of BV6 and CFZ in primary samples of DLBCL patients could reveal if the combination is effective in killing primary cells of different subtypes as we detected in the cell line system. For clinical implications it would also be important to test weather BV6/CFZ treatment as any effect on non-malignant cells i.e. PBMCs.

We could show an involvement of mitochondria for BV6/CFZ-mediated cell death but a clear proof for cytochrome c release is missing. Furthermore, it would be interesting to investigate if other factors than cytochrome c are released from mitochondria following BV6 and CFZ treatment and which role they may play in promoting cell death.

In addition, it would also be of interest if other pro-apoptotic BCL-2 proteins beside NOXA play a functional role in cell death induction after BV6/CFZ treatment. Since, BIM, BMF and tBID protein level increased after BV6/CFZ combination treatment it would be worth to investigate a genetic approach to consolidate if they also contribute to cell death induction.

Furthermore, as mention in 6.3.2 the exact involvement of IAPs for induction of cell death has to be clarified by additional immunoprecipitation studies to verify

ripoptosome formation after BV6/CFZ treatment as well as displacement studies to check for caspase displacement of XIAP by BV6 treatment.

Another interesting point which was not considered in this study is the involvement of ER stress upon proteasome inhibitor treatment and its involvement in cell death induction, since different studies could show an induction of ER stress accompanied by ROS production and induction of apoptosis after proteasome inhibitor treatment [197, 226, 230, 247].

Finally, an *in vivo* model would also support the results made in this study, regarding Smac mimetics and proteasome inhibitors as an apoptotic stimulus to antagonize tumor progression in DLBCL.

# 8      Zusammenfassung

Maligne Lymphome sind Krebserkrankungen, die von den Zellen des lymphatischen Systems ausgehen und in Hodgkin sowie Non-Hodgkin Lymphome (NHL) unterteilt werden. NHL kommen deutlich häufiger vor und 90% aller diagnostizierten Lymphome gehören zu der Gruppe der NHL. Das diffuse großzellige B-Zell Lymphom (DLBCL, *diffuse large B-cell lymphoma*) ist der häufigste Subtyp des NHL mit 40% aller neu diagnostizierten NHL Fälle. Die Tumorerkrankung tritt häufig im Alter von 60 bis 70 Jahren auf und ist eine sehr aggressive Tumorentität, die sich durch schnell wachsende Tumore in Lymphknoten, Knochenmark, Milz, Leber und anderen Organen auszeichnet. DLBCL ist eine sehr heterogene Erkrankung die anfänglich in drei verschiedene Gruppen klassifiziert wurde: aktivierter B-Zell Typ (ABC, *activated B-cell*), Keimzentrum B-Zell Typ (GCB, *germinal center B-Cell*) und mediastinaler großzelliger B-Zell Typ (PMBL, *primary mediastinal B-cell lymphoma*). Diese drei Subtypen wurden auf Grund von Genexpressionsprofilen sowie Ursprungsstudien verstellt. Zu dieser Klassifizierungen wurden später noch einmal vier weitere Subgruppen anhand von gemeinsamen genomischen Modifikationen identifiziert (MCD, BN2, N1, EZB). Diese zusätzliche neue Klassifizierung verdeutlicht noch einmal die Heterogenität von DLBCL Tumoren und die Notwendigkeit für neue gezielte Therapieansätze, da ca. 40% aller DLBCL Patienten unter Standardtherapie ein Rezidiv entwickeln oder gar keine Remission erreichen. Die Standardtherapie für DLBCL setzt sich derzeit aus einer Kombination von Immun- und Chemotherapie zusammen (R-CHOP). Die Chemotherapie besteht aus Cyclophosphamid; Doxorubicin; Vincristin; Prednison (CHOP, *cyclophosphamide, hydroxyldaunorubicin, vincristine, prednisone*) und wird durch eine Immuntherapie mit dem anti-CD20 Antikörper Rituximab (R) ergänzt.

Das Ansprechen eines Tumors auf eine Therapie hängt unter anderem von der Aktivierbarkeit seines Zelltodprogrammes ab, welches jedoch häufig durch Mutationen und Dysregulationen gestört ist und Tumorzellen daher unempfindlicher gegenüber Zelltodstimulatoren macht. Einer der am besten charakterisierten Zelltodmechanismen

ist die Apoptose, welche sich in zwei unterschiedliche Signalwege, den extrinsischen oder auch Todesrezeptorsignalweg und den intrinsischen auch mitochondrialen Signalweg einteilen lässt. Schlussendlich führen beide Signalwege zur Aktivierung von Caspasen und der Exekution von Zelltod. Die Initiierung des extrinsischen Signalweges wird über eine Liganden-Rezeptor-Interaktion von sogenannten Todesrezeptoren vermittelt. Nachdem der entsprechende Ligand (z.B. Fas, TRAIL) an den Rezeptor gebunden hat, wird ein intrazellulärer Komplex namens DISC (DISC; *death-inducing signaling complex*) gebildet. Dieser Komplex setzt sich aus FADD, Caspase-8 und cFLIP zusammen. Die Bildung des DISC führt zu einer Aktivierung von Caspase-8, die daraufhin das Signal für die Ausführung des Zelltods über zwei verschiedene Wege weitergeben kann. Zum einen kann aktivierte Caspase-8 als Initiatorcaspase weitere Effektorcaspasen wie Caspase-3 und -7 aktivieren und dadurch das Voranschreiten des Zelltods weiter begünstigen. Zum anderen kann aktivierte Caspase-8 BID zu truncated (gekürzt) BID prozessieren, was zu einer Translokation von tBID zu den Mitochondrien führt und eine Aktivierung von BAX und BAK bewirkt. Dies hat zu Folge, dass Cytochrom c aus den Mitochondrien in das Zytoplasma ausgeschüttet wird und weitere Initiator- und Effektorcaspasen aktiviert werden. Die intrinsische oder mitochondriale Apoptose wird über verschiedene Stressfaktoren wie Chemotherapeutika, DNA schädigende Substanzen, ionisierende Strahlung, Wachstumsfaktorenmangel oder zellulären Stress ausgelöst. Durch die Verteilung der BCL-2 Proteine werden das Membranpotential und die Integrität der äußeren Mitochondrienmembran kontrolliert. Die Familie der BCL-2 Proteine besteht aus drei verschiedenen Gruppen: den anti-apoptotischen (BCL-2, BCL-XL, BCL-W, MCL-1, BFL-1/A1), den pro-apoptotischen (NOXA, PUMA, BAD, BID, BIM, BIK, BMF, HRK) und den porenbildenden Proteinen (BAX, BAK, BOK). Verschiedene Stressstimuli führen zu einer Verschiebung des Gleichgewichts von pro- und anti-apoptotischen BCL-2 Proteinen zu Gunsten der pro-apoptotischen Proteine, wodurch es zu einer Aktivierung der Effektorproteine BAX und BAK kommt. Dies führt zur Permeabilisierung der äußeren mitochondrialen Membran und Freisetzung von Proteinen aus dem Intermembranraum des Mitochondriums wie Cytochrom c und Smac (*Second mitochondrial derived activator of caspases*) in das Zytoplasma. Dort bildet Cytochrom c zusammen mit der Procaspase-9 das Apoptosom, dies wiederrum resultiert in einer Aktivierung der Initiatorcaspase-9 und führt zu einer weiteren Aktivierung der Effektorcaspasen-3 und -7. In Folge dessen werden apoptotische

Zielproteine gespalten, wodurch letztendlich multiple Effekte auf Stabilität von DNA, Zytoskelett und Zellmembran entstehen.

Wichtige Regulatoren der Apoptose sind die Inhibitoren der Apoptose Proteine (IAP, *inhibitor of apoptosis protein*). Auf der einen Seite haben sie einen negativen (inhibierenden) Einfluss auf apoptotische Signalwege und auf der anderen Seite einen positiven (fördernden) Einfluss auf Signalwege, die das Überleben der Zelle positiv beeinflussen. Es sind acht IAPs beschrieben, wovon jedoch drei besonders an der Regulation von Apoptose beteiligt und Teil dieser Arbeit sind: zelluläre IAPs (*celluar IAP, cIAP*), cIAP1 und cIAP2 sowie XIAP (*X-linked IAP*). XIAP blockiert die Exekution von Apoptose durch Inhibition von Caspase-3, -7 und -9 mittels seiner BIR (*baculovirus IAP repeat*) Domäne. Des Weiteren fördert XIAP die proteasomale Degradation von Caspase-3 und -7 sowie von Smac über seine RING (*really interesting gene*) Domäne. Die zellulären IAPs weisen mit ihrer RING Domäne eine E3 Ubiquitin Ligase Funktion auf über die sie Proteine, welche in Zelltodsignalwegen involviert sind, beeinflussen können. So ubiquitinieren cIAP1 und cIAP2 z.B. RIPK1 (*Receptor-interacting protein kinase 1*) und unterbinden dadurch die Bildung des pro-apoptotischen Ripoptosoms. Außerdem ist cIAP1 in der Lage Caspase-3 und -7 zu ubiquitinieren, was einen proteasomalen Abbau dieser Proteasen zu Folge hat. Des Weiteren verhindern cIAP1/2 über die Ubiquitinierung von NIK (*NF-κB inducing kinase*) und dessen anschließender proteasomaler Abbau, die Aktivierung des anti-apoptotischen, nicht kanonischen NF-κB Signalweg. Da IAPs eine wichtige Rolle in der Zelltodregulierung spielen, tragen sie auch einen entschiedenen Beitrag zur Tumorentwicklung und Tumorprogression bei. Viele Tumore weisen eine erhöhte Expression von IAPs auf, die mit Behandlungsresistenzen und schlechten Prognosen für die Patienten einhergehen. Erhöhte Expressionslevel von cIAP1 und 2 wurden ebenfalls in primären Tumorproben von DLBCL Patienten nachgewiesen. Daher ist das zielgerichtete Angreifen oder Herunterregulieren von IAPs ein viel versprechender Therapieansatz. Für den therapeutischen Einsatz wurden IAP Antagonisten sogenannte Smac mimetics entwickelt, sie ahmen die vier N-terminalen Aminosäurereste (Ala-Val-Pro-Ile) des endogenen Smacs nach, welche für seine IAP Bindungseigenschaften benötigt werden. Smac mimetics binden an die BIR3 Domäne von cIAPs, was zu einer Konformationsänderung und Dimerisierung von zwei cIAP Proteinen führt. Darauf folgen eine Autoubiquitinierung der beiden cIAP Proteine sowie deren proteasomale

Degradation. Des Weiteren inhibieren Smac mimetics die BIR2 und BIR3 Domänen von XIAP, wodurch die Blockade von XIAP auf Caspase-3, -7 und -9 aufgehoben wird. Derzeit befinden sich Smac mimetics in prä-klinischen sowie klinischen Studien zur Therapie verschiedener Krebserkrankungen. Insbesondere in der Kombination mit anderen Medikamenten zeigen Smac mimetics *in vitro* und *in vivo* vielversprechende Ergebnisse. In der vorliegenden Arbeit wurde das bivalente Smac mimetic BV6 verwendet, welches die IAPs cIAP1/2 und XIAP antagonisiert.

Das Proteasom ist ein wesentlicher Bestandteil des Ubiquitin-Proteasom-Systems (UPS), welches für die Proteindegradation und Regulation der Homöostase innerhalb der Zelle verantwortlich ist. Das UPS kontrolliert Prozesse wie Zellzyklus und Proliferation sowie pro- und anti-apoptotische Signalwege. Das aktive 26S Proteasom ist eine multikatalytische Protease, die aus einer 20S katalytischen sowie zwei 19S regulatorischen Untereinheiten besteht. Ubiquitinierte Proteine werden in der 20S Untereinheit proteolytisch in dessen Aminosäuren gespalten. Tumorzellen haben eine hohe Proliferationsrate und daher einen höheren Umsatz an Proteinen im Vergleich zu nicht malignen Zellen. Außerdem spielt das Proteasom eine wichtige Rolle für den Zellzyklus und die Proliferation, wodurch das Proteasom zu einem geeigneten Angriffspunkt für Tumorzellen mit einer hohen Proliferationsrate wird. Tatsächlich konnte bereit gezeigt werden, dass Tumorzellen empfindlicher auf Proteasominhibition reagieren als nicht maligne Zellen. Proteasom-Inhibitoren binden an die katalytische Untereinheit des 20S Proteasom und verhindern dadurch deren enzymatische Funktion und damit verbunden die Degradation von Proteinen. Da das Proteasom in vielen zelluläre Signalwege involviert ist hat die Inhibition des Proteasoms einen Einfluss auf viele intrazelluläre Prozesse. Proteasominhibition führt zu einer Akkumulation falsch gefalteter Proteine, was wiederrum proteotoxischen Stress hervorruft und Zelltod auslöst. Des Weiteren kann die Inhibition des Proteasoms zu einer Generierung von reaktiven Sauerstoffspezies (ROS, *reactive oxygen species*) führen. Proteasominhibition fördert zu dem die Akkumulation von pro-apoptotischen Proteinen wie NOXA oder BIM. Außerdem kann Zellzyklus- und Wachstumsarrest eine Folge von Proteasominhibition sein. So sind die Folgen von Proteasom-Inhibitoren intrazellulär sehr vielseitig. Einer der ersten Proteasom-Inhibitoren bortezomib (BTZ) ist bereits für die Behandlung des Multiplen Myeloms und des Mantelzell-Lymphoms zugelassen. Die Entwicklung sogenannter *second generation* Proteasom-Inhibitoren,

hat das toxikologische Profil noch einmal verbessert und derzeit befinden sich viele Proteasom-Inhibitoren in prä-klinischen und klinischen Studien zur Behandlung verschiedener Tumorerkrankungen, entweder als Einzelbehandlung oder als Kombinationstherapie. In dieser Arbeit wurden Proteasom-Inhibitoren der zweiten Generation verwendet (carfilzomib, ixazomib, oprozomib).

Da IAPs eine wichtige Rolle für das Voranschreiten sowie die Behandlung von DLBCL spielen, wurde in der vorliegenden Arbeit zum einen das Potential von Smac mimetics in DLBCL getestet sowie die Effizienz einer Kombinationsbehandlung aus Smac mimetic und Proteasom-Inhibitor untersucht. Die Kombination von Smac mimetic und Proteasom-Inhibitoren wurde bis jetzt nur vereinzelt getestet z.B. im Multiplen Myelom, im Melanom oder in NHL. Im Falle einer kooperativen Zelltodinduktion von Smac mimetic und Proteasom-Inhibitoren sollen die molekularen Mechanismen untersucht werden mit einem speziellen Fokus auf programmierte Zelltodsignalwege.

Zunächst wurde die Wirksamkeit des Smac mimetics BV6 in DLBCL Zelllinien verschiedener Subtypen getestet. Hierbei zeigt sich, dass BV6 in allen DLBCL Zelllinien eine Reduktion der Zellviabilität hervorrufen kann, unabhängig von der Subtypenzugehörigkeit der Zelllinie (ABC, GCB, PMBL). Ebenso kann eine Einzelbehandlung mit dem Proteasom-Inhibitor carfilzomib (CFZ) eine Reduktion der Zellviabilität in allen DLBCL Zelllinien induzieren. Eine Kombinationsbehandlung von BV6 mit CFZ zeigt eine synergistische Reduktion der Zellviabilität, welches durch die Berechnung des Kombinationsindex (CI, *combination index*) und des Bliss Scores bestätigt wurde. Des Weiteren kooperiert BV6 mit anderen Proteasom-Inhibitoren (ixazomib, oprozomib) was darauf hindeutet, dass ein genereller Effekt zwischen Smac mimetic und Proteasom-Inhibitoren vorliegt, um Zellviabilität in DLBCL zu reduzieren. Neben der Reduktion der Zellviabilität führt die Kombination von BV6 und CFZ zu einer zeitabhängigen Zelltodinduktion. Zur Charakterisierung des Zelltods analysierten wir die Caspasenaktivierung, nach Behandlung mit BV6 und CFZ, als typisches Merkmal von apoptotischem Zelltod. Die Kombinationsbehandlung führt zu einer Spaltung und Aktivierung von verschiedenen Initiator- und Effektorcaspasen (Caspase-3, -7, -8 und -9). Die Verwendung des Caspasen-Inhibitors zVAD.fmk verhindert den durch BV6 und CFZ induzierten Zelltod und verdeutlicht dadurch, dass die Aktivierung der Caspasen einen wichtigen Schritt in der Zelltodinduktion darstellt. Außerdem führt die Behandlung mit BV6 und CFZ zu einem Verlust des mitochondrialen

Membranpotentials, vor und mit Beginn der Zelltodindunktion. Dies unterstützt die Hypothese, dass es sich bei dem induzierten Zelltod um intrinsische mitochondriale Apoptose handelt. Weitere mechanistische Experimente zeigen, dass der mitochondriale Signalweg kritisch für den BV6/CFZ-vermittelten Zelltod ist. Unter Behandlung mit BV6/CFZ wurde eine Aktivierung von BAX und BAK nachgewiesen, welche mit verantwortlich für die Porenbildung in der mitochondrialen Membran sind. Eine Herunterregulation dieser beiden Proteine mittels siRNA (*knockdown*) reduziert signifikant den durch BV6/CFZ-induzierten Zelltod auf ein Minimum. Im Zusammenhang mit den Mitochondrien zeigen wir auch einen Anstieg von mitochondrialem ROS, sowie eine generelle Induktion des allgemeinen ROS Levels. Eine Behandlung mit BV6/CFZ zeigt eine deutliche Akkumulation des pro-apoptotischen Proteins NOXA. Um dessen funktionelle Relevanz zu überprüfen, wurde die Proteinmenge von NOXA mittels siRNA stark reduziert. Eine Behandlung mit der Kombination aus BV6 und CFZ zeigt daraufhin eine signifikant reduzierte Zelltodindunktion, was die funktionelle Relevanz von NOXA für den BV6/CFZ-vermittelten Zelltod unterstreicht. Immunopräzipitationsstudien zeigen, dass in RIVA und U2932 Zellen NOXA konstitutiv an seinen anti-apoptotischen Bindungspartner MCL-1 gebunden ist, was die Zellen bereits darauf vorbereitet Apoptose zu durchlaufen. Dieses sogenannte „primen" für Apoptose wird durch die Behandlung mit BV6 und CFZ weiter verstärkt, da es die Bindung zwischen NOXA und MCL-1 weiter erhöht. Dadurch wird die Balance zwischen pro- und anti-apoptotischen Proteinen zu Gunsten der pro-apoptotischen Proteine verschoben und die Induktion von Apoptose begünstigt.

Zudem zeigen wir, dass eine Behandlung mit BV6 und CFZ zu einer Akkumulation von NIK führt, ein Protein welches zur Aktivierung des non-kanonischen NF-$\kappa$B Signalweges benötigt wird. Weitere Untersuchungen zeigen jedoch, dass NIK nicht an der Zelltodindunktion beteiligt ist, da eine siRNA-basierte Herunterregulierung des NIK Proteins keinen Einfluss auf die Zelltodindunktion nimmt. Ebenfalls ist der Zelltod unabhängig von dem TNF$\alpha$ Signalweg, da weder eine Behandlung mit dem TNF$\alpha$ Inhibitor Enbrel den Zelltod verringern kann noch eine zusätzliche Gabe von TNF$\alpha$ den Zelltod erhöht. Diese Ergebnisse werden durch andere Publikationen unterstützt, die ebenfalls einen Smac mimetic induzierten Zelltod unabhängig von TNF$\alpha$ und dem nicht-kanonischen NF-$\kappa$B Signalweg nachweisen konnten. Ein Abbau von cIAP

Proteinen kann neben der Akkumulation von NIK auch zu einer Förderung der Ripoptosombildung führen und auf diesem Weg die Induktion von Apoptose vorantreiben. Die Kernkomponenten des Ripoptosoms bestehen aus RIPK1, FADD und Caspase-8 und werden negativ durch cFLIP$_L$, cIAP1, cIAP2 und XIAP beeinflusst. Es ist bereits beschrieben, dass der Proteasom-Inhibitor BTZ cFLIP runterregulieren kann und Smac mimetics cIAP1, cIAP2 und XIAP antagonisieren, weshalb die Kombination von BV6 und CFZ die Formation des Ripoptosoms fördern kann. Neben der Degradation von cIAPs spielt die direkte Inhibition von Caspasen durch XIAP eine wichtige Rolle für die Induktion von Zelltod. In dieser Arbeit zeigen wir, dass eine Herunterregulation von XIAP mittels siRNA und eine anschließende Behandlung mit CFZ die Kombinationsbehandlung von BV6 und CFZ in U2932 Zellen nachahmen kann. In den RIVA Zellen hat die Herunterregulation von XIAP und anschließende Behandlung mit CFZ, keinen Nachahmungseffekt der Kombinationsbehandlung. Diese Ergebnisse lassen darauf schließen, dass die Inhibition von XIAP durch BV6 eine wichtige Rolle für die Zelltodinduktion in den U2932 Zellen spielt. U2932 Zellen besitzen ein höheres basales XIAP Proteinlevel als RIVA Zellen, was erklären könnte, dass U2932 Zellen sensitiver auf eine XIAP Runterregulation reagieren. Interessanterweise konnten wir für RIVA Zellen zeigen, dass eine gleichzeitige Herunterregulation von cIAP1 und 2 mittels siRNA und eine anschließende Behandlung mit CFZ eine Behandlung mit BV6/CFZ nachahmen kann und somit eine wichtige Rolle für die cIAPs in BV6/CFZ-vermittelten Zelltod in RIVA Zellen nachweisen. Die Wirkungsweise von BV6 scheint daher Zellkontextabhängig zu sein. Mit den cIAP *knockdown* Experimenten einhergehend hat ein Herunterregulieren der Caspase-8 Proteinmenge nur in den RIVA Zellen einen Effekt auf den Zelltod. Herabsetzten des Caspase-8 Proteinlevels führt in diesen Zellen zu einer Reduzierung des BV6/CFZ-vermittelten Zelltods. Dies lässt darauf schließen, dass in RIVA Zellen eine Degradation der cIAPs eine Ripoptosomformation begünstigen, welche jedoch von Caspase-8 abhängt, um Zelltod zu induzieren.

Insgesamt zeigen die Ergebnisse, dass in DLBCL Zelllinien, unabhängig von ihrem Subtyp, die Kombinationsbehandlung von Smac mimetic und Proteasom-Inhibitor die Zellviabilität reduziert bzw. Zelltod induziert und damit eine mögliche neue Behandlungsstrategie für diese heterogene Tumorerkrankung darstellt. Die Charakterisierung des molekularen Wirkmechanismus hat gezeigt, dass es sich um

einen apoptotischen Zelltod handelt, welcher über das Mitochondrium vermittelt wird. Eine zentrale Rolle bei der Vermittlung des Zelltodsignales spielen dabei BAX und BAK sowie das pro-apoptotische Protein NOXA.

# 9 References

1.  Elenitoba-Johnson, K.S.J. and M.S. Lim, New Insights into Lymphoma Pathogenesis. Annu Rev Pathol, 2018. 13: p. 193-217.
2.  Jiang, M., N.N. Bennani, and A.L. Feldman, Lymphoma classification update: T-cell lymphomas, Hodgkin lymphomas, and histiocytic/dendritic cell neoplasms. Expert Rev Hematol, 2017. 10(3): p. 239-249.
3.  Matasar, M.J. and A.D. Zelenetz, Overview of lymphoma diagnosis and management. Radiol Clin North Am, 2008. 46(2): p. 175-98, vii.
4.  Campo, E., et al., The 2008 WHO classification of lymphoid neoplasms and beyond: evolving concepts and practical applications. Blood, 2011. 117(19): p. 5019-32.
5.  Camicia, R., H.C. Winkler, and P.O. Hassa, Novel drug targets for personalized precision medicine in relapsed/refractory diffuse large B-cell lymphoma: a comprehensive review. Mol Cancer, 2015. 14: p. 207.
6.  Coiffier, B., Diffuse large cell lymphoma. Curr Opin Oncol, 2001. 13(5): p. 325-34.
7.  Frick, M., B. Dorken, and G. Lenz, The molecular biology of diffuse large B-cell lymphoma. Ther Adv Hematol, 2011. 2(6): p. 369-79.
8.  Alizadeh, A.A., et al., Distinct types of diffuse large B-cell lymphoma identified by gene expression profiling. Nature, 2000. 403(6769): p. 503-11.
9.  Wright, G., et al., A gene expression-based method to diagnose clinically distinct subgroups of diffuse large B cell lymphoma. Proc Natl Acad Sci U S A, 2003. 100(17): p. 9991-6.
10. Rosenwald, A., et al., The use of molecular profiling to predict survival after chemotherapy for diffuse large-B-cell lymphoma. N Engl J Med, 2002. 346(25): p. 1937-47.
11. Lenz, G., et al., Molecular subtypes of diffuse large B-cell lymphoma arise by distinct genetic pathways. Proc Natl Acad Sci U S A, 2008. 105(36): p. 13520-5.
12. Bea, S., et al., Diffuse large B-cell lymphoma subgroups have distinct genetic profiles that influence tumor biology and improve gene-expression-based survival prediction. Blood, 2005. 106(9): p. 3183-90.
13. Davis, R.E., et al., Chronic active B-cell-receptor signalling in diffuse large B-cell lymphoma. Nature, 2010. 463(7277): p. 88-92.
14. Compagno, M., et al., Mutations of multiple genes cause deregulation of NF-kappaB in diffuse large B-cell lymphoma. Nature, 2009. 459(7247): p. 717-21.
15. Kato, M., et al., Frequent inactivation of A20 in B-cell lymphomas. Nature, 2009. 459(7247): p. 712-6.
16. Ngo, V.N., et al., Oncogenically active MYD88 mutations in human lymphoma. Nature, 2011. 470(7332): p. 115-9.
17. Lenz, G., et al., Oncogenic CARD11 mutations in human diffuse large B cell lymphoma. Science, 2008. 319(5870): p. 1676-9.
18. Tagawa, H., et al., Comparison of genome profiles for identification of distinct subgroups of diffuse large B-cell lymphoma. Blood, 2005. 106(5): p. 1770-7.
19. Salmena, L., A. Carracedo, and P.P. Pandolfi, Tenets of PTEN tumor suppression. Cell, 2008. 133(3): p. 403-14.
20. Melzner, I., et al., Biallelic mutation of SOCS-1 impairs JAK2 degradation and sustains phospho-JAK2 action in the MedB-1 mediastinal lymphoma line. Blood, 2005. 105(6): p. 2535-42.

21.     Melzner, I., et al., Biallelic deletion within 16p13.13 including SOCS-1 in Karpas1106P mediastinal B-cell lymphoma line is associated with delayed degradation of JAK2 protein. Int J Cancer, 2006. 118(8): p. 1941-4.

22.     Rosenwald, A., et al., Molecular diagnosis of primary mediastinal B cell lymphoma identifies a clinically favorable subgroup of diffuse large B cell lymphoma related to Hodgkin lymphoma. J Exp Med, 2003. 198(6): p. 851-62.

23.     Savage, K.J., et al., The molecular signature of mediastinal large B-cell lymphoma differs from that of other diffuse large B-cell lymphomas and shares features with classical Hodgkin lymphoma. Blood, 2003. 102(12): p. 3871-9.

24.     Schmitz, R., et al., TNFAIP3 (A20) is a tumor suppressor gene in Hodgkin lymphoma and primary mediastinal B cell lymphoma. J Exp Med, 2009. 206(5): p. 981-9.

25.     Reddy, A., et al., Genetic and Functional Drivers of Diffuse Large B Cell Lymphoma. Cell, 2017. 171(2): p. 481-494 e15.

26.     Roschewski, M., K. Dunleavy, and W.H. Wilson, Diffuse large B cell lymphoma: molecular targeted therapy. International Journal of Hematology, 2012. 96(5): p. 552-561.

27.     Fulda, S., Tumor resistance to apoptosis. Int J Cancer, 2009. 124(3): p. 511-5.

28.     Taylor, R.C., S.P. Cullen, and S.J. Martin, Apoptosis: controlled demolition at the cellular level. Nat Rev Mol Cell Biol, 2008. 9(3): p. 231-41.

29.     Tait, S.W. and D.R. Green, Mitochondria and cell death: outer membrane permeabilization and beyond. Nat Rev Mol Cell Biol, 2010. 11(9): p. 621-32.

30.     Ashkenazi, A. and V.M. Dixit, Death receptors: signaling and modulation. Science, 1998. 281(5381): p. 1305-8.

31.     Ashkenazi, A., Targeting the extrinsic apoptosis pathway in cancer. Cytokine Growth Factor Rev, 2008. 19(3-4): p. 325-31.

32.     Kischkel, F.C., et al., Apo2L/TRAIL-dependent recruitment of endogenous FADD and caspase-8 to death receptors 4 and 5. Immunity, 2000. 12(6): p. 611-20.

33.     Li, H., et al., Cleavage of BID by caspase 8 mediates the mitochondrial damage in the Fas pathway of apoptosis. Cell, 1998. 94(4): p. 491-501.

34.     Luo, X., et al., Bid, a Bcl2 interacting protein, mediates cytochrome c release from mitochondria in response to activation of cell surface death receptors. Cell, 1998. 94(4): p. 481-90.

35.     Park, Y.H., M.S. Jeong, and S.B. Jang, Death domain complex of the TNFR-1, TRADD, and RIP1 proteins for death-inducing signaling. Biochem Biophys Res Commun, 2014. 443(4): p. 1155-61.

36.     Fuchs, Y. and H. Steller, Live to die another way: modes of programmed cell death and the signals emanating from dying cells. Nat Rev Mol Cell Biol, 2015. 16(6): p. 329-44.

37.     Micheau, O. and J. Tschopp, Induction of TNF receptor I-mediated apoptosis via two sequential signaling complexes. Cell, 2003. 114(2): p. 181-90.

38.     Creagh, E.M., H. Conroy, and S.J. Martin, Caspase-activation pathways in apoptosis and immunity. Immunol Rev, 2003. 193: p. 10-21.

39.     Adams, J.M. and S. Cory, The Bcl-2 apoptotic switch in cancer development and therapy. Oncogene, 2007. 26(9): p. 1324-37.

40.     Kale, J., E.J. Osterlund, and D.W. Andrews, BCL-2 family proteins: changing partners in the dance towards death. Cell Death Differ, 2018. 25(1): p. 65-80.

41.     Shamas-Din, A., et al., BH3-only proteins: Orchestrators of apoptosis. Biochim Biophys Acta, 2011. 1813(4): p. 508-20.

42.     Liu, Q., et al., Apoptotic regulation by MCL-1 through heterodimerization. J Biol Chem, 2010. 285(25): p. 19615-24.

43.     Ku, B., et al., Evidence that inhibition of BAX activation by BCL-2 involves its tight and preferential interaction with the BH3 domain of BAX. Cell Res, 2011. 21(4): p. 627-41.

44.     Shamas-Din, A., et al., Mechanisms of action of Bcl-2 family proteins. Cold Spring Harb Perspect Biol, 2013. 5(4): p. a008714.

45.     Letai, A., et al., Distinct BH3 domains either sensitize or activate mitochondrial apoptosis, serving as prototype cancer therapeutics. Cancer Cell, 2002. 2(3): p. 183-92.

46.     Kim, H., et al., Hierarchical regulation of mitochondrion-dependent apoptosis by BCL-2 subfamilies. Nat Cell Biol, 2006. 8(12): p. 1348-58.

47.     Kuwana, T., et al., BH3 domains of BH3-only proteins differentially regulate Bax-mediated mitochondrial membrane permeabilization both directly and indirectly. Mol Cell, 2005. 17(4): p. 525-35.

48.     Certo, M., et al., Mitochondria primed by death signals determine cellular addiction to antiapoptotic BCL-2 family members. Cancer Cell, 2006. 9(5): p. 351-65.

49.     Leber, B., J. Lin, and D.W. Andrews, Embedded together: the life and death consequences of interaction of the Bcl-2 family with membranes. Apoptosis, 2007. 12(5): p. 897-911.

50.     Singh, R., A. Letai, and K. Sarosiek, Regulation of apoptosis in health and disease: the balancing act of BCL-2 family proteins. Nat Rev Mol Cell Biol, 2019.

51.     Adrain, C. and S.J. Martin, The mitochondrial apoptosome: a killer unleashed by the cytochrome seas. Trends Biochem Sci, 2001. 26(6): p. 390-7.

52.     Birnbaum, M.J., R.J. Clem, and L.K. Miller, An apoptosis-inhibiting gene from a nuclear polyhedrosis virus encoding a polypeptide with Cys/His sequence motifs. J Virol, 1994. 68(4): p. 2521-8.

53.     Vaux, D.L. and J. Silke, Mammalian mitochondrial IAP binding proteins. Biochemical and Biophysical Research Communications, 2003. 304(3): p. 499-504.

54.     Vaux, D.L. and J. Silke, IAPs, RINGs and ubiquitylation. Nat Rev Mol Cell Biol, 2005. 6(4): p. 287-97.

55.     Yang, Y., et al., Ubiquitin protein ligase activity of IAPs and their degradation in proteasomes in response to apoptotic stimuli. Science, 2000. 288(5467): p. 874-7.

56.     Schile, A.J., M. Garcia-Fernandez, and H. Steller, Regulation of apoptosis by XIAP ubiquitin-ligase activity. Genes Dev, 2008. 22(16): p. 2256-66.

57.     Silke, J. and D. Vucic, IAP family of cell death and signaling regulators. Methods Enzymol, 2014. 545: p. 35-65.

58.     Fulda, S. and D. Vucic, Targeting IAP proteins for therapeutic intervention in cancer. Nat Rev Drug Discov, 2012. 11(2): p. 109-24.

59.     Deveraux, Q.L., et al., X-linked IAP is a direct inhibitor of cell-death proteases. Nature, 1997. 388(6639): p. 300-4.

60.     Eckelman, B.P., G.S. Salvesen, and F.L. Scott, Human inhibitor of apoptosis proteins: why XIAP is the black sheep of the family. EMBO Rep, 2006. 7(10): p. 988-94.

61.     Srinivasula, S.M., et al., A conserved XIAP-interaction motif in caspase-9 and Smac/DIABLO regulates caspase activity and apoptosis. Nature, 2001. 410(6824): p. 112-6.

62.     Shiozaki, E.N., et al., Mechanism of XIAP-mediated inhibition of caspase-9. Mol Cell, 2003. 11(2): p. 519-27.

63.     Huang, Y., et al., Structural basis of caspase inhibition by XIAP: differential roles of the linker versus the BIR domain. Cell, 2001. 104(5): p. 781-90.

64.     Chai, J., et al., Structural basis of caspase-7 inhibition by XIAP. Cell, 2001. 104(5): p. 769-80.

65.     Riedl, S.J., et al., Structural basis for the inhibition of caspase-3 by XIAP. Cell, 2001. 104(5): p. 791-800.

66.     Suzuki, Y., Y. Nakabayashi, and R. Takahashi, Ubiquitin-protein ligase activity of X-linked inhibitor of apoptosis protein promotes proteasomal degradation of caspase-3 and enhances its anti-apoptotic effect in Fas-induced cell death. Proc Natl Acad Sci U S A, 2001. 98(15): p. 8662-7.

67.     MacFarlane, M., et al., Proteasome-mediated degradation of Smac during apoptosis: XIAP promotes Smac ubiquitination in vitro. J Biol Chem, 2002. 277(39): p. 36611-6.

68.     LaCasse, E.C., et al., The inhibitors of apoptosis (IAPs) and their emerging role in cancer. Oncogene, 1998. 17(25): p. 3247-59.

69. Bertrand, M.J., et al., cIAP1 and cIAP2 facilitate cancer cell survival by functioning as E3 ligases that promote RIP1 ubiquitination. Mol Cell, 2008. 30(6): p. 689-700.

70. Varfolomeev, E., et al., IAP antagonists induce autoubiquitination of c-IAPs, NF-kappaB activation, and TNFalpha-dependent apoptosis. Cell, 2007. 131(4): p. 669-81.

71. Choi, Y.E., et al., The E3 ubiquitin ligase cIAP1 binds and ubiquitinates caspase-3 and -7 via unique mechanisms at distinct steps in their processing. J Biol Chem, 2009. 284(19): p. 12772-82.

72. Hu, S. and X. Yang, Cellular inhibitor of apoptosis 1 and 2 are ubiquitin ligases for the apoptosis inducer Smac/DIABLO. J Biol Chem, 2003. 278(12): p. 10055-60.

73. Park, Y.C., et al., A novel mechanism of TRAF signaling revealed by structural and functional analyses of the TRADD-TRAF2 interaction. Cell, 2000. 101(7): p. 777-87.

74. de Almagro, M.C. and D. Vucic, The inhibitor of apoptosis (IAP) proteins are critical regulators of signaling pathways and targets for anti-cancer therapy. Exp Oncol, 2012. 34(3): p. 200-11.

75. Kocab, A.J. and C.S. Duckett, Inhibitor of apoptosis proteins as intracellular signaling intermediates. FEBS J, 2016. 283(2): p. 221-31.

76. Scheidereit, C., IkappaB kinase complexes: gateways to NF-kappaB activation and transcription. Oncogene, 2006. 25(51): p. 6685-705.

77. Vallabhapurapu, S., et al., Nonredundant and complementary functions of TRAF2 and TRAF3 in a ubiquitination cascade that activates NIK-dependent alternative NF-kappaB signaling. Nat Immunol, 2008. 9(12): p. 1364-70.

78. Zarnegar, B.J., et al., Noncanonical NF-kappaB activation requires coordinated assembly of a regulatory complex of the adaptors cIAP1, cIAP2, TRAF2 and TRAF3 and the kinase NIK. Nat Immunol, 2008. 9(12): p. 1371-8.

79. Sun, S.C., The non-canonical NF-kappaB pathway in immunity and inflammation. Nat Rev Immunol, 2017. 17(9): p. 545-558.

80. Varfolomeev, E., et al., Cellular inhibitors of apoptosis are global regulators of NF-kappaB and MAPK activation by members of the TNF family of receptors. Sci Signal, 2012. 5(216): p. ra22.

81. Dejardin, E., The alternative NF-kappaB pathway from biochemistry to biology: pitfalls and promises for future drug development. Biochem Pharmacol, 2006. 72(9): p. 1161-79.

82. Varfolomeev, E. and D. Vucic, (Un)expected roles of c-IAPs in apoptotic and NFkappaB signaling pathways. Cell Cycle, 2008. 7(11): p. 1511-21.

83. Vince, J.E., et al., IAP antagonists target cIAP1 to induce TNFalpha-dependent apoptosis. Cell, 2007. 131(4): p. 682-93.

84. Ambrosini, G., C. Adida, and D.C. Altieri, A novel anti-apoptosis gene, survivin, expressed in cancer and lymphoma. Nat Med, 1997. 3(8): p. 917-21.

85. Vucic, D., et al., ML-IAP, a novel inhibitor of apoptosis that is preferentially expressed in human melanomas. Curr Biol, 2000. 10(21): p. 1359-66.

86. Fong, W.G., et al., Expression and genetic analysis of XIAP-associated factor 1 (XAF1) in cancer cell lines. Genomics, 2000. 70(1): p. 113-22.

87. Tamm, I., et al., Expression and prognostic significance of IAP-family genes in human cancers and myeloid leukemias. Clin Cancer Res, 2000. 6(5): p. 1796-803.

88. Li, J., et al., Human ovarian cancer and cisplatin resistance: possible role of inhibitor of apoptosis proteins. Endocrinology, 2001. 142(1): p. 370-80.

89. Li, M., et al., XIAP as a prognostic marker of early recurrence of nonmuscular invasive bladder cancer. Chin Med J (Engl), 2007. 120(6): p. 469-73.

90. Mizutani, Y., et al., Overexpression of XIAP expression in renal cell carcinoma predicts a worse prognosis. Int J Oncol, 2007. 30(4): p. 919-25.

91. Foster, F.M., et al., Targeting inhibitor of apoptosis proteins in combination with ErbB antagonists in breast cancer. Breast Cancer Res, 2009. 11(3): p. R41.

92. Hunter, A.M., E.C. LaCasse, and R.G. Korneluk, The inhibitors of apoptosis (IAPs) as cancer targets. Apoptosis, 2007. 12(9): p. 1543-68.

93. Yang, Y., et al., Targeting Non-proteolytic Protein Ubiquitination for the Treatment of Diffuse Large B Cell Lymphoma. Cancer Cell, 2016. 29(4): p. 494-507.

94. Fulda, S., Smac mimetics as IAP antagonists. Semin Cell Dev Biol, 2015. 39: p. 132-8.

95. Gaither, A., et al., A Smac mimetic rescue screen reveals roles for inhibitor of apoptosis proteins in tumor necrosis factor-alpha signaling. Cancer Res, 2007. 67(24): p. 11493-8.

96. Sun, H., et al., Design of small-molecule peptidic and nonpeptidic Smac mimetics. Acc Chem Res, 2008. 41(10): p. 1264-77.

97. Cohen, F., et al., Orally bioavailable antagonists of inhibitor of apoptosis proteins based on an azabicyclooctane scaffold. J Med Chem, 2009. 52(6): p. 1723-30.

98. Sun, H., et al., Structure-based design, synthesis, and evaluation of conformationally constrained mimetics of the second mitochondria-derived activator of caspase that target the X-linked inhibitor of apoptosis protein/caspase-9 interaction site. J Med Chem, 2004. 47(17): p. 4147-50.

99. Fulda, S., Smac Mimetics to Therapeutically Target IAP Proteins in Cancer. Int Rev Cell Mol Biol, 2017. 330: p. 157-169.

100. Feltham, R., et al., Smac mimetics activate the E3 ligase activity of cIAP1 protein by promoting RING domain dimerization. J Biol Chem, 2011. 286(19): p. 17015-28.

101. Silke, J. and P. Meier, Inhibitor of apoptosis (IAP) proteins-modulators of cell death and inflammation. Cold Spring Harb Perspect Biol, 2013. 5(2).

102. Dueber, E.C., et al., Antagonists induce a conformational change in cIAP1 that promotes autoubiquitination. Science, 2011. 334(6054): p. 376-80.

103. Gao, Z., et al., A dimeric Smac/diablo peptide directly relieves caspase-3 inhibition by XIAP. Dynamic and cooperative regulation of XIAP by Smac/Diablo. J Biol Chem, 2007. 282(42): p. 30718-27.

104. Varfolomeev, E., et al., X chromosome-linked inhibitor of apoptosis regulates cell death induction by proapoptotic receptor agonists. J Biol Chem, 2009. 284(50): p. 34553-60.

105. Dubrez, L., SMAC Mimetics: Promising Therapeutic Agents in Cancer and other Diseases. Biochemistry & Pharmacology: Open Access, 2018. 07(02).

106. Fulda, S., Promises and Challenges of Smac Mimetics as Cancer Therapeutics. Clin Cancer Res, 2015. 21(22): p. 5030-6.

107. Bedford, L., et al., Ubiquitin-like protein conjugation and the ubiquitin-proteasome system as drug targets. Nat Rev Drug Discov, 2011. 10(1): p. 29-46.

108. Ciechanover, A., The ubiquitin-proteasome pathway: on protein death and cell life. Embo j, 1998. 17(24): p. 7151-60.

109. Hershko, A., The ubiquitin system for protein degradation and some of its roles in the control of the cell division cycle. Cell Death Differ, 2005. 12(9): p. 1191-7.

110. Nalepa, G., M. Rolfe, and J.W. Harper, Drug discovery in the ubiquitin-proteasome system. Nat Rev Drug Discov, 2006. 5(7): p. 596-613.

111. Dick, L.R. and P.E. Fleming, Building on bortezomib: second-generation proteasome inhibitors as anti-cancer therapy. Drug Discov Today, 2010. 15(5-6): p. 243-9.

112. Brooks, P., et al., Subcellular localization of proteasomes and their regulatory complexes in mammalian cells. Biochem J, 2000. 346 Pt 1: p. 155-61.

113. Peters, J.M., et al., Structural features of the 26 S proteasome complex. J Mol Biol, 1993. 234(4): p. 932-7.

114. Adams, J., The proteasome: structure, function, and role in the cell. Cancer Treat Rev, 2003. 29 Suppl 1: p. 3-9.

115. DeMartino, G.N. and C.A. Slaughter, The proteasome, a novel protease regulated by multiple mechanisms. J Biol Chem, 1999. 274(32): p. 22123-6.

116. Kisselev, A.F., et al., Proteasome active sites allosterically regulate each other, suggesting a cyclical bite-chew mechanism for protein breakdown. Mol Cell, 1999. 4(3): p. 395-402.

117. Nussbaum, A.K., et al., Cleavage motifs of the yeast 20S proteasome beta subunits deduced from digests of enolase 1. Proc Natl Acad Sci U S A, 1998. 95(21): p. 12504-9.

118. Feitelson, M.A., et al., Sustained proliferation in cancer: Mechanisms and novel therapeutic targets. Semin Cancer Biol, 2015. 35 Suppl: p. S25-s54.

119. Hanahan, D. and R.A. Weinberg, Hallmarks of cancer: the next generation. Cell, 2011. 144(5): p. 646-74.

120. Crawford, L.J., B. Walker, and A.E. Irvine, Proteasome inhibitors in cancer therapy. J Cell Commun Signal, 2011. 5(2): p. 101-10.

121. Masdehors, P., et al., Increased sensitivity of CLL-derived lymphocytes to apoptotic death activation by the proteasome-specific inhibitor lactacystin. Br J Haematol, 1999. 105(3): p. 752-7.

122. Hideshima, T., et al., The proteasome inhibitor PS-341 inhibits growth, induces apoptosis, and overcomes drug resistance in human multiple myeloma cells. Cancer Res, 2001. 61(7): p. 3071-6.

123. Adams, J., The proteasome: a suitable antineoplastic target. Nat Rev Cancer, 2004. 4(5): p. 349-60.

124. Chauhan, D., T. Hideshima, and K.C. Anderson, A novel proteasome inhibitor NPI-0052 as an anticancer therapy. Br J Cancer, 2006. 95(8): p. 961-5.

125. Richardson, P.G., et al., Bortezomib or high-dose dexamethasone for relapsed multiple myeloma. N Engl J Med, 2005. 352(24): p. 2487-98.

126. Fisher, R.I., et al., Multicenter phase II study of bortezomib in patients with relapsed or refractory mantle cell lymphoma. J Clin Oncol, 2006. 24(30): p. 4867-74.

127. Bose, P., et al., Bortezomib for the treatment of non-Hodgkin's lymphoma. Expert Opin Pharmacother, 2014. 15(16): p. 2443-59.

128. Leonard, J.P., et al., Randomized Phase II Study of R-CHOP With or Without Bortezomib in Previously Untreated Patients With Non-Germinal Center B-Cell-Like Diffuse Large B-Cell Lymphoma. J Clin Oncol, 2017. 35(31): p. 3538-3546.

129. Goy, A., et al., Phase II study of proteasome inhibitor bortezomib in relapsed or refractory B-cell non-Hodgkin's lymphoma. J Clin Oncol, 2005. 23(4): p. 667-75.

130. O'Connor, O.A., et al., Phase II clinical experience with the novel proteasome inhibitor bortezomib in patients with indolent non-Hodgkin's lymphoma and mantle cell lymphoma. J Clin Oncol, 2005. 23(4): p. 676-84.

131. Richardson, P.G., et al., Frequency, characteristics, and reversibility of peripheral neuropathy during treatment of advanced multiple myeloma with bortezomib. J Clin Oncol, 2006. 24(19): p. 3113-20.

132. Lonial, S., et al., Risk factors and kinetics of thrombocytopenia associated with bortezomib for relapsed, refractory multiple myeloma. Blood, 2005. 106(12): p. 3777-84.

133. Hanada, M., et al., Epoxomicin, a new antitumor agent of microbial origin. J Antibiot (Tokyo), 1992. 45(11): p. 1746-52.

134. Meng, L., et al., Epoxomicin, a potent and selective proteasome inhibitor, exhibits in vivo antiinflammatory activity. Proc Natl Acad Sci U S A, 1999. 96(18): p. 10403-8.

135. Mushtaq, A., et al., Efficacy and toxicity profile of carfilzomib based regimens for treatment of multiple myeloma: A systematic review. Crit Rev Oncol Hematol, 2018. 125: p. 1-11.

136. Demo, S.D., et al., Antitumor activity of PR-171, a novel irreversible inhibitor of the proteasome. Cancer Res, 2007. 67(13): p. 6383-91.

137. O'Connor, O.A., et al., A Phase 1 Dose Escalation Study of the Safety and Pharmacokinetics of the Novel Proteasome Inhibitor Carfilzomib (PR-171) in Patients with Hematologic Malignancies. Clinical Cancer Research, 2009. 15(22): p. 7085-7091.

138. Moreau, P., et al., Phase 1/2 study of carfilzomib plus melphalan and prednisone in patients aged over 65 years with newly diagnosed multiple myeloma. Blood, 2015. 125(20): p. 3100-4.

139.  Muchtar, E., M.A. Gertz, and H. Magen, A practical review on carfilzomib in multiple myeloma. Eur J Haematol, 2016. 96(6): p. 564-77.

140.  Cai, Q., et al., Accelerated therapeutic progress in diffuse large B cell lymphoma. Ann Hematol, 2014. 93(4): p. 541-56.

141.  Gu, J.J., et al., The novel proteasome inhibitor carfilzomib induces cell cycle arrest, apoptosis and potentiates the anti-tumour activity of chemotherapy in rituximab-resistant lymphoma. Br J Haematol, 2013. 162(5): p. 657-69.

142.  Dasmahapatra, G., et al., Obatoclax interacts synergistically with the irreversible proteasome inhibitor carfilzomib in GC- and ABC-DLBCL cells in vitro and in vivo. Mol Cancer Ther, 2012. 11(5): p. 1122-32.

143.  Dasmahapatra, G., et al., In vitro and in vivo interactions between the HDAC6 inhibitor ricolinostat (ACY1215) and the irreversible proteasome inhibitor carfilzomib in non-Hodgkin lymphoma cells. Mol Cancer Ther, 2014. 13(12): p. 2886-97.

144.  Weigert, O., et al., Sequence-dependent synergy of the proteasome inhibitor bortezomib and cytarabine in mantle cell lymphoma. Leukemia, 2007. 21(3): p. 524-8.

145.  O'Connor, O.A., et al., The combination of the proteasome inhibitor bortezomib and the bcl-2 antisense molecule oblimersen sensitizes human B-cell lymphomas to cyclophosphamide. Clin Cancer Res, 2006. 12(9): p. 2902-11.

146.  Perez-Galan, P., et al., The proteasome inhibitor bortezomib induces apoptosis in mantle-cell lymphoma through generation of ROS and Noxa activation independent of p53 status. Blood, 2006. 107(1): p. 257-64.

147.  Perez-Galan, P., et al., BCL-2 phosphorylation modulates sensitivity to the BH3 mimetic GX15-070 (Obatoclax) and reduces its synergistic interaction with bortezomib in chronic lymphocytic leukemia cells. Leukemia, 2008. 22(9): p. 1712-20.

148.  Paoluzzi, L., et al., The BH3-only mimetic ABT-737 synergizes the antineoplastic activity of proteasome inhibitors in lymphoid malignancies. Blood, 2008. 112(7): p. 2906-16.

149.  Ackler, S., et al., The Bcl-2 inhibitor ABT-263 enhances the response of multiple chemotherapeutic regimens in hematologic tumors in vivo. Cancer Chemother Pharmacol, 2010. 66(5): p. 869-80.

150.  Dai, Y., M. Rahmani, and S. Grant, Proteasome inhibitors potentiate leukemic cell apoptosis induced by the cyclin-dependent kinase inhibitor flavopiridol through a SAPK/JNK- and NF-kappaB-dependent process. Oncogene, 2003. 22(46): p. 7108-22.

151.  Bhalla, S., et al., PCI-24781 induces caspase and reactive oxygen species-dependent apoptosis through NF-kappaB mechanisms and is synergistic with bortezomib in lymphoma cells. Clin Cancer Res, 2009. 15(10): p. 3354-65.

152.  Heider, U., et al., Synergistic interaction of the histone deacetylase inhibitor SAHA with the proteasome inhibitor bortezomib in cutaneous T cell lymphoma. Eur J Haematol, 2009. 82(6): p. 440-9.

153.  Paoluzzi, L., et al., Romidepsin and belinostat synergize the antineoplastic effect of bortezomib in mantle cell lymphoma. Clin Cancer Res, 2010. 16(2): p. 554-65.

154.  Paoluzzi, L., et al., The anti-histaminic cyproheptadine synergizes the antineoplastic activity of bortezomib in mantle cell lymphoma through its effects as a histone deacetylase inhibitor. Br J Haematol, 2009. 146(6): p. 656-9.

155.  Rao, R., et al., Role of CAAT/enhancer binding protein homologous protein in panobinostat-mediated potentiation of bortezomib-induced lethal endoplasmic reticulum stress in mantle cell lymphoma cells. Clin Cancer Res, 2010. 16(19): p. 4742-54.

156.  Roue, G., et al., The Hsp90 inhibitor IPI-504 overcomes bortezomib resistance in mantle cell lymphoma in vitro and in vivo by down-regulation of the prosurvival ER chaperone BiP/Grp78. Blood, 2011. 117(4): p. 1270-9.

157.  Roue, G., et al., Selective inhibition of IkappaB kinase sensitizes mantle cell lymphoma B cells to TRAIL by decreasing cellular FLIP level. J Immunol, 2007. 178(3): p. 1923-30.

158. Georgakis, G.V., et al., Activity of selective fully human agonistic antibodies to the TRAIL death receptors TRAIL-R1 and TRAIL-R2 in primary and cultured lymphoma cells: induction of apoptosis and enhancement of doxorubicin- and bortezomib-induced cell death. Br J Haematol, 2005. 130(4): p. 501-10.

159. Smith, M.R., F. Jin, and I. Joshi, Bortezomib sensitizes non-Hodgkin's lymphoma cells to apoptosis induced by antibodies to tumor necrosis factor related apoptosis-inducing ligand (TRAIL) receptors TRAIL-R1 and TRAIL-R2. Clin Cancer Res, 2007. 13(18 Pt 2): p. 5528s-5534s.

160. Lin, J.H., et al., IRE1 signaling affects cell fate during the unfolded protein response. Science, 2007. 318(5852): p. 944-9.

161. Ron, D. and P. Walter, Signal integration in the endoplasmic reticulum unfolded protein response. Nat Rev Mol Cell Biol, 2007. 8(7): p. 519-29.

162. Ling, Y.H., et al., Reactive oxygen species generation and mitochondrial dysfunction in the apoptotic response to Bortezomib, a novel proteasome inhibitor, in human H460 non-small cell lung cancer cells. J Biol Chem, 2003. 278(36): p. 33714-23.

163. Yu, C., et al., The hierarchical relationship between MAPK signaling and ROS generation in human leukemia cells undergoing apoptosis in response to the proteasome inhibitor Bortezomib. Exp Cell Res, 2004. 295(2): p. 555-66.

164. Hideshima, T., et al., NF-kappa B as a therapeutic target in multiple myeloma. J Biol Chem, 2002. 277(19): p. 16639-47.

165. Hideshima, T., et al., Bortezomib induces canonical nuclear factor-kappaB activation in multiple myeloma cells. Blood, 2009. 114(5): p. 1046-52.

166. Luciano, F., et al., Phosphorylation of Bim-EL by Erk1/2 on serine 69 promotes its degradation via the proteasome pathway and regulates its proapoptotic function. Oncogene, 2003. 22(43): p. 6785-93.

167. Rizzatti, E.G., et al., Noxa mediates bortezomib induced apoptosis in both sensitive and intrinsically resistant mantle cell lymphoma cells and this effect is independent of constitutive activity of the AKT and NF-kappaB pathways. Leuk Lymphoma, 2008. 49(4): p. 798-808.

168. Bonvini, P., et al., Bortezomib-mediated 26S proteasome inhibition causes cell-cycle arrest and induces apoptosis in CD-30+ anaplastic large cell lymphoma. Leukemia, 2007. 21(4): p. 838-42.

169. Strauss, S.J., et al., The Proteasome Inhibitor Bortezomib Acts Independently of p53 and Induces Cell Death via Apoptosis and Mitotic Catastrophe in B-Cell Lymphoma Cell Lines. Cancer Research, 2007. 67(6): p. 2783-2790.

170. Matta, H. and P.M. Chaudhary, The proteasome inhibitor bortezomib (PS-341) inhibits growth and induces apoptosis in primary effusion lymphoma cells. Cancer Biol Ther, 2005. 4(1): p. 77-82.

171. Nasr, R., et al., Efficacy and mechanism of action of the proteasome inhibitor PS-341 in T-cell lymphomas and HTLV-I associated adult T-cell leukemia/lymphoma. Oncogene, 2005. 24(3): p. 419-30.

172. Mato, A.R., T. Feldman, and A. Goy, Proteasome inhibition and combination therapy for non-Hodgkin's lymphoma: from bench to bedside. Oncologist, 2012. 17(5): p. 694-707.

173. Xia, Z., et al., Opposing effects of ERK and JNK-p38 MAP kinases on apoptosis. Science, 1995. 270(5240): p. 1326-31.

174. Lauricella, M., et al., JNK and AP-1 mediate apoptosis induced by bortezomib in HepG2 cells via FasL/caspase-8 and mitochondria-dependent pathways. Apoptosis, 2006. 11(4): p. 607-25.

175. Lei, K. and R.J. Davis, JNK phosphorylation of Bim-related members of the Bcl2 family induces Bax-dependent apoptosis. Proc Natl Acad Sci U S A, 2003. 100(5): p. 2432-7.

176. Hussain, A.R., et al., Prognostic significance of XIAP expression in DLBCL and effect of its inhibition on AKT signalling. J Pathol, 2010. 222(2): p. 180-90.

177. Schirmer, M., et al., Intrinsic and chemo-sensitizing activity of SMAC-mimetics on high-risk childhood acute lymphoblastic leukemia. Cell Death Dis, 2016. 7: p. e2052.

178. Ramakrishnan, V., et al., Smac mimetic LCL161 overcomes protective ER stress induced by obatoclax, synergistically causing cell death in multiple myeloma. Oncotarget, 2016. 7(35): p. 56253-56265.
179. Bhatti, I.A., B.A. Abhari, and S. Fulda, Identification of a synergistic combination of Smac mimetic and Bortezomib to trigger cell death in B-cell non-Hodgkin lymphoma cells. Cancer Lett, 2017. 405: p. 63-72.
180. Chauhan, D., et al., Targeting mitochondrial factor Smac/DIABLO as therapy for multiple myeloma (MM). Blood, 2007. 109(3): p. 1220-7.
181. Lecis, D., et al., Novel SMAC-mimetics synergistically stimulate melanoma cell death in combination with TRAIL and Bortezomib. Br J Cancer, 2010. 102(12): p. 1707-16.
182. Hsu, Y.T. and R.J. Youle, Bax in murine thymus is a soluble monomeric protein that displays differential detergent-induced conformations. J Biol Chem, 1998. 273(17): p. 10777-83.
183. Chou, T.C., Theoretical basis, experimental design, and computerized simulation of synergism and antagonism in drug combination studies. Pharmacol Rev, 2006. 58(3): p. 621-81.
184. Ianevski, A., et al., SynergyFinder: a web application for analyzing drug combination dose-response matrix data. Bioinformatics, 2017. 33(15): p. 2413-2415.
185. Vanden Berghe, T., et al., Regulated necrosis: the expanding network of non-apoptotic cell death pathways. Nat Rev Mol Cell Biol, 2014. 15(2): p. 135-47.
186. Petersen, S.L., et al., Autocrine TNFalpha signaling renders human cancer cells susceptible to Smac-mimetic-induced apoptosis. Cancer Cell, 2007. 12(5): p. 445-56.
187. Pop, C. and G.S. Salvesen, Human caspases: activation, specificity, and regulation. J Biol Chem, 2009. 284(33): p. 21777-81.
188. Westphal, D., et al., Molecular biology of Bax and Bak activation and action. Biochim Biophys Acta, 2011. 1813(4): p. 521-31.
189. Griffiths, G.J., et al., Cell Damage-induced Conformational Changes of the Pro-Apoptotic Protein Bak In Vivo Precede the Onset of Apoptosis. The Journal of Cell Biology, 1999. 144(5): p. 903-914.
190. Desagher, S., et al., Bid-induced Conformational Change of Bax Is Responsible for Mitochondrial Cytochrome c Release during Apoptosis. The Journal of Cell Biology, 1999. 144(5): p. 891-901.
191. Chipuk, J.E. and D.R. Green, How do BCL-2 proteins induce mitochondrial outer membrane permeabilization? Trends Cell Biol, 2008. 18(4): p. 157-64.
192. Smith, V.M., et al., Specific interactions of BCL-2 family proteins mediate sensitivity to BH3-mimetics in diffuse large B-cell lymphoma. Haematologica, 2019.
193. Smith, A.J., et al., Noxa/Bcl-2 protein interactions contribute to bortezomib resistance in human lymphoid cells. J Biol Chem, 2011. 286(20): p. 17682-92.
194. Vela, L., et al., Direct interaction of Bax and Bak proteins with Bcl-2 homology domain 3 (BH3)-only proteins in living cells revealed by fluorescence complementation. J Biol Chem, 2013. 288(7): p. 4935-46.
195. Dai, H., et al., Transient binding of an activator BH3 domain to the Bak BH3-binding groove initiates Bak oligomerization. J Cell Biol, 2011. 194(1): p. 39-48.
196. Du, H., et al., BH3 domains other than Bim and Bid can directly activate Bax/Bak. J Biol Chem, 2011. 286(1): p. 491-501.
197. Fribley, A., Q. Zeng, and C.Y. Wang, Proteasome inhibitor PS-341 induces apoptosis through induction of endoplasmic reticulum stress-reactive oxygen species in head and neck squamous cell carcinoma cells. Mol Cell Biol, 2004. 24(22): p. 9695-704.
198. Dixon, S.J., et al., Ferroptosis: an iron-dependent form of nonapoptotic cell death. Cell, 2012. 149(5): p. 1060-72.
199. Candas, D. and J.J. Li, MnSOD in oxidative stress response-potential regulation via mitochondrial protein influx. Antioxid Redox Signal, 2014. 20(10): p. 1599-617.
200. Cillessen, S.A., et al., Small-molecule XIAP antagonist restores caspase-9 mediated apoptosis in XIAP-positive diffuse large B-cell lymphoma cells. Blood, 2008. 111(1): p. 369-75.

201.   Ward, G.A., et al., ASTX660, a Novel Non-peptidomimetic Antagonist of cIAP1/2 and XIAP, Potently Induces TNFalpha-Dependent Apoptosis in Cancer Cell Lines and Inhibits Tumor Growth. Mol Cancer Ther, 2018. 17(7): p. 1381-1391.

202.   Runckel, K., et al., The SMAC mimetic LCL-161 displays antitumor activity in preclinical models of rituximab-resistant B-cell lymphoma. Blood Adv, 2018. 2(23): p. 3516-3525.

203.   Yang, C., et al., LCL161 increases paclitaxel-induced apoptosis by degrading cIAP1 and cIAP2 in NSCLC. J Exp Clin Cancer Res, 2016. 35(1): p. 158.

204.   Tian, A., et al., Synergistic effects of IAP inhibitor LCL161 and paclitaxel on hepatocellular carcinoma cells. Cancer Lett, 2014. 351(2): p. 232-41.

205.   Carter, B.Z., et al., Synergistic targeting of AML stem/progenitor cells with IAP antagonist birinapant and demethylating agents. J Natl Cancer Inst, 2014. 106(2): p. djt440.

206.   Weisberg, E., et al., Smac mimetics: implications for enhancement of targeted therapies in leukemia. Leukemia, 2010. 24(12): p. 2100-9.

207.   Wagner, L., et al., Smac mimetic sensitizes glioblastoma cells to Temozolomide-induced apoptosis in a RIP1- and NF-kappaB-dependent manner. Oncogene, 2013. 32(8): p. 988-97.

208.   Stadel, D., et al., Requirement of nuclear factor kappaB for Smac mimetic-mediated sensitization of pancreatic carcinoma cells for gemcitabine-induced apoptosis. Neoplasia, 2011. 13(12): p. 1162-70.

209.   Yazbeck, V., et al., A Phase II Trial of Bortezomib and Vorinostat in Mantle Cell Lymphoma and Diffuse Large B-cell Lymphoma. Clin Lymphoma Myeloma Leuk, 2018. 18(9): p. 569-575.e1.

210.   Evens, A.M., et al., A phase I/II trial of bortezomib combined concurrently with gemcitabine for relapsed or refractory DLBCL and peripheral T-cell lymphomas. Br J Haematol, 2013. 163(1): p. 55-61.

211.   Chauhan, D., et al., A novel orally active proteasome inhibitor induces apoptosis in multiple myeloma cells with mechanisms distinct from Bortezomib. Cancer Cell, 2005. 8(5): p. 407-19.

212.   Craxton, A., et al., NOXA, a sensor of proteasome integrity, is degraded by 26S proteasomes by an ubiquitin-independent pathway that is blocked by MCL-1. Cell Death Differ, 2012. 19(9): p. 1424-34.

213.   Fernandez, Y., et al., Differential regulation of noxa in normal melanocytes and melanoma cells by proteasome inhibition: therapeutic implications. Cancer Res, 2005. 65(14): p. 6294-304.

214.   Hausmann, M., et al., BCL-2 modifying factor (BMF) is a central regulator of anoikis in human intestinal epithelial cells. J Biol Chem, 2011. 286(30): p. 26533-40.

215.   Puthalakath, H., et al., Bmf: a proapoptotic BH3-only protein regulated by interaction with the myosin V actin motor complex, activated by anoikis. Science, 2001. 293(5536): p. 1829-32.

216.   Day, C.L., et al., Localization of dynein light chains 1 and 2 and their pro-apoptotic ligands. Biochem J, 2004. 377(Pt 3): p. 597-605.

217.   Kutuk, O. and A. Letai, Displacement of Bim by Bmf and Puma rather than increase in Bim level mediates paclitaxel-induced apoptosis in breast cancer cells. Cell Death Differ, 2010. 17(10): p. 1624-35.

218.   Baou, M., et al., Role of NOXA and its ubiquitination in proteasome inhibitor-induced apoptosis in chronic lymphocytic leukemia cells. Haematologica, 2010. 95(9): p. 1510-8.

219.   Miller, L.A., et al., BH3 mimetic ABT-737 and a proteasome inhibitor synergistically kill melanomas through Noxa-dependent apoptosis. J Invest Dermatol, 2009. 129(4): p. 964-71.

220.   Qin, J.Z., et al., Proteasome inhibitors trigger NOXA-mediated apoptosis in melanoma and myeloma cells. Cancer Res, 2005. 65(14): p. 6282-93.

221.   Mei, Y., et al., Noxa/Mcl-1 balance regulates susceptibility of cells to camptothecin-induced apoptosis. Neoplasia, 2007. 9(10): p. 871-81.

222. Geserick, P., et al., The ratio of Mcl-1 and Noxa determines ABT737 resistance in squamous cell carcinoma of the skin. Cell Death Dis, 2014. 5: p. e1412.

223. Gomez-Bougie, P., et al., Noxa up-regulation and Mcl-1 cleavage are associated to apoptosis induction by bortezomib in multiple myeloma. Cancer Res, 2007. 67(11): p. 5418-24.

224. Perez-Galan, P., et al., The BH3-mimetic GX15-070 synergizes with bortezomib in mantle cell lymphoma by enhancing Noxa-mediated activation of Bak. Blood, 2007. 109(10): p. 4441-9.

225. Willis, S.N., et al., Proapoptotic Bak is sequestered by Mcl-1 and Bcl-xL, but not Bcl-2, until displaced by BH3-only proteins. Genes Dev, 2005. 19(11): p. 1294-305.

226. Obeng, E.A., et al., Proteasome inhibitors induce a terminal unfolded protein response in multiple myeloma cells. Blood, 2006. 107(12): p. 4907-16.

227. Lee, A.H., et al., Proteasome inhibitors disrupt the unfolded protein response in myeloma cells. Proc Natl Acad Sci U S A, 2003. 100(17): p. 9946-51.

228. Lipchick, B.C., E.E. Fink, and M.A. Nikiforov, Oxidative stress and proteasome inhibitors in multiple myeloma. Pharmacol Res, 2016. 105: p. 210-5.

229. Maharjan, S., et al., Mitochondrial impairment triggers cytosolic oxidative stress and cell death following proteasome inhibition. Sci Rep, 2014. 4: p. 5896.

230. Weniger, M.A., et al., Treatment-induced oxidative stress and cellular antioxidant capacity determine response to bortezomib in mantle cell lymphoma. Clin Cancer Res, 2011. 17(15): p. 5101-12.

231. Cao, X.H., et al., ROS-Ca(2+) is associated with mitochondria permeability transition pore involved in surfactin-induced MCF-7 cells apoptosis. Chem Biol Interact, 2011. 190(1): p. 16-27.

232. Fulda, S., Molecular pathways: targeting inhibitor of apoptosis proteins in cancer--from molecular mechanism to therapeutic application. Clin Cancer Res, 2014. 20(2): p. 289-95.

233. Thu, Y.M. and A. Richmond, NF-kappaB inducing kinase: a key regulator in the immune system and in cancer. Cytokine Growth Factor Rev, 2010. 21(4): p. 213-26.

234. Wittwer, T. and M.L. Schmitz, NIK and Cot cooperate to trigger NF-kappaB p65 phosphorylation. Biochem Biophys Res Commun, 2008. 371(2): p. 294-7.

235. Boutaffala, L., et al., NIK promotes tissue destruction independently of the alternative NF-kappaB pathway through TNFR1/RIP1-induced apoptosis. Cell Death Differ, 2015. 22(12): p. 2020-33.

236. Allensworth, J.L., et al., Smac mimetic Birinapant induces apoptosis and enhances TRAIL potency in inflammatory breast cancer cells in an IAP-dependent and TNF-alpha-independent mechanism. Breast Cancer Res Treat, 2013. 137(2): p. 359-71.

237. Eschenburg, G., et al., Smac mimetic LBW242 sensitizes XIAP-overexpressing neuroblastoma cells for TNF-alpha-independent apoptosis. Cancer Res, 2012. 72(10): p. 2645-56.

238. Cheung, H.H., et al., Smac mimetic compounds potentiate interleukin-1beta-mediated cell death. J Biol Chem, 2010. 285(52): p. 40612-23.

239. Feoktistova, M., et al., cIAPs block Ripoptosome formation, a RIP1/caspase-8 containing intracellular cell death complex differentially regulated by cFLIP isoforms. Mol Cell, 2011. 43(3): p. 449-63.

240. Tenev, T., et al., The Ripoptosome, a signaling platform that assembles in response to genotoxic stress and loss of IAPs. Mol Cell, 2011. 43(3): p. 432-48.

241. Sayers, T.J., et al., The proteasome inhibitor PS-341 sensitizes neoplastic cells to TRAIL-mediated apoptosis by reducing levels of c-FLIP. Blood, 2003. 102(1): p. 303-10.

242. Chan, H., D.P. Bartos, and L.B. Owen-Schaub, Activation-dependent transcriptional regulation of the human Fas promoter requires NF-kappaB p50-p65 recruitment. Mol Cell Biol, 1999. 19(3): p. 2098-108.

243. Singh, N.P., M. Nagarkatti, and P.S. Nagarkatti, Role of dioxin response element and nuclear factor-kappaB motifs in 2,3,7,8-tetrachlorodibenzo-p-dioxin-mediated regulation of Fas and Fas ligand expression. Mol Pharmacol, 2007. 71(1): p. 145-57.
244. Baetu, T.M., et al., Disruption of NF-kappaB signaling reveals a novel role for NF-kappaB in the regulation of TNF-related apoptosis-inducing ligand expression. J Immunol, 2001. 167(6): p. 3164-73.
245. Fakler, M., et al., Small molecule XIAP inhibitors cooperate with TRAIL to induce apoptosis in childhood acute leukemia cells and overcome Bcl-2-mediated resistance. Blood, 2009. 113(8): p. 1710-22.
246. Gerges, S., K. Rohde, and S. Fulda, Cotreatment with Smac mimetics and demethylating agents induces both apoptotic and necroptotic cell death pathways in acute lymphoblastic leukemia cells. Cancer Lett, 2016. 375(1): p. 127-132.
247. Ri, M., Endoplasmic-reticulum stress pathway-associated mechanisms of action of proteasome inhibitors in multiple myeloma. Int J Hematol, 2016. 104(3): p. 273-80.

# 10 Danksagung

Zunächst möchte ich mich bei Frau Prof. Dr. Simone Fulda bedanken, für die Möglichkeit meine Doktorarbeit in ihrem Labor am Institut für experimentelle Tumorforschung in der Pädiatrie durchzuführen sowie für ihren Support, fachliche Diskussionen und Ratschläge während meiner Zeit als Doktorandin. Außerdem möchte ich mich bei Herrn Prof. Dr. Volker Dötsch für die Betreuung meiner Arbeit am Fachbereich 14 und die Übernahme des Gutachtens bedanken.

Ein Dank geht auch an alle aktuellen und ehemaligen Mitarbeiter der AG Fulda für das angenehme Arbeitsklima, das freundliche Miteinander und die ständige Hilfsbereitschaft. Ein besonderer Dank geht dabei an Christina Hugenberg für ihre stetige Hilfe in bürokratischen sowie nicht-bürokratischen Angelegenheiten. Vielen Dank auch an Dani und Sonja, die den Laboralltag am Laufen halten und uns viel Arbeit abnehmen. Ebenso möchte ich Meike herzlich danken für ihre tolle Betreuung, Ratschläge und Unterstützung. Ein besonderes Dankeschön geht auch an Svenja, Lisa, Vanessa, Jessi, Lara, Sjoerd, Jens und Anne für die schöne gemeinsame Zeit im Büro/Labor, die fachlichen sowie fachfremden Diskussionen und die moralische Unterstützung.

Vielen Dank Svenja für die tolle gemeinsame Zeit, die wir im und außerhalb des Labors zusammen hatten. Ohne dich wäre die Zeit hier definitiv nicht so schön gewesen und nicht so schnell vergangen.

Ein ganz besonderer Dank geht auch an alle, die mich während meiner Schwangerschaft so toll im Labor unterstützt haben.

Ein Dankeschön auch an Paul, für seinen Support in Formatierungsfragen.

Zum Schluss möchte ich meiner Familie danken für ihre Unterstützung und Hilfe in den letzten Jahren und meinem Mann Christoph, der mich immer unterstütz hat und mir jederzeit mit Rat und Tat und Motivation beiseite stand.

# 11 Curriculum Vitae

## **Personal Data:**

| | |
|---|---|
| **Name** | Anna Dietz geb. Schwendler |
| **Address** | Kiedricherstraße 11, 65197 Wiesbaden |
| **E-Mail** | anna@dietz.world |
| **Phone** | 0176/ 311 97 310 |
| **Date and place of birth** | 08.06.1990, Wiesbaden |

## **Academic education:**

| | |
|---|---|
| **06/2016-date** | **Goethe-University-Frankfurt** |
| | PhD student at the Institute for experimental cancer research in pediatrics |
| | Course of study: Biochemistry |
| | Degree: Dr. phil. nat. (prospective) |
| **10/2015-04/2016** | **Philipps University Marburg** |
| | Research assistant at the Institute of Anatomy and Cell Biology |
| **10/2013-10/2015** | **Philipps University Marburg** |
| | Course of study: Human biology |
| | Degree: Master of Science (1.3) |
| **04/2013-06/2013** | **Paul Ehrlich Institute, Langen** |
| | Internship at the research group Experimental Allergology |
| **04/2010-05/2013** | **Johannes Gutenberg University Mainz** |
| | Course of study: Biology |
| | Degree: Bachelor of Science (2.1) |

| 10/2009- 12/2009 | **Helmholtz Institute of Biomedical Engineering, Aachen** |
|---|---|
| | Internship at the research groups Tissue Engineering & Biomaterials as well as Cardiovascular Engineering |
| 06/2000-06/2009 | **Leibniz Gymnasium, Wiesbaden** |
| | Qualification: Abitur (2.1) |

## Publications:

| 03/2020 | **International Journal of Cancer** |
|---|---|
| | *Proteasome inhibitors and Smac mimetics cooperate to induce cell death in Diffuse Large B-cell Lymphoma by stabilizing NOXA and triggering mitochondrial apoptosis* (Dietz et al. 2019) |
| 10/2019 | **Hematologica** |
| | *Specific interactions of BCL-2 family proteins mediate sensitivity to BH3-mimetics in diffuse large B-cell lymphoma* (Smith et al. 2019, co-authorship) |
| 01/2018 | **Frontiers in Pharmacology** |
| | *Neurotrophic, cytoprotective and anti-inflammatory effects of St. John's wort extract on differentiated mouse hippocampal HT-22 neurons* (Bonaterra et al. 2018, shared first authorship) |

## Special skills:

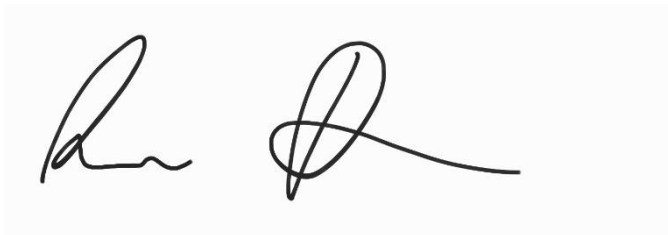| Languages | German (native) |
|---|---|
| | English (Business fluent) |
| | French (basic knowledge) |
| Computer skills | Microsoft Word, Excel, PowerPoint (competent knowledge) |
| | SigmaPlot (basic knowledge) |
| | ImageJ (basic knowledge) |

## 12 Eidesstattliche Erklärung

Ich, Anna Dietz geb. Schwendler, erkläre hiermit an Eides Statt, dass ich die vorgelegte Dissertation

*„Mechanisms of Smac mimetic and proteasome inhibitor-induced cell death in diffuse large B-cell lymphoma"*

selbstständig angefertigt und mich anderer Hilfsmittel als der in ihr angegebenen nicht bedient habe, insbesondere, dass alle Entlehnungen aus anderen Schriften mit Angabe der betreffenden Schrift gekennzeichnet sind.

Ich versichere, nicht die Hilfe einer kommerziellen Promotionsvermittlung in Anspruch genommen, sowie die Grundsätze der guten wissenschaftlichen Praxis beachtet zu haben.

Frankfurt am Main, den 17.03.2020